The Fatigue Behaviour of Tension Lap Spliced Reinforced Concrete Beams Strengthened with Fibre Reinforced Polymer Wrapping

by

Rayed Alyousef

A thesis

presented to the University of Waterloo

in fulfillment of the

thesis requirement for the degree of

Doctor of Philosophy

in

Civil Engineering

Waterloo, Ontario, Canada, 2016

AUTHOR'S DECLARATION

I hereby declare that I am the sole author of this thesis. This is a true copy of the thesis, including any required final revisions, as accepted by my examiners.

I understand that my thesis may be made electronically available to the public.

Abstract

Many reinforced concrete structures containing lap splices were constructed before modern bond and fatigue design codes came into existence and are subjected to fatigue loading, which may lead to a bond failure even when the applied load is far below the ultimate load for a bond failure under a monotonic loading. Fatigue loads result in a deterioration of the bond interaction between the steel and concrete and interrupt the force transfer mechanism resulting in an increased deflection, an increased number of cracks and their widths, and a decreased load carrying capacity of reinforced concrete elements of structures. Some of these structures require strengthening to enhance their bond strength at lap splices.

This study was aimed at increasing our understanding of the behaviour of the bond between the steel bar and the concrete along the lap splice region for structures subjected to cyclic loading. An additional aim of the study was to investigate the effect of fatigue loading on the bond between concrete and steel, and the ability of the new high and low modulus fiber-reinforced polymer (FRP) sheets to enhance the fatigue performance of a tension lap splice.

Fifty three beams were cast and tested under monotonic and fatigue loading. The beams dimensions were 2200 mm in length, 350 mm in height and 250 mm in width. Each beam was reinforced with two 20M bars lap spliced in the constant moment region of the tension zone and two 10M bars in the compression zone outside the constant moment region. The test variables were the concrete cover, the presence or absence of FRP wrapping, the type of the FRP wrapping glass or carbon fiber-reinforced polymer (GFRP or CFRP), the type of loading and the fatigue load range. The minimum load applied was 10% of the static bond capacity of the specimen. The maximum load was varied to obtain fatigue lives between 1,000 and 1,000,000 cycles. The test frequency for all cyclic tests was 1.3 Hz.

The results of the tests under monotonic load showed that the GFRP wrapped beams had an increase in bond strength of approximately 25% compared to the unwrapped beams for each of the concrete covers. However, the CFRP wrapped beams had a percentage increase in bond strength that decreased as the concrete cover increased. The CFRP wrapped beams had

increases in bond strength of 71%, 60% and 44% compared to the unwrapped beams for concrete covers of 20 mm, 30 mm and 50 mm, respectively.

The results of the tests under fatigue load showed that all beams failed by a bond failure except for those beams that exceeded the fatigue life limits for a longitudinal bar. As expected, these beams failed by fatigue rupture of the longitudinal steel bars. The GFRP and CFRP sheets increased the fatigue strength (measured as the applied load range for a given fatigue life) of the wrapped beams for all concrete covers compared to that of the unwrapped beams. The longitudinal splitting cracks for the FRP wrapped beams were finer in width and larger in number compared to those cracks for the unwrapped beams.

A crack growth model was developed to calculate the fatigue life of the bond specimens and to calculate the slip and the deflection due to stress changes in the steel and concrete due to cracking, and compare it to the measured slip and deflection. There is also a good agreement between the calculated number of cycles with the actual fatigue data for all different wrapping conditions and all different concrete cover thicknesses. Also, only a small amount of the inelastic slip and the inelastic deflection are due to the stress changes in the steel and concrete due to splitting cracking. The remaining inelastic slip and inelastic deflection which are due to deformation of the concrete in front of the steel rebar lugs is much larger.

Acknowledgements

First and foremost, I would like to thank and praise Allah for helping and guiding me through this work and giving me the patience and health necessary to complete my PhD degree.

I will always be grateful to have had the opportunity of working with my previous supervisor Professor Khaled Soudki, may his soul rest in peace. He supported me and provided help and guidance in planning my research project.

I would like to express my sincere gratitude and appreciation to my friend, my supervisor and my civil engineer godfather Prof. Tim Topper for his patient help, guidance, encouragement, support and wonderful supervision and above all friendship. His immeasurable dedication, commitment and care for his students, his wealth of knowledge, and patience with his students and his love for research has been a great inspiration. I have been extremely lucky to have a supervisor who cared so much about my work, and who answered my questions and queries so quickly. Words cannot express my sincere appreciation for his help, guidance and everything else he did for me. Special thanks are due to my supervisor Prof. Adil Al-Mayah for his support and guidance. Without his inspirational guidance, his enthusiasm, his encouragement and his unselfish help, I could not have finished my doctoral work in University of Waterloo. I would also like to thank my committee members, Professor(s) Mark Green, Hamid Jahed, Scott Walbridge and Tarek Hegazy for reviewing my thesis, evaluating my research, and for their insightful feedback. Special thanks to NDT group (Prof: Giovanni Cascante, Maria Jose and Fernando Tallavo) for their help and assistance, without you guys the completion of the NDT part cannot be complete.

I also would also like to thank my colleagues who assisted me throughout various stages of this study: Rizwan Azam, Mohamed Zawam, Maria Jose, Adham El Menoufy, Taha Younes, Noran Abdel-Wahab, Mohamed Yakhlaf, Amr Ab-del-Havez. Without them the completion of this work would have been much more difficult.

Special thanks are extended to my friends: Hisham Alabduljabbar, Ayman Shihata, Omar Alromyah, Talal Alharbi, Suliman AL Othman, Omar Alghamdi, Mohammed Algaej, Abdulaziz Alaskar, Suliman AL Mushari, Mohamed El Badawe, Yasir Alhamadi, Khaled Aldosiry and my brother in-law Mohammed Alyousef for their sincerity, support, and encouragement during my academic journey.

The help of Douglas Hirst, Richard Morrison and Rob Sluban from Civil Engineering in the lab work is appreciated and acknowledged.

I am also grateful to Prince Sattam bin Abdul-Aziz University in Al-Kharj, Saudi Arabia for fully sponsoring my scholarship and also for the continued support from Saudi Arabian Cultural Bureau in Canada throughout my study.

Finally, a heartfelt gratitude to my mother and father, my wife, my daughter, brothers, sisters, my brother in-law, and best friends Hisham, AbdulAziz and Suliman for their true endless love and honest support that inspired me to work hard and achieve the PhD degree. I dedicate this thesis to my mother Latifa and father Abdullah, my wife Hadeel, my little daughter Reem, brothers (Mohammed, Ali, Yousef, Ayoub and Yaquop), sister (Haifa and Sara), amazing brother in-law Ali and to my best friend Hisham with love and appreciation.

Dedication

To my beloved family; my parents, Abdullah Alyousef, Latifa Alyousef, my wife Hadeel Alyousef and my daughter Reem.

Table of Contents

List of Figures

List of Tables

Chapter 1 Introduction

1.1 General

A lap splice is a simple, cost effective, and efficient connection method commonly used to transfer the force between lapped steel rebars in a reinforced concrete member. Short lap splices are weak in bond strength. Many reinforced concrete structures subjected to cyclic loading were constructed before modern bond and fatigue design codes were available. One of the main issues faced in determining the adequacy of existing structures is the low bond strength of short lap splices. Failure of the bond between the steel rebar and the concrete in the absence of stirrups often occurs by splitting of the concrete cover on the tension face or side face of a beam and is a problem that affects the serviceability and safety of reinforced concrete structures under both monotonic and fatigue loads.

Structures such as bridges and marinas are subjected to cyclic loading. As the ratio of live load to dead load increases, the fatigue limit state starts to govern the design through the effect of repeated loading (ACI 215, 1974). Damage in concrete structures may accumulate under service loads that are far below the ultimate loads under monotonic loading. Fatigue failure is the most likely extreme scenario that will occur due to repeated loading (ACI 215, 1974). Damage of the concrete structure may materialize in the form of an increased number of cracks, increased crack widths and an increase in the deflection. These factors are greatly influenced by the quality of the bond between the steel and the concrete. Accurate calculations of the bond strength between steel and concrete will have a significant impact on evaluating the residual strength of concrete structures (Oh and Kim, 2007; ACI 408R, 2003).

Fiber reinforced polymer (FRP) sheets offer an excellent solution for the rehabilitation and strengthening of deteriorated and deficient concrete members. In addition to their high strength to weight ratio, durability in service environments and high fatigue strength, FRP sheets can be easily bonded to the external surface of reinforced concrete slabs, beams, and columns (ACI 440, 2008). For lap splices, the FRP sheets prevent the concrete cover from splitting, which leads to an increase in the force that is transferred between lap splice bars by the concrete.

1.2 Research Motivation

1.2.1 Research Needs

Fatigue loading leads to a decrease in the strength and ductility of the lap splice. However, many reinforced concrete structures containing lap splices were constructed before modern bond and fatigue design codes came into existence. Therefore, some of these structures require strengthening to enhance their bond strength at lap splices. The repair of reinforced concrete beams using FRP sheets has become popular as a new technique for strengthening methods. From the literature review, the majority of the research on strengthening the bond strength of the reinforced concrete beams containing lap splices was performed under monotonic loading. To the author's knowledge, no one has investigated the effect of FRP sheet wrapping on the bond strength of reinforced concrete beams containing lap splices under fatigue loading. The absence of experimental data on the strengthening of reinforced concrete beams containing lap splices reinforced with FRP sheets under fatigue loading has delayed the development of a model able to predict the fatigue performance of the bond between steel and concrete.

1.2.2 Scope of Research

This study was designed to address the needs discussed above and enhance our knowledge of the bond strength of the lap splice region under fatigue loading. It investigated the effectiveness and feasibility of using FRP wrapping sheets to improve the performance of reinforced concrete beams with a lap splice under monotonic and fatigue loading. Experiments were performed to investigate the behaviour of wrapped and unwrapped concrete beams containing lap splices under monotonic and fatigue loading for different wrapping materials and concrete covers. In addition, a crack growth model was developed to predict the fatigue life of beams. Furthermore, non-destructive tests were performed to assess the damage of the rebar-concrete bond during fatigue loading.

1.2.3 Research Objectives

This research has the following objectives:

- To test the effect of FRP sheet wrapping on the bond strength of reinforced concrete beams with lap splices under monotonic and fatigue loading for different concrete cover thicknesses.
- To develop an analytical model to predict the fatigue life of unwrapped and wrapped lap spliced reinforced concrete beams.

1.3 Thesis Structure

The thesis is divided into seven chapters. Chapter one provides an introduction, discusses research needs, describes the scope of the research, and the research objectives and thesis structure. Chapter two provides background and a literature review covering bond between steel and concrete, strengthening using fiber reinforced polymer sheets and fatigue of bond in concrete structures. . Chapter three describes the experimental program, test matrix, specimen fabrication, material properties, FRP repair, and test setup. Chapter four consists of the experimental results under both monotonic and fatigue loading. Chapter five provides the modeling of the experimental work which includes Wahab et al., 2015 shear stress modeling, the model used in the current study, the procedure used to derive the constants for the model and a comparison of the experimental results with the model predictions . Chapter six gives the results of ultrasound tests using the surface wave technique and discuss their use in detecting structural deterioration. Conclusion and recommendation for future work are provided in chapter seven.

Chapter 2 Background and Literature Review

Many existing reinforced concrete members containing lap splices need to be rehabilitated to bring their bond strength up to the current code requirements. Several strengthening methods have been used to increase the bond strength such as increasing the concrete cover of the member, replacing the old concrete cover with a new high strength concrete, adding a transverse reinforcement either internal as stirrups or external as a steel plate and adding a wrapping of external FRP sheet. These strengthening methods have limitations. Increasing the concrete cover of the reinforced concrete member, replacing the old concrete cover with new high strength concrete and adding transverse reinforcement may require more space during construction than is available. A drawback of using steel plate is the problem of steel corrosion. Moreover, it increases the dead load on the reinforced concrete structure (Lerchental, 1970; Kajfasz et al., 1970; Swamy et al., 1987; Jones et al., 1988; Oehlers, 1992). On the contrary, the FRP sheet wraps do not suffer from the above drawbacks. They are compact and light due to their high strength to weight ratios and do not corrode. Also they have high fatigue strengths and are easily bonded to the external surface of a reinforced concrete member (ISIS, 2001).

2.1 Bond of the Steel Reinforcement in Concrete

Reinforced concrete structures are comprised of concrete that is strong in compression and steel that is strong and ductile in tension. “The bond between reinforcing bars and concrete has been acknowledged as a key to the proper performance of reinforced concrete structures for well over 100 years” (ACI 408R, 2003). Continuous research efforts in the recent years have provided a better understanding of bond behaviour.

In reinforced concrete structures, the external loads are applied to the concrete and not directly to the reinforced steel bar. Concrete is weak in tension, once the concrete cracks, all the tensile force due to the applied load is transferred to the steel bar at the cracked sections. Some of the tensile force is transferred back to the concrete in between the cracks. A shear stress (bond stress) between the steel and the surrounding concrete occurs as the stress of the steel bar change along its length. All current

design bond strength codes aim to provide enough bond length to ensure that the steel bar yields before a bond failure happens.

2.1.1 Bond Mechanism

There are three mechanisms that determine the stress transfer between the concrete and a deformed steel bar in a concrete beam, namely:

A: a chemical adhesion between the steel and the concrete,

B: friction between the steel and the concrete, and

C: a mechanical anchorage of the reinforcing steel ribs against the concrete

The bond forces between the deformed steel bar and the concrete are shown in Figure 2.1. The chemical adhesion and friction are the main bond components for plain steel bars, although the roughness of the surfaces of the bars may also result in some mechanical interlock between the concrete and the steel. The mechanical interlocking between the concrete and the steel for deformed bars gives much higher bond strengths than those due to chemical adhesion and friction. The forces due to the bearing of the bar ribs against the concrete create the majority of the bond strength that prevents the relative slip between deformed bars and surrounding concrete.

Adhesion prevents bars from slipping during the early stage of loading. As the load increases, the steel bars start to move breaking the adhesion and activating the bearing and friction forces. Friction and bearing forces play the major role in load transfer mechanism for ribbed steel bars, while friction forces on the surface of the reinforcing bars are reduced with a further increase in the slip (ACI 408R, 2003).

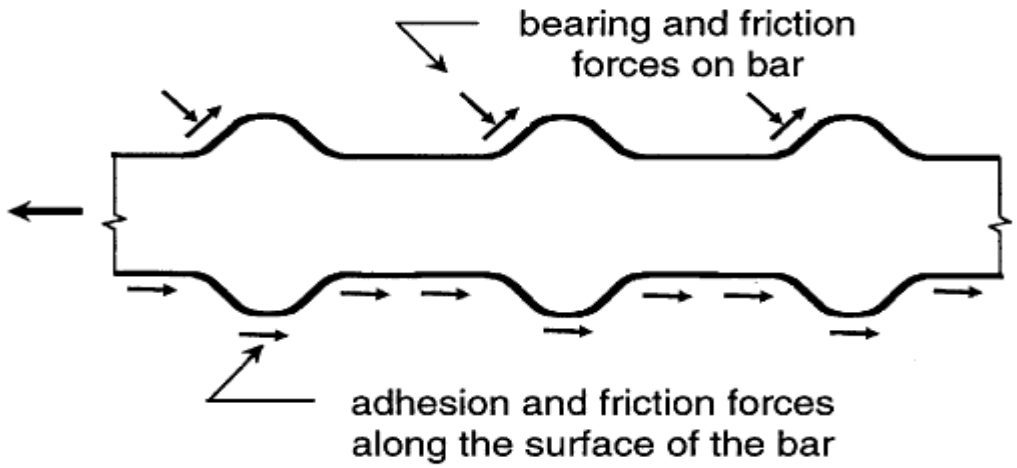

Figure 2.1 Bond mechanism of deformed reinforcement in concrete due to adhesion, bearing and friction (ACI 408R, 2003)

Much of the tensile force in the steel bars at the cracks is redistributed to the surrounding concrete in the regions between cracks by shear stress. The component of the shear stress acts at an angle β to the steel bar ribs as shown in Figure 2.2 (Goto,1971; Ferguson and Briceno, 1969, Canbay and Frosch, 2005). The shear force results in a radial hope stress that develops circumferential tensile stresses in the surrounding concrete along the development length as shown in Figure 2.3.

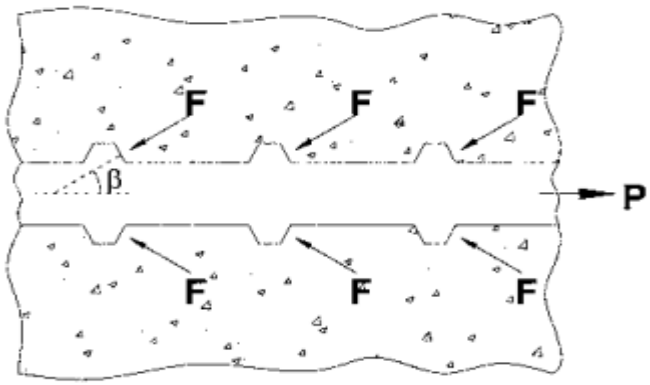

Figure 2.2 Shear stress component (Canbay and Frosch, 2005)

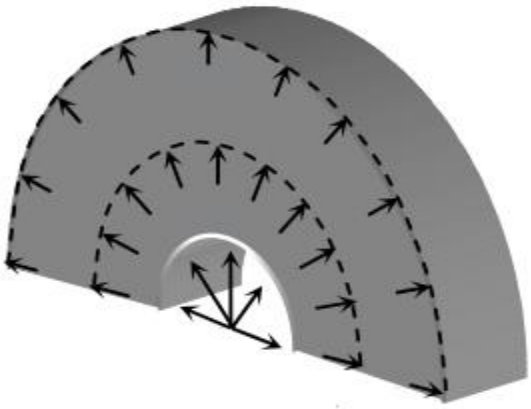

Figure 2.3 The resultant circumferential tensile stresses in the surrounding concrete (Tastani and Pantazopoulou 2012)

Two modes of failure of the bond between the steel and the concrete have been reported namely: splitting and pullout (Orangun et al., 1977; Eligehausen et al., 1983; FIP, 2000; ACI 408R, 2003) as shown in Figure 2.4. The pullout failure happens when the confinement of the steel bar, which is controlled by the amount of concrete cover, the concrete compressive strength, and the constraint by stirrups or FRP wrapping, is high. This failure occurs by a shearing off of the steel bar ribs from the surrounding concrete (ACI 408R, 2003). On the other hand, the splitting failure takes place when the concrete cover is small and the confinement of the steel bar is insufficient and; hence, splitting cracks develop at the steel bar ribs (ACI 408R, 2003). The splitting cracks are parallel to the steel bar at the thinner of the side or bottom concrete covers or the half of the spacing between the steel bars (ACI 408.2R, 2012). A bond pullout failure is preferable to a splitting failure because a pullout failure is gradual in nature and provides a warning of failure in the form of an increase in deflection before full failure occurs while a splitting failure occurs suddenly. .

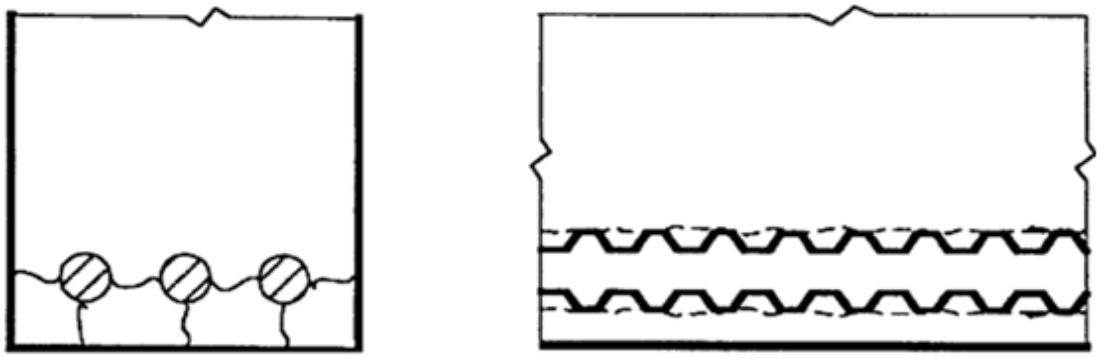

(a) Splitting Failure (b) Pullout Failure

Figure 2.4 Bond failure type (ACI 408R, 2003)

2.1.2 Factors Affecting Bond Behaviour

There are many factors affecting the bond strength of reinforced concrete beams, such as the concrete compressive strength, the concrete cover, the steel bar size, the steel bar anchorage / splice length, the amount of the transverse reinforcement, the yield strength of the steel bar, the casting position of the steel bars, the type and rating of the loading and the steel surface condition and coatings. Some of these factors are discussed below.

2.1.2.1 Concrete Compressive Strength (f'_c)

The concrete shear strength depends on the tensile strength of the concrete, and the tensile strength of the concrete is proportional to the square root of the comprehensive strength of concrete$\sqrt{f'_c}$. Therefore, the bond strength of concrete has a strong relationship with the square root of the comprehensive strength of concrete, especially for ordinary concrete ($f'_c < 55\ MPa$) (ACI 408R, 2003; ACI 408.2R, 2012; Carino and Lew, 1982; Tepfers 1973; Orangun et al., 1977). Force transfer takes place between concrete and steel by bearing and friction, and the failure can occur in the concrete by tensile splitting or shear. Therefore, the concrete compressive strength becomes a key parameter of bond behaviour (Orangun et al., 1977). Generally, an increase in concrete compressive strength will lead to an increase in the bond strength but with slower rate than the increase in concrete compressive strength and the failure becomes more brittle (Azizinamini et al., 1999; Alavi-Fard and Marzouk, 2002; ACI 408R, 2003; El-Azab and Mohamed, 2014).

2.1.2.2 Concrete Cover

The concrete cover is the clear distance from a steel reinforcing bar to an external surface of a beam and the half distance between steel bars. The smaller of the side or bottom concrete cover thicknesses or the spacing between the bars governs the splitting failure for a given lap splice length and confinement level. The mode of failure for the lap splice has been found to be strongly affected by the thickness of the concrete cover (Tepfers 1973; Orangun et al. 1977; Darwin et al. 1996a; ACI 408R, 2003 and ACI 408.2R, 2012). For a lap splice without stirrups or FRP confinement, the thickness of the concrete cover and the concrete tensile strength govern the splitting bond strength capacity (ACI 408R.2003). Increasing the thickness of the concrete cover leads to an increase in the force transfer between the concrete and the steel bar resulting in a higher bond strength. The relationship between the concrete cover and the bond strength is not linear, because the distribution of the tensile strength of the concrete surrounding the lap splice is not constant (Canbay and Frosch 2005). The effectiveness of the concrete cover decreases as the concrete cover increases.

2.1.2.3 Bar Size

For the same development length, a small bar develops a greater bond stress than a large bar (ACI 408.2R, 2012). Therefore, in order to develop the same bond stress in bars of two different sizes within the development length, a longer development length is required for the larger bar. Using many small bars instead of few large bars is always recommended to improve bond performance when an adequate clear distance between the bars is maintained.

2.1.2.4 Anchorage/Splice Length

The increase in the bond force at failure under the influence of a monotonic loading is not proportional to an increase in the anchorage length as long as the minimum required development length is provided. An increase in the anchorage length will result in a decrease in the maximum bond stress (ACI 408.2R, 2012). An increase in the anchorage length however, will result in an increase of the number of cycles to cause a pullout failure under cyclic loading (ACI 408.2R, 2012; MacKay et al., 1989).

2.1.2.5 Transverse Reinforcement

An additional confinement force is provided through steel stirrups transverse reinforcement, which limits the growth of splitting cracks and increases the bond strength and the ductility of a splice (ACI 408R, 2003). Therefore, the required splice length depends on the confinement provided by the transverse reinforcement. The amount and the distribution of the transverse reinforcement will determine whether a splitting tensile failure occurs. The concrete after cracking will be confined if the transverse reinforcement is properly detailed. Under the cyclic loads, the resistance to splitting failure is significantly increased by transverse reinforcement (ACI 408.2R, 2012; Tepfers, 1973; Tepfers, 1980; Tepfers, 1988; Sparling and Rezansoff, 1986).

2.1.2.6 Type and Rate of Loading

The bond strength under monotonic loading is greater than that under fatigue loading. The fatigue loading results in a deterioration of the bond strength represented by an increased number of cracks, increased crack widths and an increase in the deflection. Rehm and Eligehausen 1979 studied the effect of the type of loading on bond performance. They concluded that, fatigue loading (reversed or uni-direction) caused more deterioration of bond than monotonic loading. Shah and Chung 1986 studied the effect of loading rate on the bond strength and concluded that a slow loading rate resulted in a lower bond strength and more deterioration of the bond along the anchorage length compared to a faster loading rate.

2.1.3 Bond Test Specimens

2.1.3.1 Beam-End Specimen

Based on the ASTM standard, a half of the beam specimen is used in this test, which represents a simplified version of the RILEM test, as shown in Figure 2.5. A tension force is applied directly to the reinforcing bar by the test frame. Tension is created in the concrete around the bar while moment and shear forces are developed by the bearing points on the sample to create a reaction force similar to that developed at the end of a full reinforced concrete beam.

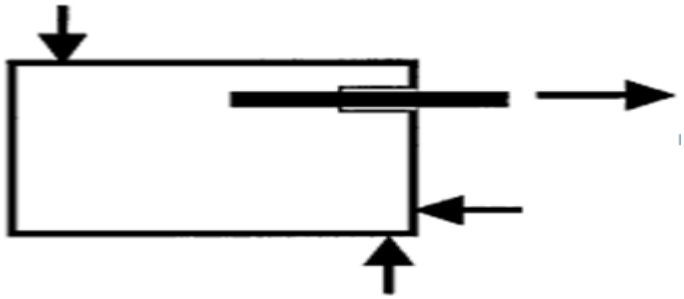

Figure 2.5 Beam-End specimens (ACI 408R, 2003)

2.1.3.2 Beam Anchorage Specimen

The flexural beams can be used to integrate the contributions of the components found in real beams into bond tests. The free end slip can be monitored by extending a reinforcing bar beyond the ends of the beams in the case of standard beams. In addition, pockets may be incorporated outside the bond area to allow internal slip and tensile stress in the steel to be measured. Plastic sleeves can be used to de-bond the reinforcing bar outside the constant moment region to control the bond length of the bar. The test is further simplified by using standard simply supported test beams as shown in Figure 2.6.

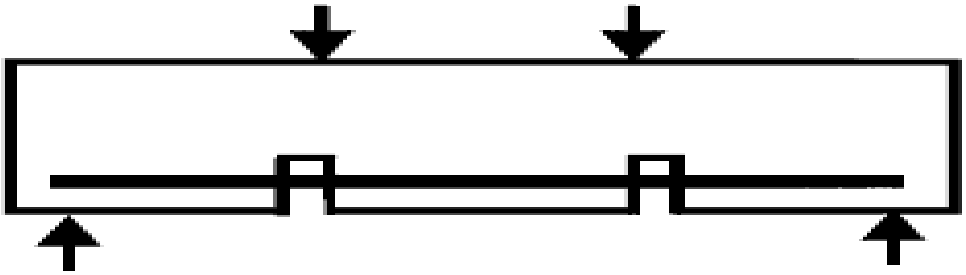

Figure 2.6 Beam anchorage specimens (ACI 408R, 2003)

2.1.3.3 Lap Splice Beam Specimen

Large scale beam specimens are used as lap splice specimens to measure the bond between lap-splice bars as shown in Figure 2.7. The lap splice is placed in a central constant moment region. This makes the fabrication rather convenient, and produces similar bond strength values to those obtained using a beam anchorage specimen. Realistic measures of the bond strength in an actual structure are obtained from the beam anchorage specimen and the splice beam specimen.

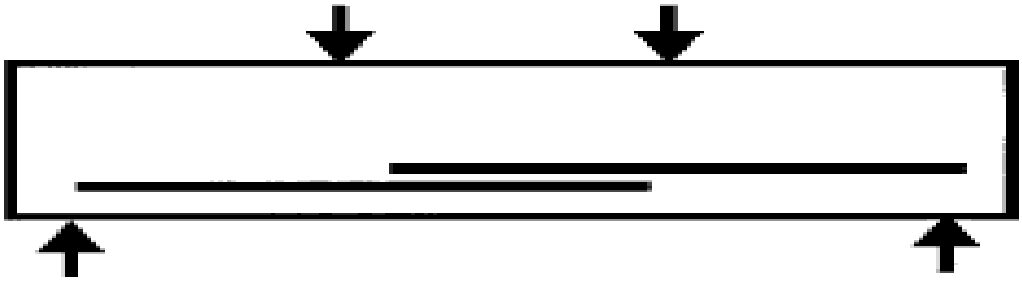

Figure 2.7 Splice beam specimen (ACI 408R, 2003)

2.2 Fiber Reinforced Polymers (FRP)

Fiber Reinforced Polymers (FRP) are composite materials that consist of fibres and a matrix as shown in Figure 2.8. There are four types of FRP material commonly used civil engineering applications namely: Carbon Fiber Reinforced Polymers (CFRP), Glass Fiber Reinforced Polymers (GFRP), Aramid Fiber Reinforced Polymers (AFRP) and Basalt Fiber Reinforced Polymers (BFRP). The strength of the FRP depends on the type and the volume of the FRP. These FRP's have higher strengths than the conventional reinforced steel and their stress strain relation is linear until failure as shown in Figure 2.9. FRP sheets have good mechanical properties such as a high strength to weight ratio, good durability, a high fatigue strength and corrosion free (ACI 440, 2008). They can easily be bonded to external surfaces of reinforced concrete as a strengthening and/or repair measure to increase the service life of damaged or deficient concrete members such as slabs, beams and columns.

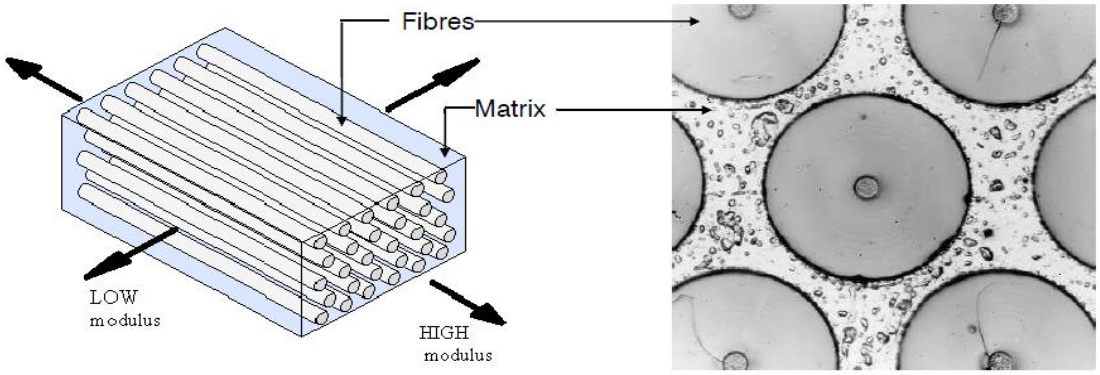

Figure 2.8 Components of FRP (Badawi, 2007)

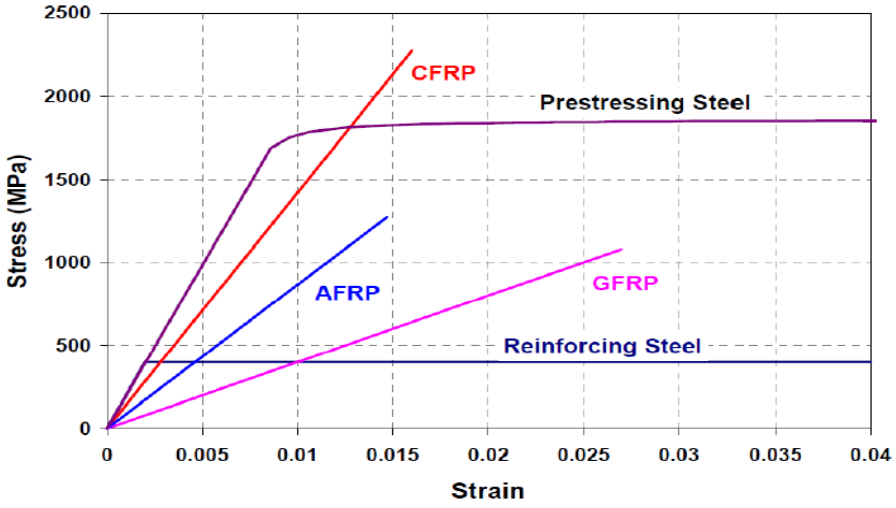

Figure 2.9 Stress-strain behaviour of steel reinforcement and FRP (ISIS Canada, 2008)

2.2.1 Fibres

The strength of FRP sheets use to carry the tensile forces in reinforced concrete structures depends on three factors: the type of the FRP (CFRP, GFRP, AFRP and BFRP), the volume of the FRP and the orientation of the FRP fibres.

2.2.1.1 Carbon Fibres

Excellent properties are demonstrated by the carbon fibre reinforced polymer (CFRP) composites, that have an excellent tensile strength, good corrosion resistance, a high fatigue strength, a low coefficient of thermal expansion and a high strength to weight ratio. However, they are expensive compared with other FRP products.

2.2.1.2 Glass Fibres

Glass fibre reinforced polymer (GFRP) materials have a high tensile strength compared to reinforced steel bars, a satisfactory heat resistance and a low electrical conductivity and a relatively low production cost compared to CFRP composites. However, GFRP composites have a lower stiffness and a lower specific strength than CFRP composites.

2.2.2 Matrix

A matrix is used to hold and bind the fibres in FRP together. A resin matrix is used to transfer stress to the fibres from the concrete and to protect the fibres against

environmental attack and damage due to handling. Epoxies, vinyl esters and polyesters are the commonly used resin types. The suitability of a resin is dependent on its ease of application, compatibility with the fibres, and ability to bind with the substrate (ACI 440, 2008). It is very important that the maximum strain of the resin be higher than that of the fiber so that it remains uncracked under load and protects the fiber from mechanical damage and environmental attack. Figure 2.10 shows the tensile stress-strain relationships of the FRP components.

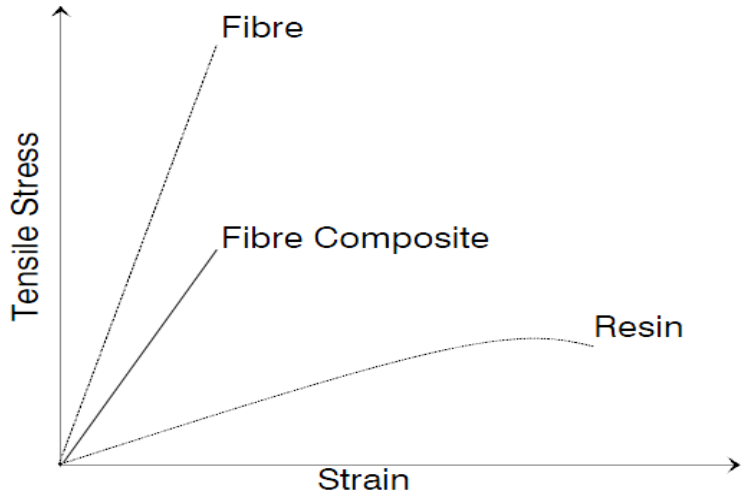

Figure 2.10 Tensile stress-strain relationship of the FRP components (ACI 440R, 1996)

2.3 Use of FRP for Repair and Strengthening

Nowadays, the service loads applied to infrastructure are increasing and this trend is expect to continue. The continuous updating of bond and fatigue requirements has resulted in existing structures having inadequate strengths to meet current code requirements. There are many reasons to strengthen existing structural members such as deficiencies in the design or construction of the structure members and changes in the use of structure members not taken account of in their original design. Badawi 2007 illustrated the strengthening necessity of a reinforced concrete member as shown in Figure 2.11.

FRP materials have been used for repair and strengthen concrete structures to increase their flexural, shear and bond strength. They are used both internally and externally. Their internal applications are in common new concrete construction and their external applications are in existing concrete structures to provide additional strength and to repair any damage. Flexural strength is increased by wrapping the FRP sheets

around beams to confine the concrete and increase the shear and bond capacity. Damage due to corrosion and repeated loading can be reduced by wrapping the sheets around RC columns and beams. The strength and ductility of the columns and the beams is also increased by wrapping with these sheets. Design rules and specifications are provided by the ACI code and ISIS Canada for strengthening using FRP (ACI 440, 2008; ISIS 2008).

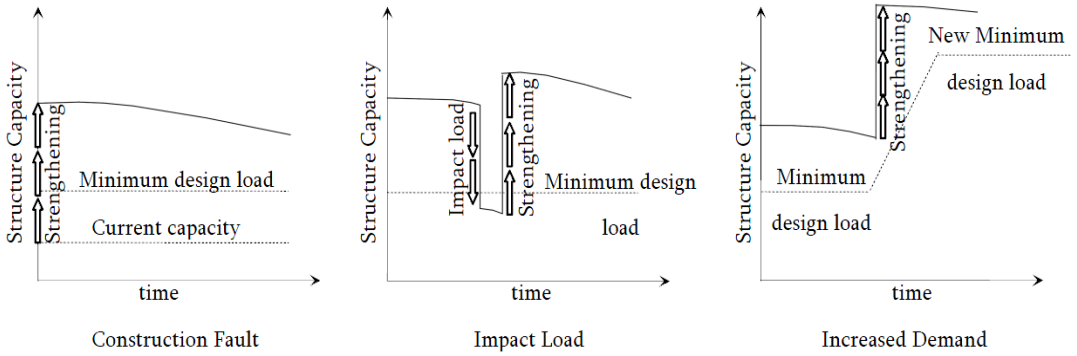

Figure 2.11 Necessity of concrete structure strengthening (Badawi, 2007)

2.4 Effect of Confinement on the Bond Behaviour in Reinforced Concrete Beams Containing a Lap splice

2.4.1 Effect of Stirrups

Garcia et al. (2013) reported that transverse reinforcement by stirrups resulted in a delay in the propagation of splitting cracks for various concrete covers ranging from 14 mm to 30 mm. Also, a significant increase in the maximum load and deflection was observed in beams with stirrups compared to unconfined beams. Transverse reinforcement confined the splice bars and delayed the spalling of the concrete cover. Seliem et al. (2009) observed that beams with stirrups exhibited a gradual bond failure rather than the abrupt failure of beams without stirrups. The amount and distribution of the transverse reinforcement and the constraint it provides were found to play a role in changing the mode of failure from bond splitting to a pullout failure (Orangun et al., 1977; Tepfers 1973; Pacholka et al., 1999; Sakurada et al., 1993; Lukose et al., 1982; Rezansoff et al., 1992). They found that transverse reinforcement confined the concrete cover after cracks initiated and increased the resistance to splitting failure. Tocci (1981) studied the effect of the amount of the transverse reinforcement along a lap splice under fatigue loading, and concluded that stirrups delayed the propagation

of cracks; however, they did not prevent a splitting failure. At a given stress level, beams with a clear concrete cover of 65 mm that contained transverse reinforcement had a longer fatigue life than similar beams without transverse reinforcement (Tocci 1981). Increasing the amount of the transverse reinforcement can lead to a change in the mode of failure from bond failure to fatigue failure of the main reinforcement (Rezansoff et al., 1993). Studies conducted at Cornell University by Hungspreug (1981) and Fagundo et al. (1979) concluded that the concrete confinement along the splices at high intensity loads deteriorated rapidly and that a heavy transverse confinement along a lap splice was required to maintain the bond strength when concrete deteriorates.

Similarly, when internal transverse reinforcement along a lap splice under unidirectional fatigue loading was studied a heavy transverse reinforcement changed the failure mode from a bond failure to a fatigue failure of the main reinforcement (Rezansoff et al. 1993). Increasing the number of stirrups along a lap splice under fatigue loading resulted in an increase in the fatigue life at a given stress level compared to that for a lap splice with fewer stirrups.

2.4.2 Effect of the Thickness of the Concrete Cover on the Bond Strength

In beams without stirrups, the smallest of the two covers or half spacing between the steel bars is assumed to control the lap-splice strength for a given development length of the splice. This is because the magnitude of the confinement forces that are generated by the concrete around the bars increases with cover thickness. The relationship between the thickness of the concrete cover and the bond strength, b_s, is nonlinear and can be expressed by the ratio of the square root of the concrete cover c to bar diameter d_c, $b_s = \sqrt{c/d_c}$ (Canbay and Frosch, 2005). The concrete cover and the bar spacing determine the type of bond failure observed under monotonic loading in laboratory tests (Untrauer, 1965; Tepfers, 1973; Orangun et al., 1977; Eligehausen, 1979; Darwin et al., 1996). The efficiency of the concrete cover decreases as the concrete cover increases (Canbay and Frosch, 2005). When the concrete cover or the bar spacing is small, a splitting tensile failure takes place at short anchorage lengths as shown in Figure 2.4a. However, for a large concrete cover, it is possible for a pullout failure to occur as shown in Figure 2.4b. A pullout failure can happen in the presence

of some splitting cracks if the bonded length of the steel bar has a high level of confinement due to stirrups or an FRP sheet. A splitting bond failure results in lower bond strength than a pullout bond failure (ACI 408R, 2003). The effect of the concrete cover is more pronounced under cyclic loading conditions than for monotonic loading. It was reported that repeated loads lead to an increase in the crack propagation rate (ACI 408.2R, 2012). Also, the concrete cover has an effect on the bond-slip curve. As the concrete cover and the bar spacing increase, the bend in the bond-slip curve becomes sharp (ACI 408.2R, 2012).The confinement effect produced by using FRP wrapping is expected to decrease with an increasing concrete cover because the confinement stresses in the concrete adjacent to the steel bars will be reduced as the cover thickness increases.

2.4.3 Effect of the FRP Wrapping on the Bond Strength

Many researchers have studied the effect of external confinement (FRP sheets) on the bond strength of splices under monotonic loading. Garcia et al. (2013) concluded that beams wrapped with CFRP sheet experienced narrower splitting cracks than unwrapped beams and had a greater bond strength and bar slip compared to unwrapped beams. Also, they observed that the CFRP sheet served to confine the concrete cover and delayed the propagation of splitting cracks. They attributed this behaviour to an increase in the force transferred between the concrete cover and the lap splice bars.

Hamad et al. (2004) studied the effect of FRP sheets on lap splice bond strength using a 20 mm clear concrete cover under monotonic load. The investigated test variables were the presence or absence of GFRP wrapping sheets, the configuration of the GFRP wrap (one wrap, two wraps or a continuous strip) and the number of GFRP layers. They concluded that wrapping with GFRP sheets increased the bond strength and the deflection without changing the failure mode and as the amount of GFRP sheets increased in area and in thickness, the bond strength and the deflection of a beam increased. Soudki and Sherwood (2000), (2003), and Shihata (2011) studied the effect of wrapping with CFRP sheets on the bond strength of a corroded lap splice under monotonic loading. The test variables were the percentage of corrosion of the steel bar and the clear concrete cover 30 mm or 40 mm. The result showed that the

CFRP sheets increased the bond strength and the deflection. The failure mode was not affected by the CFRP wrapping.

Bousias et al. (2007) came to the conclusion that the number of FRP layers was not proportional to the bond resistance capacity. Bournas and Triantafillou (2011) concluded that the bond strength between lap-spliced bars and the surrounding concrete could be improved by the use of a FRP sheet wrapping that delayed the appearance of longitudinal cracks.

Hamad et al., (2004a), (2004b), (2004c) and Rteil, (2002) studied the effect on bond strength of FRP wrapping sheets applied along the lap splice under monotonic loading. The test variables were the type of the FRP sheets (CFRP or GFRP), the concrete compressive strength (28 MPa or 70 MPa), the configuration of the FRP along the lap splice (strip width and the spacing between the strips) and the number of the FRP layers. It was concluded that the FRP wrapping sheets improved the bond strength of the lap splice and that the improvement varied from 8% to 34% compared to the unwrapped beams The FRP sheets led to more ductal failure compared to the unwrapped beams. Based on their results, they proposed an equation to calculate the effect of the FRP sheets on the bond strength as shown below:

$$K_{tr\prime f} = \frac{C_1 * A_{tr,f} * f_{fe}}{s_f * d_b * n_b} \leq 0.25 ,$$

$K_{tr',f}$ = equivalent to the normalized bond strength contribution of the FRP sheet, C_1 = proportionality constant= $\frac{1}{16.6}$, $A_{tr,f}$ = total cross sectional area of FRP (mm^2), f_{fe} = the effective stress in the FRP laminate (MPa), s_f = width of FRP sheets (mm), d_b = diameter of steel rebar (mm) and n_b = the number of spliced bars.

Under fatigue loading, the FRP wrapping increased the fatigue bond strength and the deflection of reinforcing concrete beam compared to unwrapped beams (Alyousef et al., 2015; Alyousef et al., 2016a; Alyousef et al., 2016b; Alyousef et al., 2016c (accepted); Rteil et al., 2007; Rteil, 2007). For the same area of material, the use of external FRP confinement is more efficient and effective than stirrups in controlling splitting cracks (Hamad et al., 2004; Hamad et al., 2004; Hamad and Rteil 2006; Tarabia et al., 2010).

2.4.3.1 FRP Confinement Mechanism

FRP wrapping sheets have been used to increase the bond strength between a steel bar and the surrounding concrete in reinforced concrete structures. The FRP sheets wrapping increases the confinement and the transfer of stress between the concrete and the steel over the bonded region which increases the load carrying capacity and the ductility of a structure. For a column, the confinement is more efficient for a circular section than for square or rectangular sections where the confining stress is transmitted to the concrete surface at four corners (Parvin and Brighton. 2014). Confinement efficiency can be improved for square and rectangular sections by increasing the corner radius (Bakis et al., 2002).

For the beam, the forces due to the FRP wrapping sheets resist the splitting forces due to shear in the spliced bars. As the distance between the wrapping sheets and the spliced bars increases with increased cover thickness the bars become more remote from the wrapping and the confining stresses decrease.

2.5 Fatigue Load

For many years, it has been known that the steel reinforcing bars fail by bar rupture under repeated load at a significantly lower stress than that under a single monotonic load. In addition, fatigue failure occurs suddenly without any warring by rupture of the steel bar (ACI 215R-1974). This fatigue failure of the steel bar is characterized by a fracture surface that shows two regions: a rough surface and smooth surface as shown in Figure 2.12. The smooth surface occurs on the side closest to the maximum tension zone. This smooth surface is due to the rubbing of the crack faces during cracks growth (ACI 215R-1974). As the cross section of the steel bar decreases, the steel bar is no longer able to carry the applied stress leading to a ductile failure which causes the rough surface.

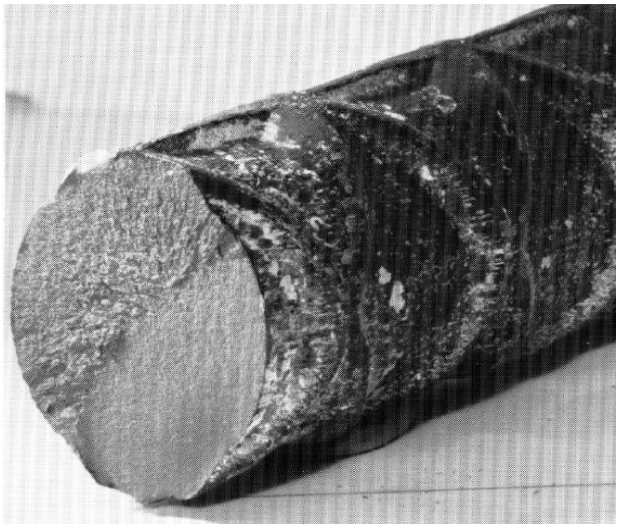

Figure 2.12 Fatigue failure of the reinforced steel bar (ACI 215R, 1974)

Badawi 2007 illustrated graphically a stress versus time graph for a fatigue test together with the definitions of important terms used in the analysis of the fatigue data as shown in Figure 2.13. The figure defines the minimum, the maximum and the mean stress. The fatigue data are usually presented as an S-N plot. The S-N plot plots the fatigue life (number of cycle) versus stress range on logarithm scales as shown in Figure 2.14. The reinforced steel bar has a fatigue limit (endurance limit) at which the stress versus fatigue life curve becomes flat as shown on Figure 2.14. The fatigue limit is sometimes defined as the maximum stress can be applied to a material without causing a fatigue failure. The fatigue limit for a steel reinforcing bar various from 35% to 60% of yield stress (ACI 215R-1974).

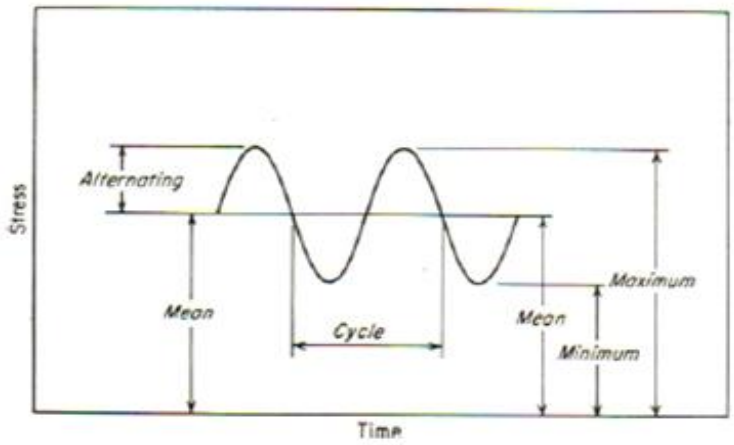

Figure 2.13 Fatigue term used in analysis (Badawi, 2007)

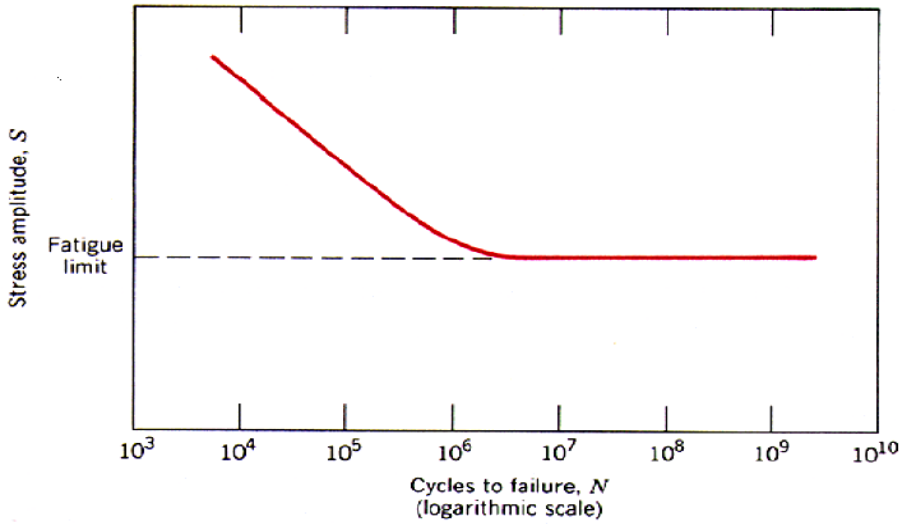

Figure 2.14 S-N curve (Badawi, 2007)

2.5.1 Steel

The factors affecting the fatigue failure of the steel reinforcement of beams under fatigue loading are: the geometry of the steel bar, the size of the steel bar, the applied stress range, the mean stress applied and the yield strength of the bar (Soretz 1974; Tepfers 1973; Rezansoff 1978; Rezansoff et al. 1988; ACI 215R, 1974; Tilly and Tan, 1979; Rabbat and Corley, 1984; Zacaruk 1990). Stress concentrations due to changes in the bars geometry like ribs lead to the initiation of cracks in the steel rebar. Cyclic loading propagates these cracks to cause fatigue failure of the reinforcing steel rebar.

The size of the diameter of the reinforcing steel bar affects the fatigue life. At a given stress, the fatigue life decreases as the diameter of the steel bar increases. This phenomenon is partly due to the increase in probability of having a large flaw in the larger volume of a larger diameter bar Mallet 1991; Bannantine et al., 1990; ACI 215R, 1974).

The following equation was developed by ACI 215 (1974) for the limit of the flexural stress within a reinforcing steel bar that allows a designer to assume an infinite fatigue life for the reinforcing steel rebar :

$$S_r = 161 - 0.33 * S_{min} \quad (MPa)$$

S_r= Stress range in reinforced steel bar (MPa)

S_{min}= Minimum applied stress in the reinforced bar (MPa)

Helgason and Hanson (1974) who studied the fatigue failure of reinforcing steel rebar provided the following equation to estimate the fatigue failure limit for a reinforcing bar:

$$log_{10}N = 6.696 - 0.0055f_r \qquad (MPa)$$

N= Fatigue failure limit

f_r= Applied stress range in a steel rebar (MPa)

Tilly and Tan, 1979 studied the effect of mean stress on the fatigue strength of a steel reinforcing bar and concluded that as the applied mean stress decreases the fatigue life of the reinforcing steel bar increases as shown in Figure 2.15.

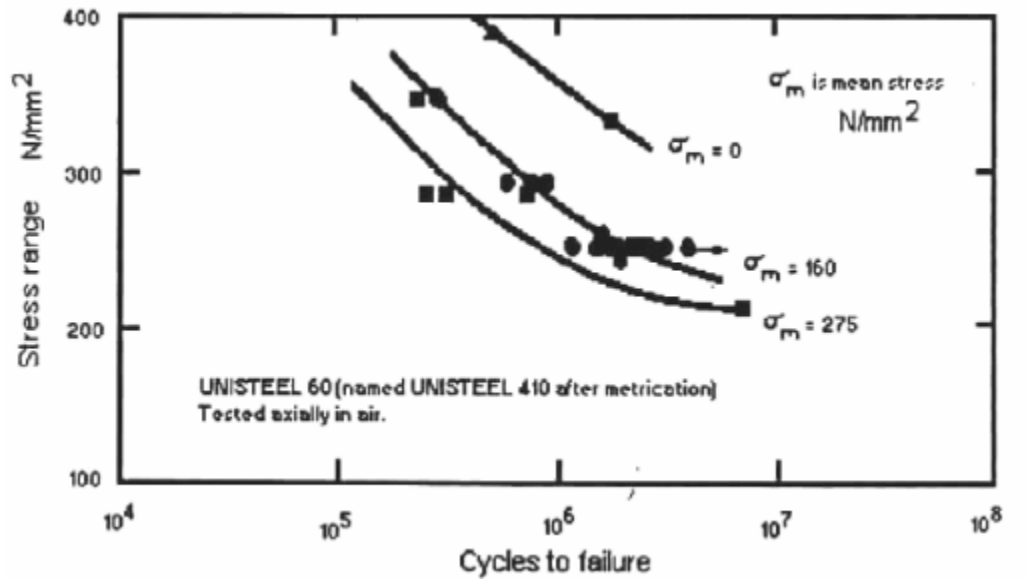

Figure 2.15 Effect of mean stress on the fatigue life of the steel (Tilly and Tan, 1979)

2.5.2 Effect of Repeated Load on Bond Behaviour

When the tensile stress exceeds the tensile strength of the concrete under repeated loading, splitting cracks occur and propagate as loading continues until a bond failure occurs. The propagation of splitting cracks deteriorates the bond and leads to a cyclic failure at a bond stress level below the ultimate stress level under static load. Perry and Jundi (1969) studied bond behaviour under fatigue loading focusing on the shear stress distribution, using a pullout specimen test. It was concluded that the peak bond stress initially occurred at the loaded end and then moved toward to the unloaded end as the number of cycles increased. The reduction of the limiting bond stress at the

loaded end due to fatigue loading varied from 65% to 90%. Plizzari et al. (2002) studied the effect of stirrup transverse reinforcement confinement on bond behaviour under repeated load using a pullout specimen test. They reported that increased confinement due to adding transverse reinforcement led to an increased bond fatigue strength, a decreased slip rate and a reduction in the number of splitting cracks.

Under a fatigue loading, the deterioration of bond is not related to the peak stress, but to the peak slip of the reinforcement (Balazs and Koch, 1992). Fatigue loading leads to an increase in the slip between the reinforcing bar and the concrete. The slip rate under repeated loading is dependent on the load level, the frequency of loading, the strength of the concrete and the amount of confinement. Bond failure under fatigue loading may occur by pullout of the bar or by splitting of the concrete cover.

2.5.3 FRP Wrapping Confinement

Fiber reinforced polymer wrapping sheets have been used for strengthening the bond of corroded bars under fatigue loading (Rteil et al. 2007, Rteil 2007 and Al-Hammoud, 2012.). The parameters of their studies were corrosion level, bonded length, concrete cover, type of loading and the applied load range. It was concluded that, the FRP wrapping sheets increased the fatigue strength of both corroded and non-corroded reinforced concrete beams compared to unwrapped beams. Also, for some beams, the FRP wrapping sheets increased the bond strength enough to change the mode of failure from bond failure between the steel and the concrete to a bar rupture failure. The failure modes observed included bond failure, bar rupture and FRP failure (by rupture or delamination) as shown in Figure 2.16.

a) Rupture of CFRP sheets b) Concrete splitting cracks

Figure 2.16 Mode of failure for strengthened beam (Rteil 2017)

2.6 Slip between Steel Bars and Concrete

Fatigue loading leads to an increase in the slip between the reinforcing bar and the concrete with the number of load cycles. This increase in the slip of the steel bar results in a deterioration of the bond strength (FIB, 2000). It is interesting to note that, under a fatigue loading, the main effect of bond deterioration is not related to the peak stress, but to the peak slip of the reinforcement (Balazs, 1991). The slip rate under repeated load is dependent on the load level, the strength of the concrete and the amount of confinement (ACI 408.2R, 2012). Harajli et al. (2002, 2004) and Harajli (2009, 2006) studied the effect of FRP wrapping on the bond stress-slip behaviour of a splitting bond failure under monotonic load. It was reported that there are four stages of slip before failure as shown in **Error! Reference source not found.**. In the irst stage, the stiffness of the bond stress versus slip relationship is similar to that for a pullout failure. The bond resistance in this first stage is attributed to the chemical adhesion and friction between the bar and the concrete and lasts until tensile cracks develop in the concrete. The second stage begins as the tensile cracks develop and is characterized by a bond stress versus slip curve that is lower than that for a pullout failure and continues until the cracks propagate to the surface. Then a third stage begins which is characterized by a sudden and rapid drop in the bond stress and is usually considered to be a bond failure. Finally, there is a fourth stage characterized by a continuing decrease in bond stress and an increase in slip.

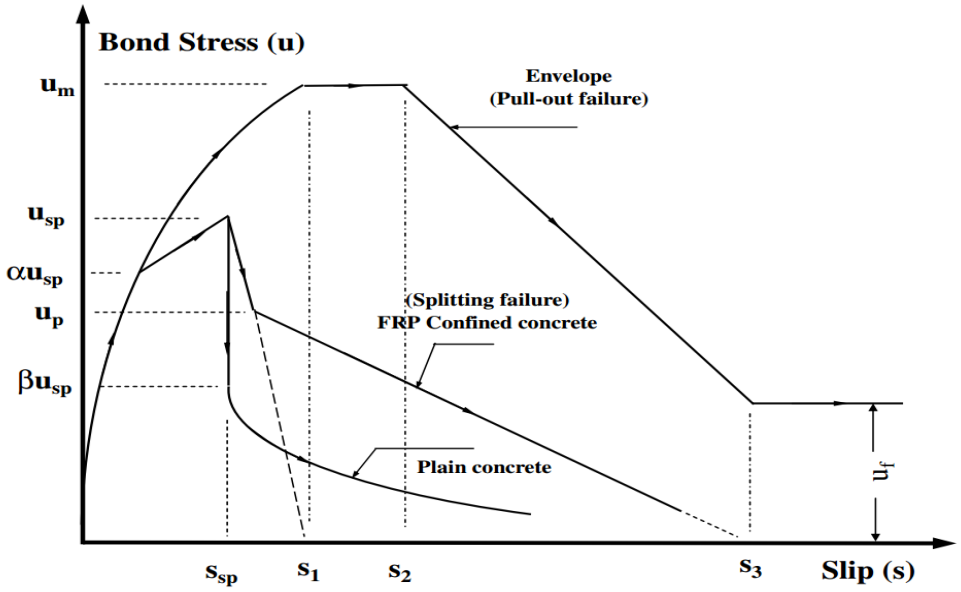

Figure 2.17 Monotonic envelopes of local bond stress–slip models

Chapter 3 Experimental Program

3.1 Introduction

The experimental program of this research consisted of three phases using three different concrete clear covers. A total of fifty three beams were constructed and tested under monotonic and fatigue loading. The beams were divided into three groups with different concrete covers. The dimensions of each beam were 250 mm wide, 350 mm high and 2200 mm long. The test specimens were designed to fail in bond rather than in flexure. Three beams from each group were tested under monotonic loading while the rest of beams were tested under fatigue loading. The primary objective of this study is to investigate the effect of repeated loading on the bond between concrete and steel, and the ability of FRP sheets to enhance the fatigue performance of a tension lap splice. This chapter describes the test matrix, the design of the test specimen and its fabrication, the material properties, the formwork and concrete placement, the strengthening of the beams with FRP wrapping sheets, the instrumentation, and the test setup.

3.2 Test Matrix

The 53 beams were constructed and tested were divided into three groups as shown in Figure 3.2. The beams were divided into three groups that were Group 1 (20 mm concrete cover), Group 2 (30 mm concrete cover) and Group 3 (50 mm concrete cover). The first phase constructed and tested was Group 2 (17 beams), the second phase was Group 3 (19 beams) and the third phase Group 1 (17 beams). Nine beams were tested under monotonic loading and forty four beams were tested under fatigue loading. Fifteen beams were unwrapped, eighteen beams were wrapped with GFRP sheets and twenty beams were wrapped with CFRP sheets. Each series of each group had a specimen that was loaded monotonically to failure, while the other beams from each series of each group were subjected to fatigue loading. The test variables for each group were the presence or absence of FRP sheet wrapping, the type of FRP sheet wrapping (GFRP sheets or CFRP sheet), the loading type (monotonic or fatigue) and the fatigue load range.

The beam notation used was in the form of three parts: AA-BB-CC. The first part was represented the wrapping condition (UN, GFRP or CFRP), the second part was represented the group number (G1, G2 or G3) and the last part was represented the static load or fatigue load range (ST or fatigue load range) as shown in Figure 3.1.

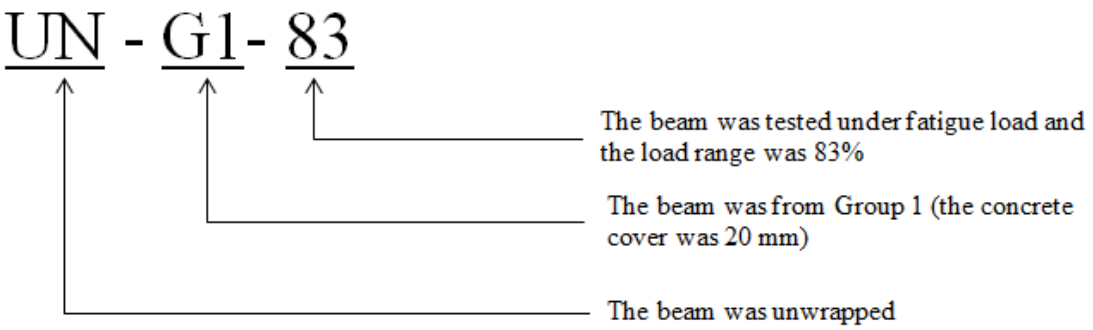

Figure 3.1 Beam notation

A minimum applied load of 10% of the ultimate monotonic failure load was used for all fatigue tests as shown in Table 3.1. This minimum load was applied to represent the dead load on the structure member and to prevent beam movement at the minimum load. The maximum load was varied to obtain fatigue lives between 1,000 and 1,000,000 cycles. After each beam was tested, the maximum applied load was increased or decreased for the following beam so that its estimated fatigue life lay between 1,000 and 1,000,000 cycles. After more than two test results were obtained, a linear log-log curve fitted to the previous data was used to choose subsequent load levels. A fatigue life of 1,000,000 cycles was taken as a runout fatigue life. Beams that had reached a million cycles without failure were tested again at a higher load level.

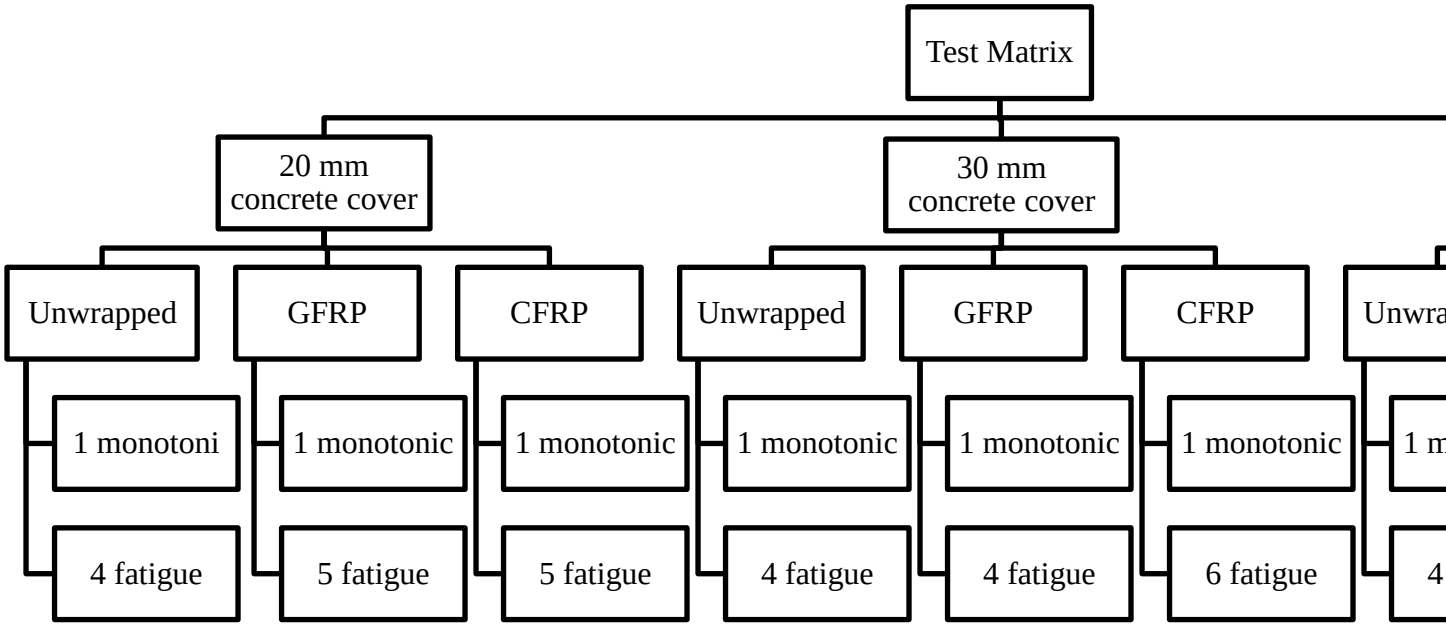

Figure 3.2 Test matrix

Table 3.1 Details of test matrix

Group	Wrapping	Beam notation	Loading	Minimum	Maximum
Group 1 (20 mm concrete cover)	Unwrapped	UN-G1-ST	Monotonic	-	-
		UN-G1-83	Fatigue	10	93
		UN-G1-78	Fatigue	10	88
		UN-G1-75	Fatigue	10	85
		UN-G1-65	Fatigue	10	75
		UN-G1-55	Fatigue	10	65
	GFRP wrapping	GFRP-G1-ST	Monotonic	-	-
		GFRP-G1-83	Fatigue	10	93
		GFRP-G1-78	Fatigue	10	88
		GFRP-G1-75	Fatigue	10	85
		GFRP-G1-65	Fatigue	10	75
		GFRP-G1-61	Fatigue	10	71
	CFRP wrapping	CFRP-G1-ST	Monotonic	-	-
		CFRP-G1-80	Fatigue	10	90
		CFRP-G1-73	Fatigue	10	83
		CFRP-G1-67	Fatigue	10	77
		CFRP-G1-65	Fatigue	10	75
		CFRP-G1-62	Fatigue	10	72
Group 2 (30 mm concrete cover)	Unwrapped	UN-G2-ST	Monotonic	-	-
		UN-G2-80	Fatigue	10	90
		UN-G2-70	Fatigue	10	80
		UN-G2-63	Fatigue	10	73
		UN-G2-59	Fatigue	10	69
		UN-G2-55	Fatigue	10	65
	GFRP wrapping	GFRP-G2-ST	Monotonic	-	-
		GFRP-G2-80	Fatigue	10	90
		GFRP-G2-75	Fatigue	10	85
		GFRP-G2-70	Fatigue	10	80
		GFRP-G2-63	Fatigue	10	73
		GFRP-G2-58	Fatigue	10	68

	CFRP wrapping	CFRP-G2-ST	Monotonic	-	-
		CFRP-G2-80	Fatigue	10	90
		CFRP-G2-76	Fatigue	10	86
		CFRP-G2-71	Fatigue	10	81
		CFRP-G2-69	Fatigue	10	79
		CFRP-G2-63	Fatigue	10	73
		CFRP-G2-59	Fatigue	10	69
Group 3 (50 mm concrete cover)	Unwrapped	UN-G3-ST	Monotonic	-	-
		UN-G3-85	Fatigue	10	95
		UN-G3-83	Fatigue	10	93
		UN-G3-75	Fatigue	10	85
		UN-G3-70	Fatigue	10	80
		UN-G3-63	Fatigue	10	73
	GFRP wrapping	GFRP-G3-ST	Monotonic	-	-
		GFRP-G3-82	Fatigue	10	92
		GFRP-G3-80	Fatigue	10	90
		GFRP-G3-73	Fatigue	10	83
		GFRP-G3-72	Fatigue	10	82
		GFRP-G3-67	Fatigue	10	77
		GFRP-G3-60	Fatigue	10	70
	CFRP wrapping	CFRP-G3-ST	Monotonic	-	-
		CFRP-G3-81	Fatigue	10	91
		CFRP-G3-76	Fatigue	10	86
		CFRP-G3-73	Fatigue	10	83
		CFRP-G3-66	Fatigue	10	76
		CFRP-G3-59	Fatigue	10	69
		CFRP-G3-53	Fatigue	10	63

3.3 Design of the Test Specimens

The beams cross section and reinforcing details were the same for all beams. The beam was 2200 mm long, 250 mm wide and 350 mm in height. Two symmetric applied loads provided a constant moment region at the mid span of the beam. The span between two supports was

1800 mm divided into three equal length regions, two shear span regions and a constant moment region containing the lap splice. The splice length was 300 mm to maintain the minimum length allowed by the ACI and the Canadian standards, and to ensure a bond failure before the steel yielding. Each beam was reinforced with two 20M steel rebars spliced at the mid span. The lab splice was placed in the constant moment region to study the effect of the FRP wrapping on the bond strength where the nominal stress is uniform and there is no shear stress. Two 10M deformed bars were used in the compression zone outside the constant moment region. This test beam was designed without internal transverse reinforcing stirrups within the constant moment region of the splice to allow a separation of the effect of confinement by the U-shaped FRP sheets on the bond strength from the effect of confinement by stirrups. The internal transverse reinforcement in the shear spans consisted of 10M stirrups distributed at 100 mm spacing. The ratio of the lap splice length to the steel bar diameter l_s/d_b was 15.

The clear side and bottom concrete covers were 20 mm, 30 mm and 50 mm for Group 1, Group 2 and Group 3, respectively. The ratios of the clear concrete cover to the steel bar diameter c/d_b were 1, 1.5 and 2.5 for Group 1, Group 2 and group 3, respectively. Figure 3.3 shows the dimensions and steel reinforcement details for all beams in Group 2 (30 mm concrete cover) and Group 3 (50 mm concrete cover). All beams in Group 1 (20 mm concrete cover) had steel bars that were de-bonded by Polyvinyl chloride (PVC) tube from the edge of the lap splice zone to the end of the beam as shown in Figure 3.4. These bars were used to measure the bond slip.

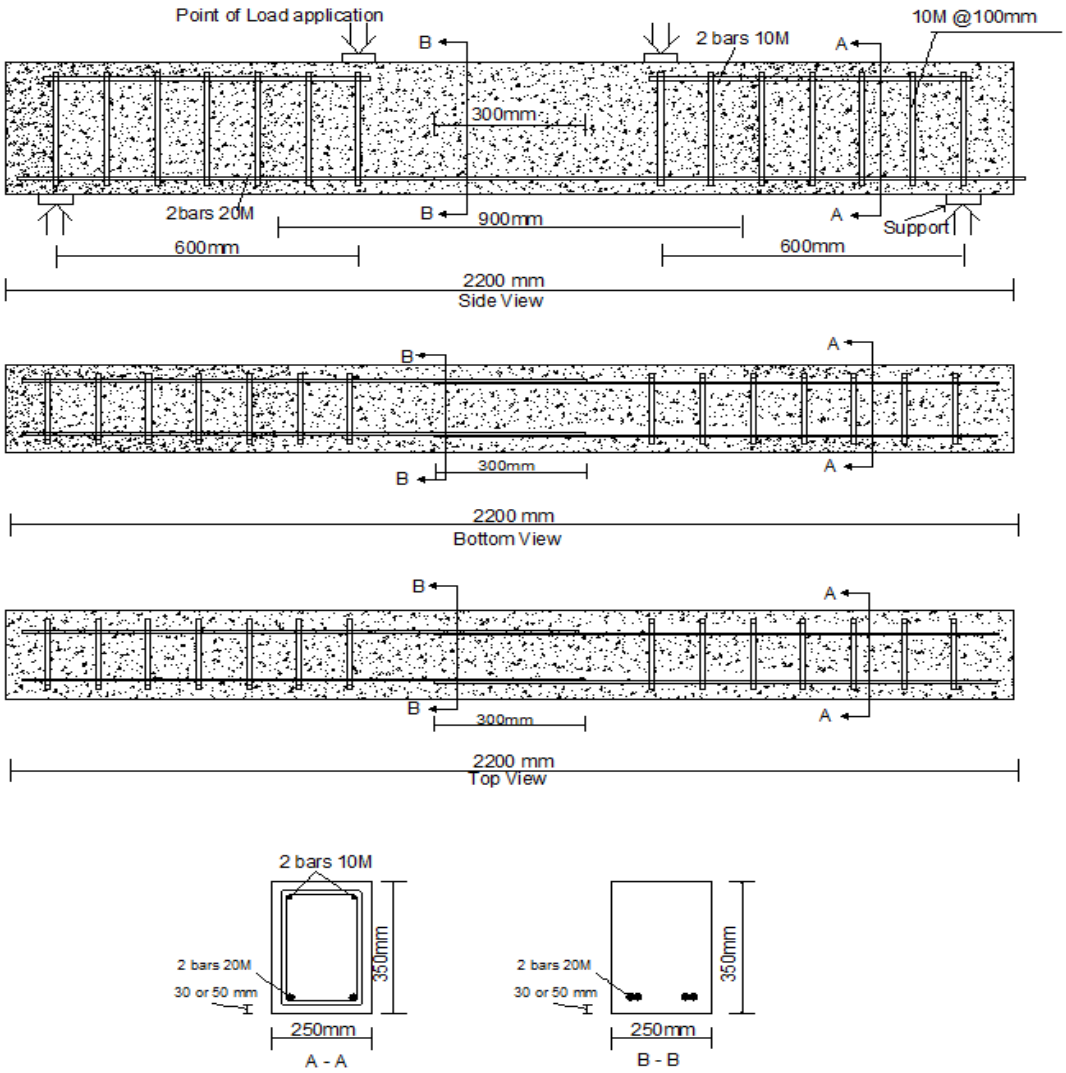

Figure 3.3 Beam cross-section and reinforcement layout along the span for Group 2 and Group 3

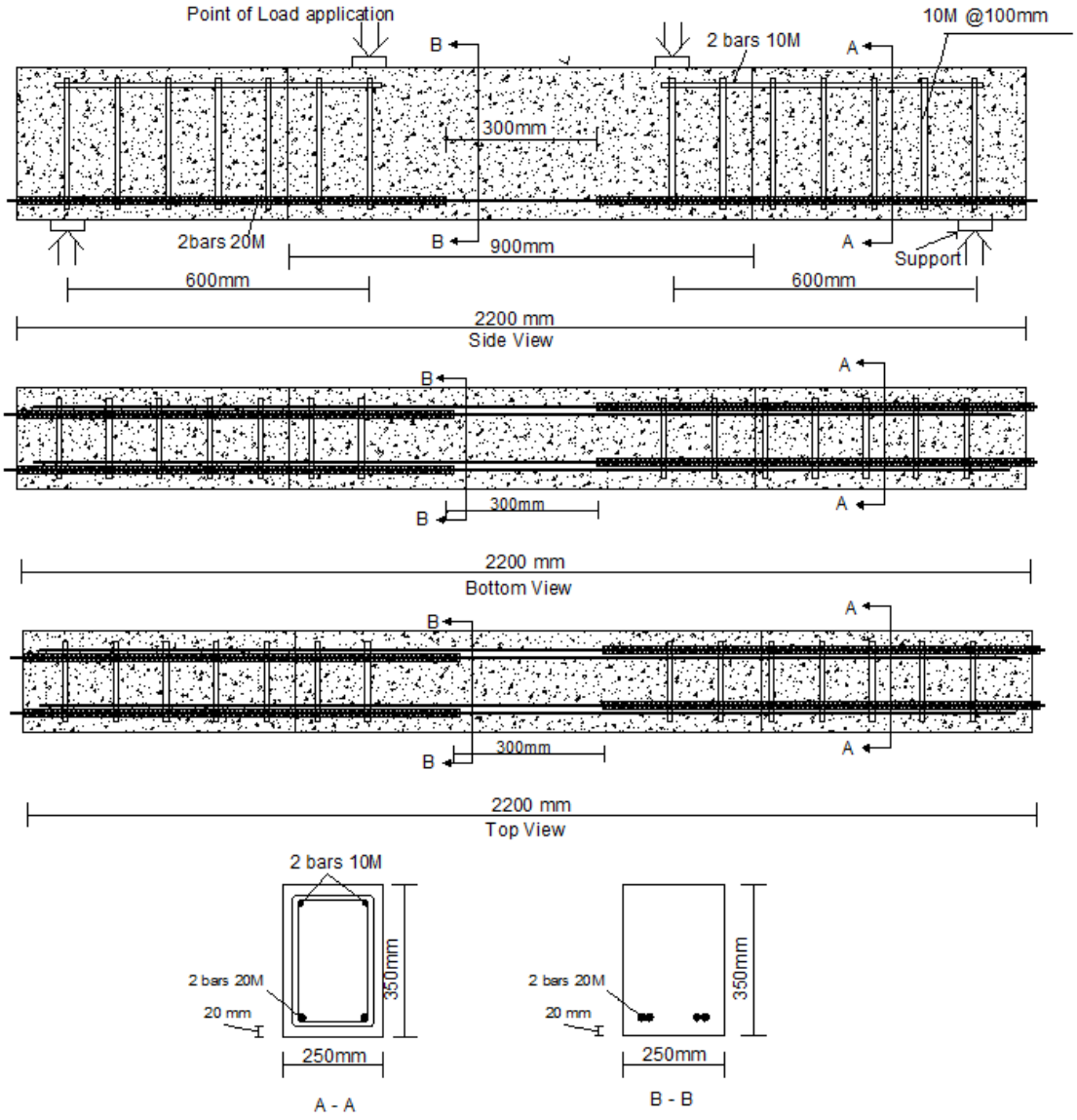

Figure 3.4 Beam cross-section and reinforcement layout along the span for Group 1

3.4 Specimen Fabrication

3.4.1 Formwork and Steel Cages

Sixteen forms were built to cast sixteen beams at the same time for each group to maintain a uiform concrete compressive strength for each group. The formwork consisted of a C channel on the bottom and plywood side sheets. The plywood side sheet dimensions were a 370 mm height a 20 mm width and a 2200 mm length. The C channel was 250 mm wide and 65 mm in height. For easy removal of the beams from the formwork after casting, the inside face of the formwork was coated with oil. Figure 3.5 shows the details of the formwork and Figure 3.6 shows the formwork and the cage inside it.

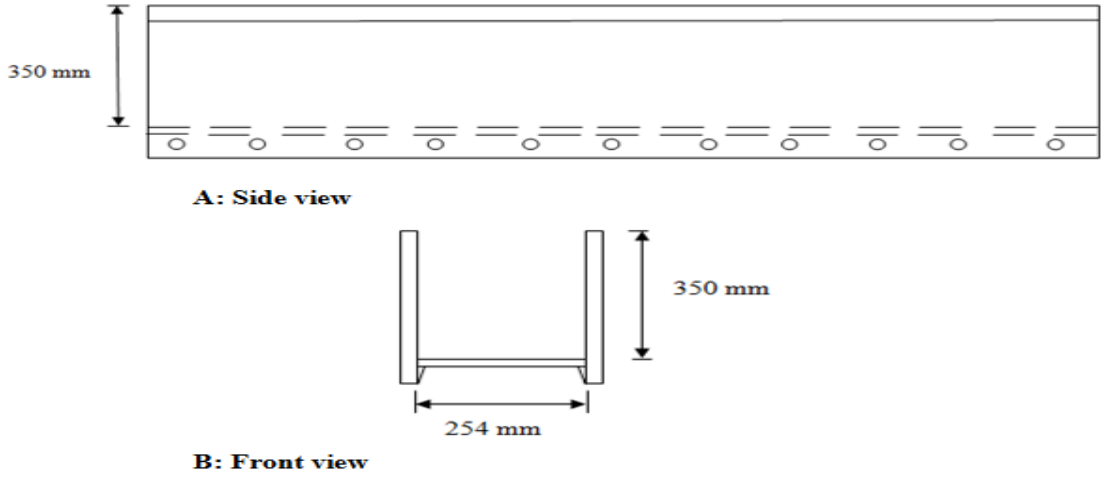

Figure 3.5 Details of the formwork

Figure 3.6 Cage inside formwork

3.4.2 Concrete Placement and Curing

Four cubic meters of ready mix concrete was supplied from a local ready mix plant for each group. Vibration with a hand held vibrator was used for concrete compaction to avoid segregation. After the concrete was compacted, a trowel was used to finish the surface. Two hours after casting, the concrete surface was covered with wet burlap for curing. The beams were removed from the forms after two weeks. Different stages concrete placement and curing are shown in Figure 3.7.

Concrete placing process

Concrete surface after finishing

Concrete curing

Figure 3.7 Stages of concrete placement and curing

3.5 Material Properties

Four batches of concrete were used in this study. For each group, one separate batch was used, and the fourth batch provided extra beams to all groups to replace those beams that failed by fatigue of reinforcement rather than by a bond failure. Three of the four batches consisted of sixteen beams for each group, and the fourth batch (extra batch) consisted of five beams. The first batch was cast for Group 2 (30 mm concrete cover), then the second batch was for Group 3 (50 mm concrete cover), the third batch was for Group 1 (20 mm concrete) and fourth batch was the extra beams.

The materials used in this study were concrete, steel bar, FRP sheets and epoxy. The mechanical properties for all those materials are given below:

3.5.1 Concrete

All concrete batches had the same components and quantities of each component. The concrete components per cubic meter were 1110 kg of coarse aggregate (20 mm maximum aggregate size), 865 kg of fine aggregate, 220 kg of Portland cement, 60 kg of slag and fly ash, 325 ml/100kg of a high strength water reducing superplasticizer and 200 liters of water. The water to cement ratio was 0.55, and the slump was 180 mm. All specimens were cast in a horizontal position. For each batch, a minimum of twenty concrete cylinders 100 mm x 200 mm were cast from same batch as the beams. The average concrete compressive strength was monitored by testing three 100 mm × 200 mm cylinders at various ages for each batch as shown in Figure 3.8. The average concrete compressive strength was 42 MPa, 33 MPa and 35 MPa at the 28-day specified strength based on standard (CSA A23.3-2004) for Group 1, Group 2 and Group 3, respectively.

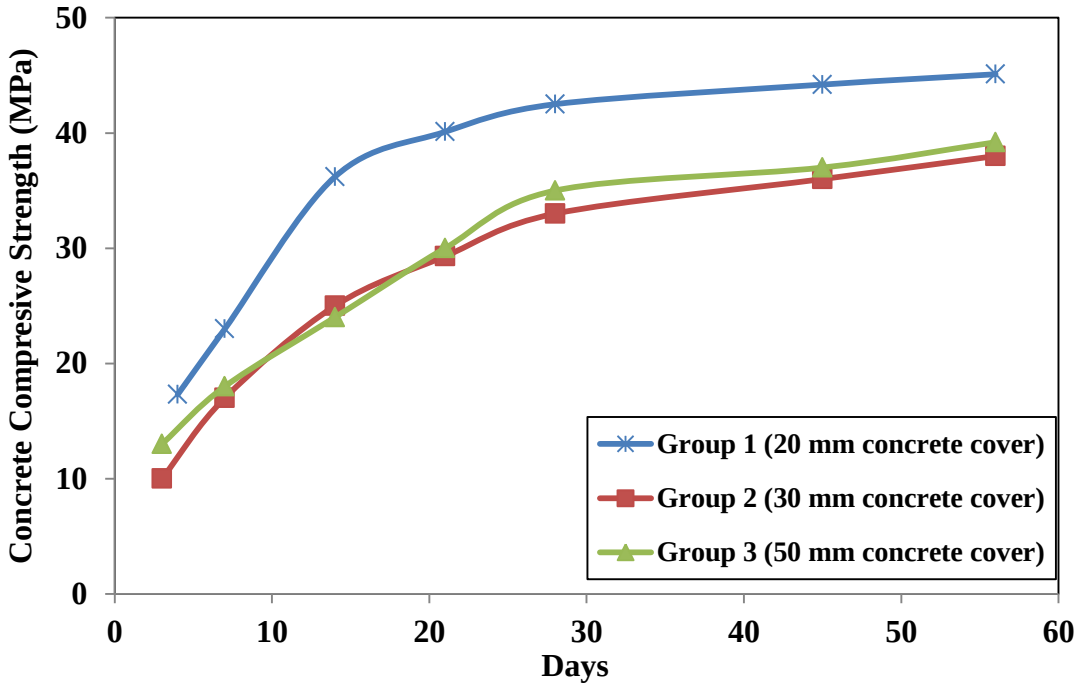

Figure 3.8 Average concrete strength at different ages for all groups

3.5.2 Steel Reinforcement

The average nominal yield stress for the Grade 400 deformed steel bars were 435 MPa, 453 MPa and 427 MPa for Group 1, Group 2 and Group 3, respectively, as provided by the supplier.

3.5.3 FRP Sheets and Matrix

Two types of FRP wrapping sheets were used in this study. The GFRP sheet used was SikaWrap 430G and the CFRP sheet used was SikaWrap 900C. Table 3.2 summarizes the properties of the FRP wrapping sheets, as provided by Sika Canada. The weights of the GFRP sheet and the CFRP sheet were 430 g/m^2 and 900 g/m^2, respectively.

The CFRP wrapping sheets were used with two types of epoxies that were Sikadur 300 and Sikadur 330. The concrete surface was primed with Sikadur 330 and the CFRP sheets were saturated with Sikadur 300 and then the CFRP sheets were placed on the concrete surface. However, the GFRP wrapping sheets used only Sikadur 330. The properties of the two types of epoxies used in the study are shown in Table 3.2, as provider by Sika Canada.

Table 3.2 Properties of FRP wrapping sheets and epoxies

Property	Carbon fiber wrapped sheet				Glass fiber wrapped sheet		
	CFRP wrap 900C fiber properties	epoxy 300	epoxy 330	CFRP wrap 900C cured laminated	GFRP wrap 430G fiber properties	epoxy 330	GFRP wrap 430G cured laminated
Tensile strength (MPa)	3,800	55	30	1120	2,250	30	540
Tensile modulus (MPa)	242,000	1,720	--	100,000	70,000	--	26,500
Elongation (%)	1.55	3	1.5	1.1	2.8	1.5	2.21
Thickness (mm)	--	--	--	1.3	--	--	0.508

3.6 FRP Repair and Application

3.6.1 FRP Repair Scheme

The FRP repair scheme was kept the same for all the repaired beams. After preparing the concrete surface, one layer of U-shaped FRP sheet with a 950 mm in length was used to cover the constant moment region at the mid span of the beam. The widths of the FRP sheets were 600 mm for Group 2 and Group 3 and 900 mm for Group 1as shown in Figure 3.9 and Figure 3.10, respectively.

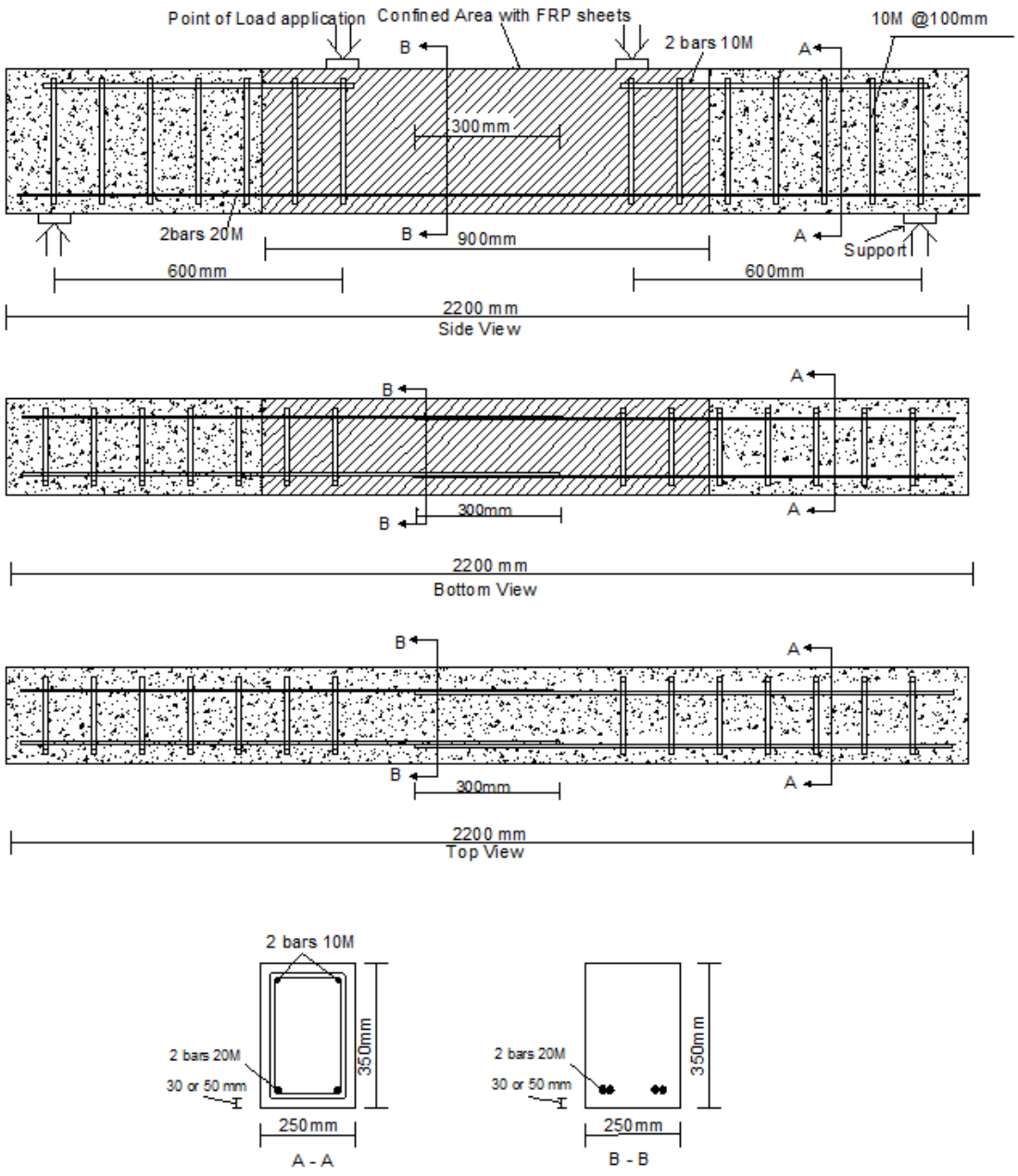

Figure 3.9 FRP repair scheme for Group 2 and Group 3

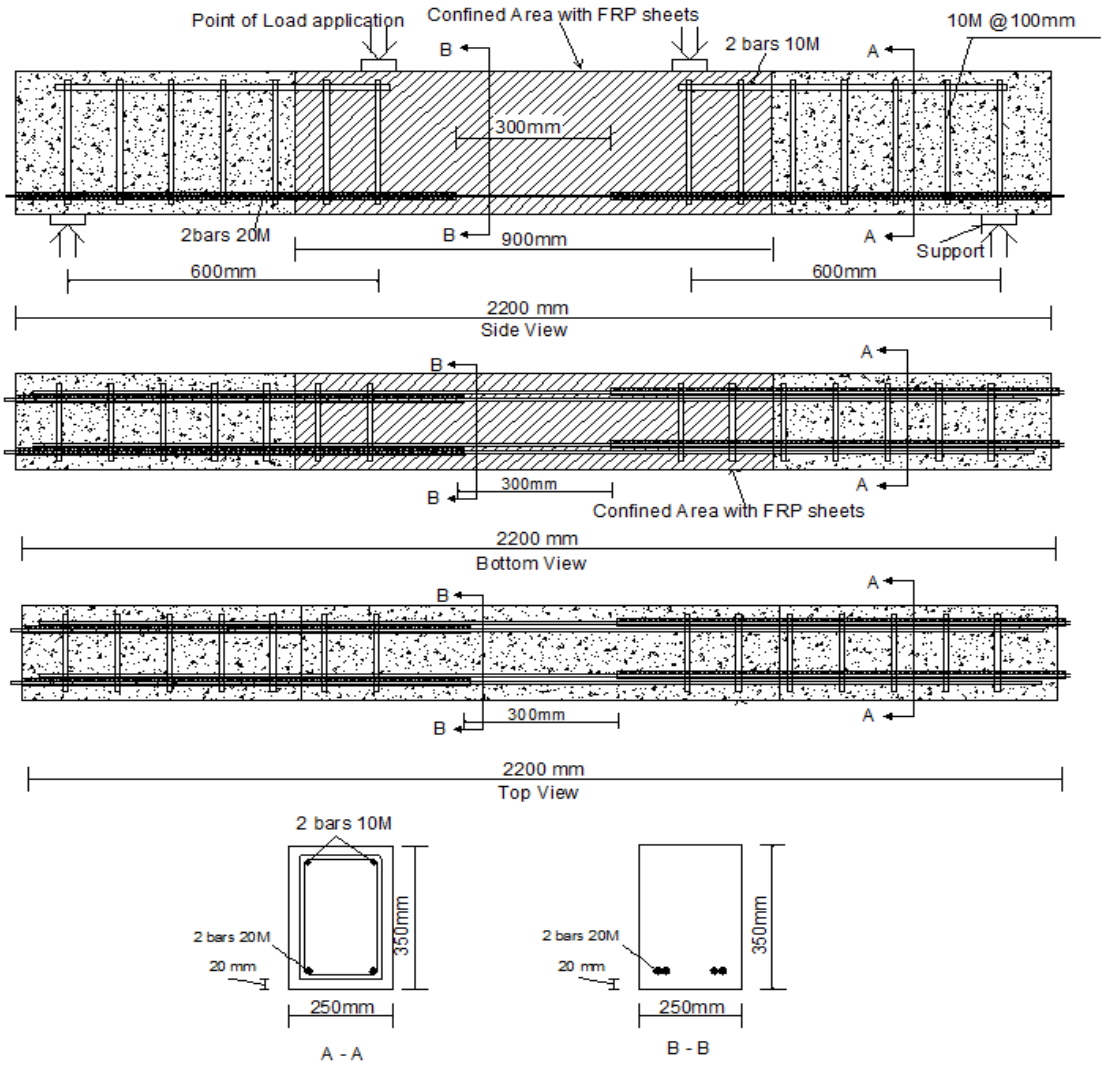

Figure 3.10 FRP repair scheme for Group 1

3.6.2 Surface Preparation

Prior to the application of the FRP sheets, the concrete surface was sandblasted to remove weak surface material and expose the aggregate to get a sufficiently rough surface to ensure a good bond between the FRP sheets and the concrete. ACI 440 (2008) recommends rounding of the specimen corners to avoid a localized stress concentration in the FRP sheet. Figure 3.11 shows the concrete corners after sandblasting.

Figure 3.11 Concrete service after sandblasted

3.6.3 Installation of the FRP

The CFRP and GFRP sheets were cut to the chosen dimensions. The epoxy Sikadur 330 was prepared by mixing its two components using a low speed drill, and then applied to the concrete surface using a brush. The CFRP sheets were impregnated with Sikadur 300 and then installed on the beam while the GFRP was installed without being impregnated with Sikadur 300. A manual pressure was applied to the CFRP and GFRP sheets by using a threaded roller to remove any air voids at the concrete/FRP interface and achieve a good bond between concrete surface and FRP sheets. Figure 3.12 shows installation of the CFRP/GFRP wrapping sheets.

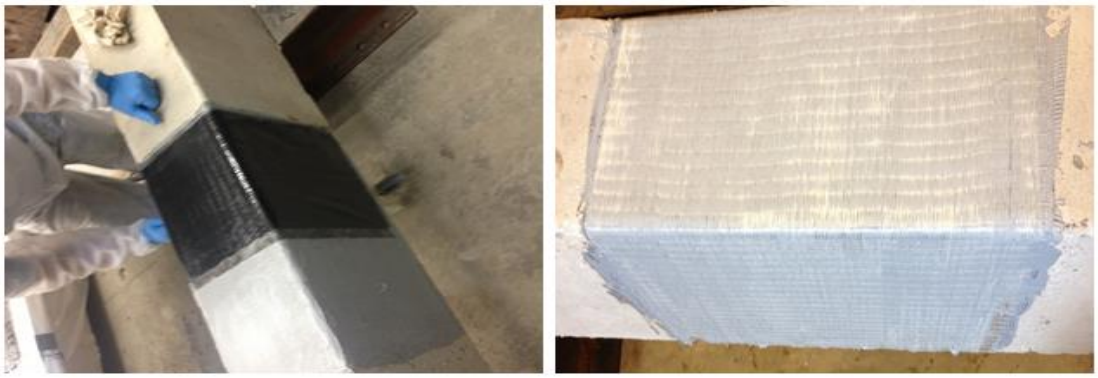

Figure 3.12 Installation of FRP wrapping sheets

3.7 Instrumentation

All beams were instrumented with eight 5 mm strain gauges on the steel reinforcement to measure the strain distribution along lap splice in the constant moment region. For Group 2 and Group 3, a total of nine strain gages were used for each beam and the location of the strain gauges on the steel reinforcement are shown in Figure 3.13. For Group 1, a total of sixteen steel strain gages were used for each beam and the location of the strain gauges on the steel reinforcement are shown in Figure 3.14. Also, all beams were instrumented with one 50 mm strain gauge on the concrete compression surface at the mid span.

For each beam of Group 2 and Group 3, the mid span deflection was monitored by using one linear variable differential transducer (LVDT) with a 50 mm range and an accuracy of 0.01 mm. For each beam of Group 1, five linear variable differential transducers (LVDT) were used to measure the mid-span deflection and the slip of the four extended de-bonded steel bars.

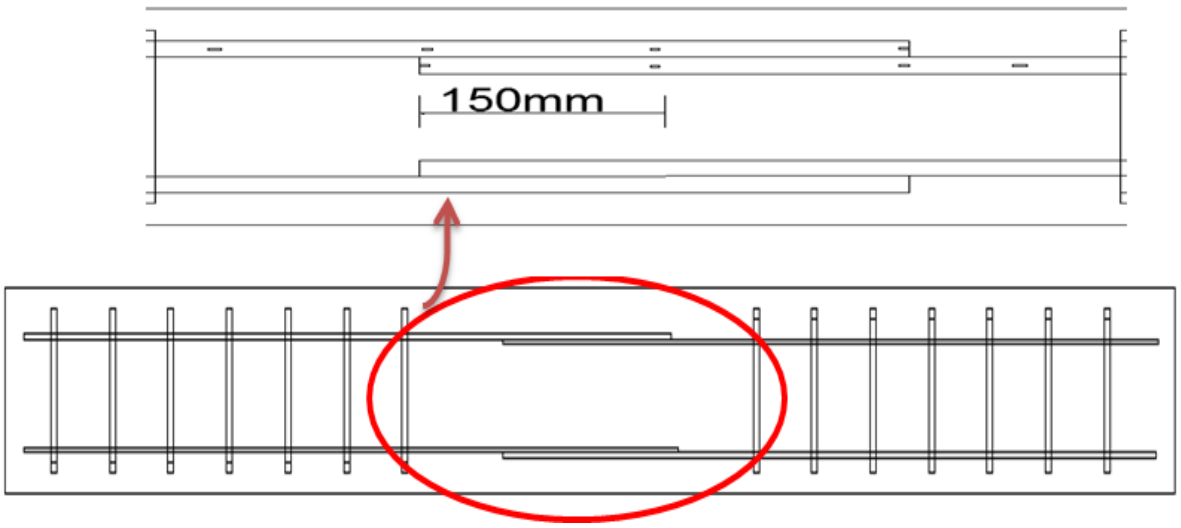

Figure 3.13 The location of the strain gauges along the lap splice for Group 2 and Group 3

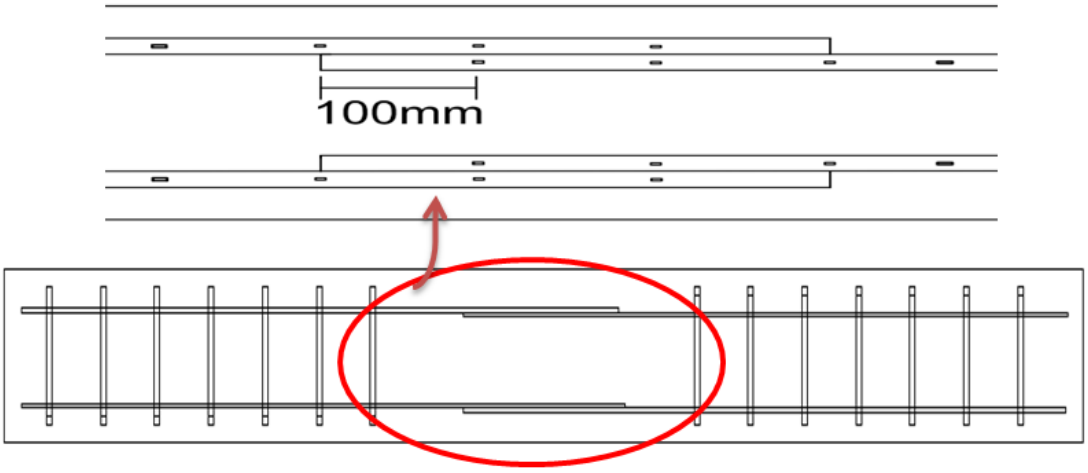

Figure 3.14 The location of the strain gauges along the lap splice for Group 1

3.8 Test Setup and Loading Procedure

All specimens were tested under four-point bending for both monotonic and fatigue loadings. The loading system produced a constant moment region in the middle of the span that included the lap splice region, as shown in Figure 3.15. In the monotonic load tests, the beam was loaded in displacement control at a rate of 0.15 mm per minute until the beam failed.

All fatigue tests were performed in load control. At the beginning of each test, the load was increased manually using the set point of the controller to reach the desired maximum load. Then the load was decreased manually to the mean load. Then the controller was used to automatically apply a cyclic loading between the desired minimum and maximum loads in a sine wave mode with a frequency of 1.3 Hz.

Figure 3.15 Loading test setup

Chapter 4 Experimental Results and Discussion

4.1 Introduction

This chapter presents the test results for the monotonic and fatigue bond strength between reinforcing steel bars and the surrounding concrete along the tension lap splice for unstrengthened and strengthened beams with different FRP sheets. Fifty three beams were cast and tested under monotonic and fatigue loading. The beams were divided into three groups having different concrete covers Group 1 (20 mm concrete cover), Group 2 (30 mm concrete cover) and Group 3 (50 mm concrete cover). Group 1, Group 2 and Group 3 consisted of 17 beams, 17 beams and 19 beams, respectively. Each group was divided into three series unwrapped beams, GFRP wrapped beams and CFRP wrapped beams. Each series had a specimen that was loaded monotonically to failure to determine the monotonic load and bond capacity of the specimens, while the other beams from each series were subjected to fatigue loading. The test variables for each group were the presence or absence of FRP sheet wrapping, the type of FRP wrapping sheet (GFRP or CFRP sheets), the loading type (monotonic or fatigue) and the fatigue load range.

The main goal of this research was to investigate the effect of fatigue loading on the bond between concrete and steel, and the ability of FRP sheets to enhance the fatigue performance of a tension lap splice. The discussion of the experimental results will focus on the behaviour of the tested specimens under monotonic and fatigue loading including the bond strength, the strain behaviour and the variation of fatigue life with the applied load range and stress range. For Group 1, the behaviour of the slip of the steel bars under monotonic and fatigue loading will be discussed.

4.2 Monotonic Test Results

For each group, three beams one unwrapped beam, one GFRP beam and one CFRP beam were tested under monotonic loading. Table 4.1 summarizes the maximum loads, the deflections at maximum load and the modes of failure of the monotonic beam tests. All the

beams failed by a splitting bond failure. For Group 1 and Group 3, the steel reinforcement of the CFRP wrapped beam reached the yield stress level, but the beam failed by a splitting bond failure.

Table 4.1 Maximum loads and mode of failure for all beams

Group	Specimen notation	Max. load (kN)	Deflection at Max. load (mm)	Failure mode
Group 1	UN-G1-ST	180	3.25	Bond failure
	GFRP-G1-ST	230	4.8	Bond failure
	CFRP-G1-ST	307	10.1	Bond failure
Group 2	UN-G2-ST	161	3.22	Bond failure
	GFRP-G2-ST	200	4.63	Bond failure
	CFRP-G2-ST	258	6.74	Bond failure
Group 3	UN-G3-ST	209	5.24	Bond failure
	GFRP-G3-ST	265	12.48	Bond failure
	CFRP-G3-ST	300	25.24	Bond failure

4.2.1 General Behaviour and Mode of Failure

For all the unwrapped beams, the first cracks developed were flexural cracks within the constant moment region at both ends of the lap splice. As the loading increased, more vertical and diagonal flexural cracks appeared within and outside the constant moment region. As the loading increased further, splitting cracks parallel to the lap splice appeared at both ends of the lap splice. The longitudinal splitting cracks increased in length from both ends of the lap splice as the load increased further as shown in Figure 4.1. Figure 4.2 shows measurements of crack length from one end of the splice versus load in the monotonic test of an unwrapped beam with a 20 mm cover. The maximum length of the bottom splitting cracks

reached 120 mm from both ends of the lap splice before failure occurred. These splitting cracks led to a loss of bond between the steel bar and the surrounding concrete. When the bottom splitting cracks reached a length of 120 mm the beam experienced a sudden failure marked by a rapid drop in the load carrying capacity. At failure, longitudinal splitting side cracks occurred along the lap splice region. Chunks of the concrete cover fell down as the failure occurred due to the absence of stirrup or FRP sheet confinement. These observations for the unwrapped beams under monotonic loading were similar to those reported by (Seliem et al., 2009; Tarabia et al., 2010 and Garcia et al., 2013).

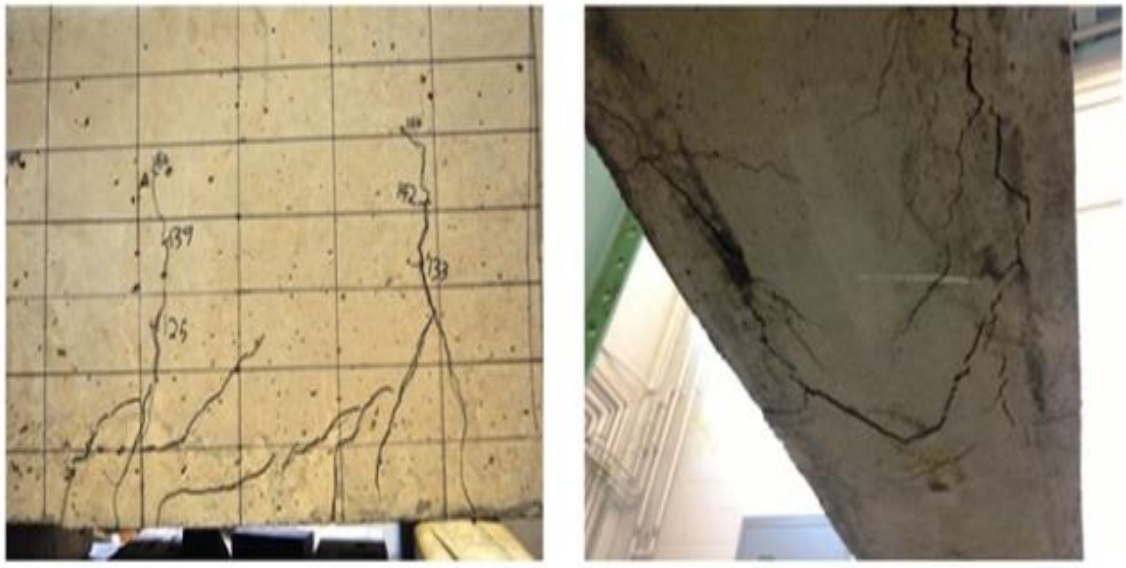

Figure 4.1 Mode of failure for the unwrapped beam

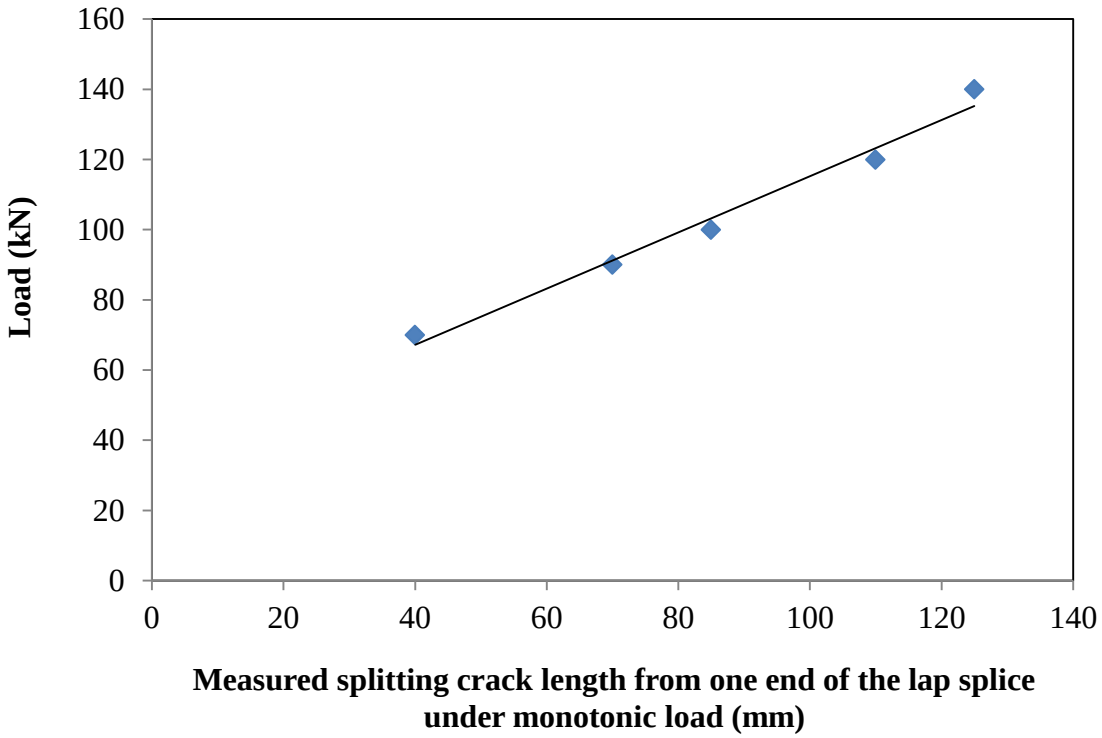

Figure 4.2 Increase in splitting crack length with monotonic load for the unwrapped beam with 20 mm concrete cover

For all the FRP wrapped beams, the first visible cracks were flexural cracks at both ends of the lap splice. As the load increased, the FRP sheet split vertically to reveal flexural cracks. The FRP sheet prevented the visual monitoring of splitting cracks. After the test the FRP sheet was removed and splitting cracks were observed along the entire lap splice length as shown in Figure 4.3. The failure for the unwrapped and GFRP wrapped beams was by splitting. However, in the CFRP wrapped beam under monotonic loading a partial failure by pullout was followed by a splitting failure.

The lap spliced beam wrapped with FRP sheets carried more applied load even after the longitudinal splitting cracks occurred all along the entire lap splice length. This is attributed to the fact that the FRP sheets held and confined the concrete cover even after the splitting cracks extended over the whole lap splice region. Similar behaviour was observed when a lap

spliced beam with stirrups and FRP wrapping was able to carry more applied load even after the longitudinal splitting cracks occurred along the entire length of the lap splice region (Rezansoff et al., 1993; Tocci 1981; Tepfers 1973; Garcia et al., 2013).

Figure 4.3 Mode of failure for wrapped beam

4.2.2 Strain Behaviour

The typical strain distributions along the lap splice for the unwrapped beam are shown in Figure 4.4. The figure shows the strains (microstrain) measured at the strain gauge locations for load intervals of 30 kN. The values of the strain gauge readings at the loaded end of the lap splice and outside the lap splice but within the constant moment region were almost the same. At a high load level just before failure, the strain gauge reading at G2 from the beginning of the lap splice jumped, indicating a de-bonding between the steel bar and the concrete. The strain distribution along the lap splice was found to be similar to that reported by other researchers (Tepfers, 1973; Judge et al., 1990; Tepfers 1980).

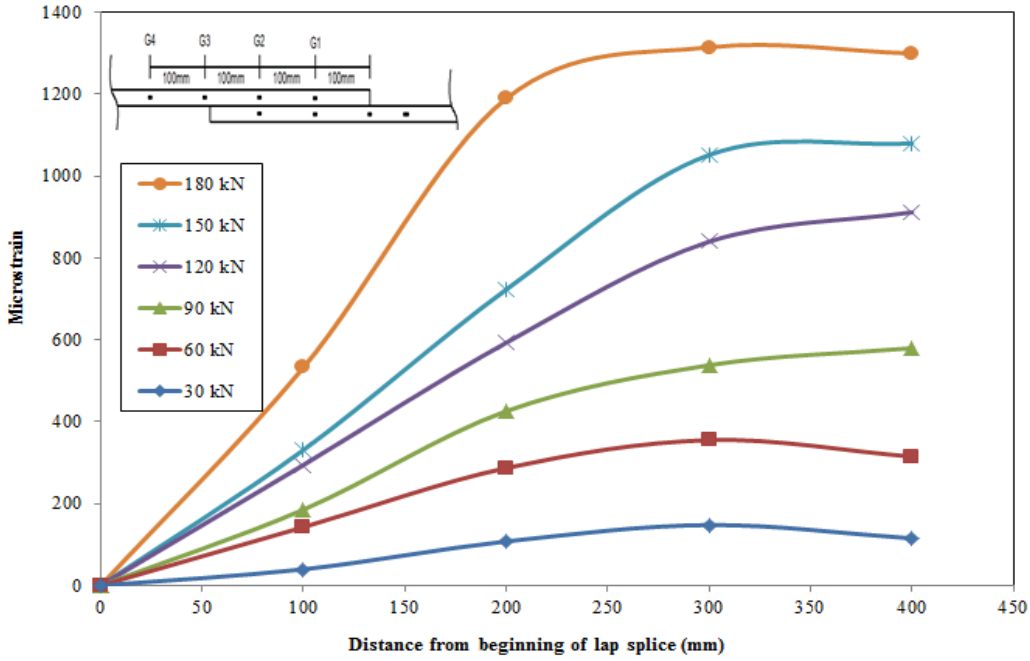

Figure 4.4 Strain distribution along the lap splice for the unwrapped beam UN-G1-ST

Figure 4.5 shows typical strain distributions along the lap splice for a GFRP wrapped beam for various load levels. Before the concrete cracked, both the concrete and the steel bars carried the tensile force, and the strain profile followed the linear behaviour of an uncracked concrete section along the lap splice length as shown in Figure 4.5. Once the concrete cracked above 80 kN, all the tensile force at the crack locations was carried by the steel bar and the strain readings increased at gauges near the crack locations. The values of the strain at the loaded end of the lap splice and the strain located outside the lap splice but within the constant moment region were slightly different from each other. As the load increased further, the strain distributions were similar. Just before failure, the strain gauge reading at 200 mm from the beginning of the lap splices jumped and the slope from there to the end of the splice decreased, this suggested that a partial de-bonding had occurred between the concrete and the steel bar for 100 mm length closest to the loaded end.

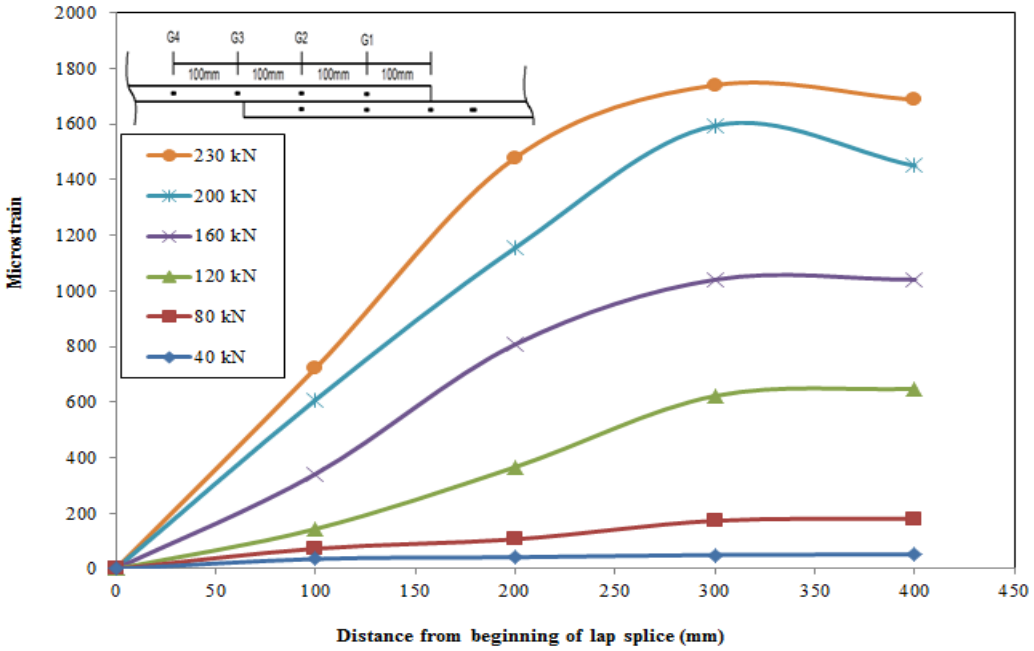

Figure 4.5 Strain distribution along the lap splice for the GFRP wrapped beam GFRP-G1-ST

4.2.3 Load Deflection Curve

The load deflection curves for Group 1, Group 2 and Group 3 are shown in Figure 4.6, Figure 4.7 and Figure 4.8 respectively. For all of the different concrete covers, the initial stiffness for the unwrapped, GFRP wrapped and CFRP wrapped beams was almost the same. As the load increased, the mid-span deflection increased until cracks appeared in the constant moment region. At that point, the slope of the load versus deflection graph decreased and continued to decrease as the load increased to its maximum value. After the concrete cracked, the stiffness for the FRP wrapped beams of Group 1 and Group 3 was higher than that of the unwrapped beams. However, for Group 2, the stiffness for all beams under monotonic loading was about the same until failure. For all the unwrapped beams, a brittle and sudden failure occurred once the side splitting cracks occurred. The confinement provided by the stiffer CFRP wrapping was greater than that provided by the GFRP wrapping and resulted in a greater strength and ductility.

For Group 1, the load deflection curves obtained from the tests are shown in Figure 4.6. The ultimate loads for the unwrapped, the GFRP wrapped and the CFRP wrapped beams were 180 kN, 230 kN and 307 kN, respectively. The GFRP and CFRP wrapping sheets increased the maximum load by 28% and 71% compared to the unwrapped beam, respectively. The deflection at the ultimate load increased by 48% and 378% for the GFRP wrapped and CFRP wrapped beams, respectively.

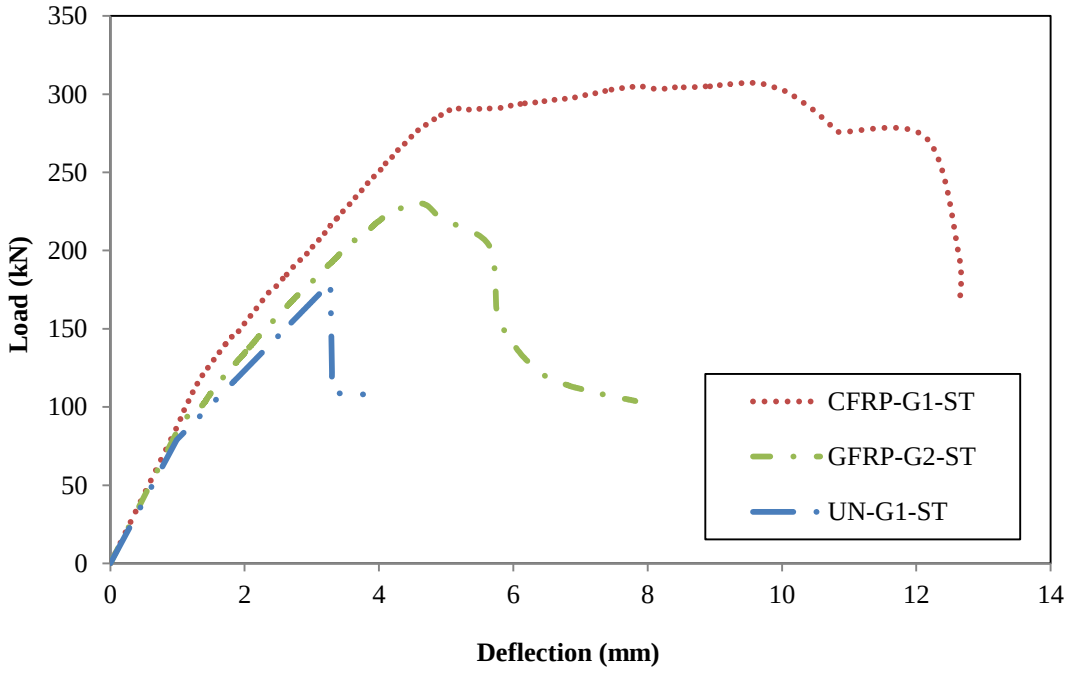

Figure 4.6 Load - deflection curves for unwrapped and FRP wrapped beams of Group 1 (20 mm concrete cover)

For Group 2, the concrete compressive strength was 33 MPa which was less than the concrete compressive strength for Group 1. Figure 4.7 shows the load deflection curves for all beams of Group 2 under monotonic loading. The maximum loads for the unwrapped, the GFRP wrapped and the CFRP wrapped beams were 161 kN, 200 kN and 258 kN, respectively. The GFRP and CFRP wrapping sheets increased the maximum load by 24% and 60% compared to the unwrapped beam, respectively. The deflections at the maximum

load were 3.22 mm, 4.63 mm and 6.74 mm for the unwrapped, the GFRP wrapped and the CFRP wrapped, respectively. The GFRP and CFRP wrapping sheets increased the deflection at the maximum load by 44% and 109% compared to the unwrapped beam, respectively.

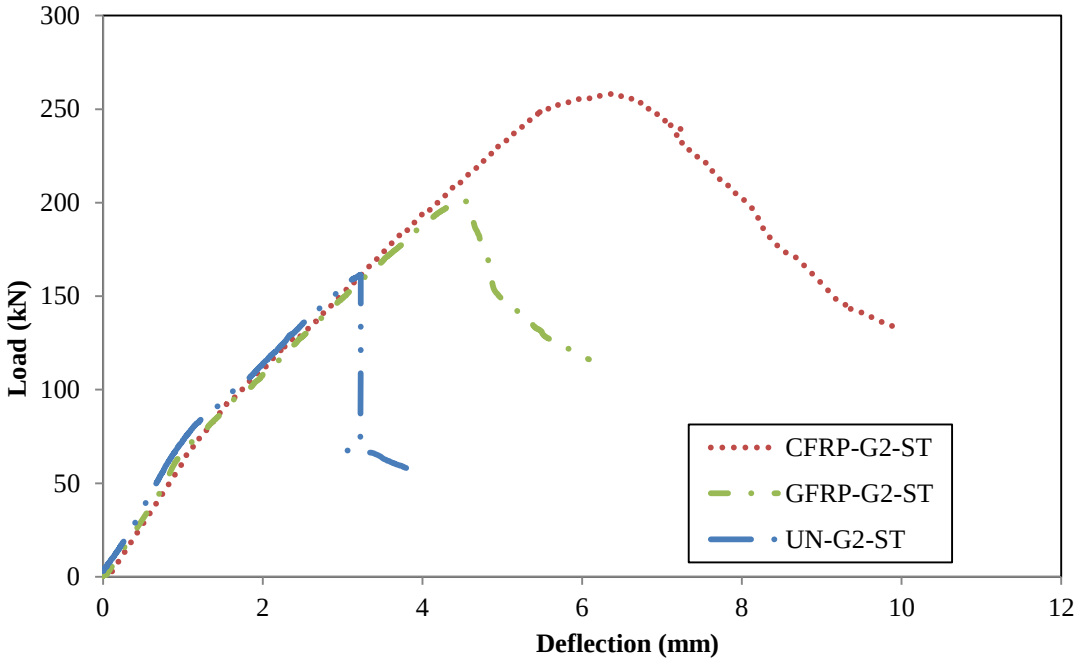

Figure 4.7 Load - deflection curves for unwrapped and FRP wrapped beams of Group 2 (30 mm concrete cover)

For Group 3, the concrete compressive strength was 35 MPa. The load deflection curves obtained from the tests are shown in Figure 4.8. The ultimate loads for the unwrapped, the GFRP wrapped and the CFRP wrapped beams were 209 kN, 265 kN and 300 kN, respectively. The GFRP and CFRP wrapping sheets increased the maximum load by 27% and 44% compared to the unwrapped beam, respectively. The deflection at the ultimate load was increased by 138% and 482% for the GFRP wrapped and CFRP wrapped beams, respectively.

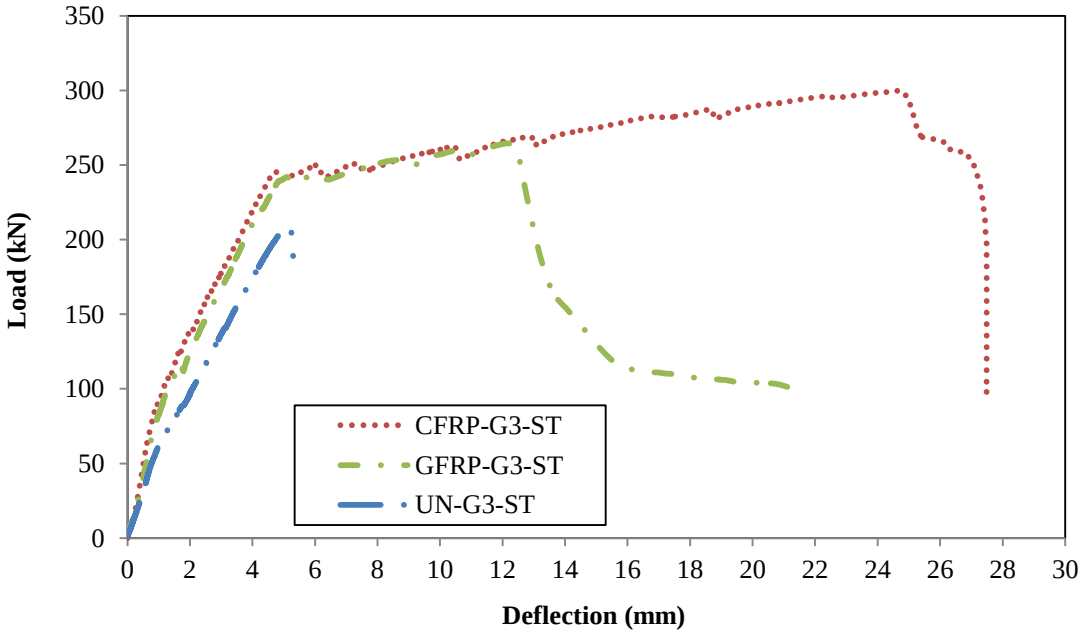

Figure 4.8 Load - deflection curves for unwrapped and FRP wrapped beams of Group 3 (50 mm concrete cover)

4.2.4 Bond Strength

The average bond strength is defined as the average shear stress between the steel rebars and the surrounding concrete adjacent to the bars over the length of the splice. The average shear stress at failure is calculated as the force in a steel rebar at failure divided by the surface area of the bar over the length of the splice. The bond strength is calculated from the following equation:

$$\tau = \frac{A_b f_s}{\pi d_b l} = \frac{f_s d_b}{4\, l} \qquad 4.1$$

where A_b is the bar area (mm^2); f_s is the steel stress (MPa); d_b is the steel bar diameter (mm) and l is the lap splice length (mm)

The stress f_s in the steel rebar at the failure of the beam is obtained from the load on the beam at failure based on a cracked section analysis of the cross section. Orangun et al. (1977) developed an analytical model to predict the average bond strength as shown below:

$$\tau = \left[0.10 + \frac{c}{4d_b} + \frac{4.2d_b}{l_d}\right]\sqrt{f'_c} \qquad 4.2$$

where u is the average bond strength (MPa); c is the concrete cover (mm); d_b is the steel bar diameter (mm); l_d is the lap splice length (mm) and f'_c is the concrete compressive strength (MPa).

Hamad et al. (2004) studied the effect of FRP wrapping sheets on the bond strength of a lap splice under monotonic loading and proposed the following experimental parameter to capture the effect of the FRP wrapping on the bond strength along the lap splice:

$$K_{tr,f} = \frac{C_1 A_{tr,f} f_{fe}}{s_f d_b n_b} \leq 0.25 \qquad 4.3$$

where C_1 is a proportionality constant which is equal to $\frac{1}{16.6}$, $A_{tr,f}$ is the total cross sectional area of FRP (mm^2), f_{fe} is the effective stress in the FRP laminate (MPa), s_f is the width of the FRP (mm), d_b is the diameter of the steel rebar (mm) and n_b is the number of spliced bars. The $K_{tr,f}$ factor can be used to predict the effectiveness of the confinement due to the external FRP wrapping on the bond strength.

Table 4.2 shows results for the actual bond strength, the predicted bond strength and the enhancement of the ratio of the bond strength to that of an unwrapped beam due to the FRP wrapping for the beams tested under monotonic loading. The effectiveness of the CFRP wrapping sheets was greater than that of the GFRP wrapping sheets due to their greater stiffness. The bond ratio is given by the actual bond strength divided by the predicted bond strength. The increment in bond ratio increased as the stiffness of the FRP sheet increased. The bond ratio varied between 95% and 134%. The Orangun et al. (1977) and Hamad et al.

(2004) equations give a good prediction of the average bond strength for all different concrete covers thickness and different wrapping conditions of the lap splice. The ratio of the actual bond strength to the predicted bond strength for the CFRP wrapped beams was 134%, 115% and 111% for Group 1 (20 mm concrete cover), Group 2 (30 mm concrete cover) and Group 3 (50 mm concrete cover), respectively. The ratio of the actual bond strength to the predicted bond strength value for the GFRP wrapped beams was 113%, 99% and 106% for Group 1, Group 2 and Group 3, respectively. The limitation of 0.25 for $K_{tr,f}$ in the Hamad et al. (2004) equation gives a $K_{tr,f}$ value for the GFRP sheets of 0.14. However, the $K_{tr,f}$ value for the new high strength CFRP sheets is 0.89 which is more than three times the value using this limitation. The limitation of 0.25 for $K_{tr,f}$ preceded the introduction of new high stiffness CFRP sheets and is too conservative for the new high strength CFRP sheet and especially so for a small concrete cover. The calculation of $K_{tr,f}$ is shown in the Appendix.

Table 4.2 Test results and analytical predictions of bond strength for all groups

Group	Specimen notation	Prediction of concrete bond strength (MPa)	Prediction of FRP bond strength (MPa)	Prediction of total bond (MPa)	Actual bond strength (MPa)	Effect of FRP to enhance the bond ratio (%)	Ratio of Actual bond stress to prediction bond stress (%)
Group 1	UN-G1-ST	4.08	--	4.08	4.46	--	109
	GFRP-G1-ST	4.08	0.97	5.05	5.73	128	113
	CFRP-G1-ST	4.08	1.62	5.70	7.64	171	134
Group 2	UN-G2-ST	4.34	--	4.34	4.14	--	95
	GFRP-G2-ST	4.34	0.85	5.19	5.15	124	99
	CFRP-G2-ST	4.34	1.43	5.77	6.63	160	115
Group 3	UN-G3-ST	5.95	--	5.95	5.73	--	96
	GFRP-G3-ST	5.95	0.88	6.83	7.26	127	106
	CFRP-G3-ST	5.95	1.47	7.42	8.23	144	111

4.2.5 Bond Stress versus Slip Responses

The slip was measured only for Group 1 beams. The local bond stress versus slip responses for the unwrapped, GFRP wrapped and CFRP wrapped beams tested under monotonic load are shown in Figure 4.9. Slip initiated in the unwrapped beam at a lower bond stress than in the wrapped beams. The FRP sheet along the lap splice delayed and confined the growth of the splitting cracks before failure and improved the splitting bond strength compared to the unwrapped beams. Also, the FRP sheets delayed the slip of the steel reinforcement to a

higher bond stress than that exhibited by the unwrapped beams. The load to initiate slip of the steel bar increased as the stiffness of the FRP sheet increased. The increase in bond strength is attributed to the amount of confinement.

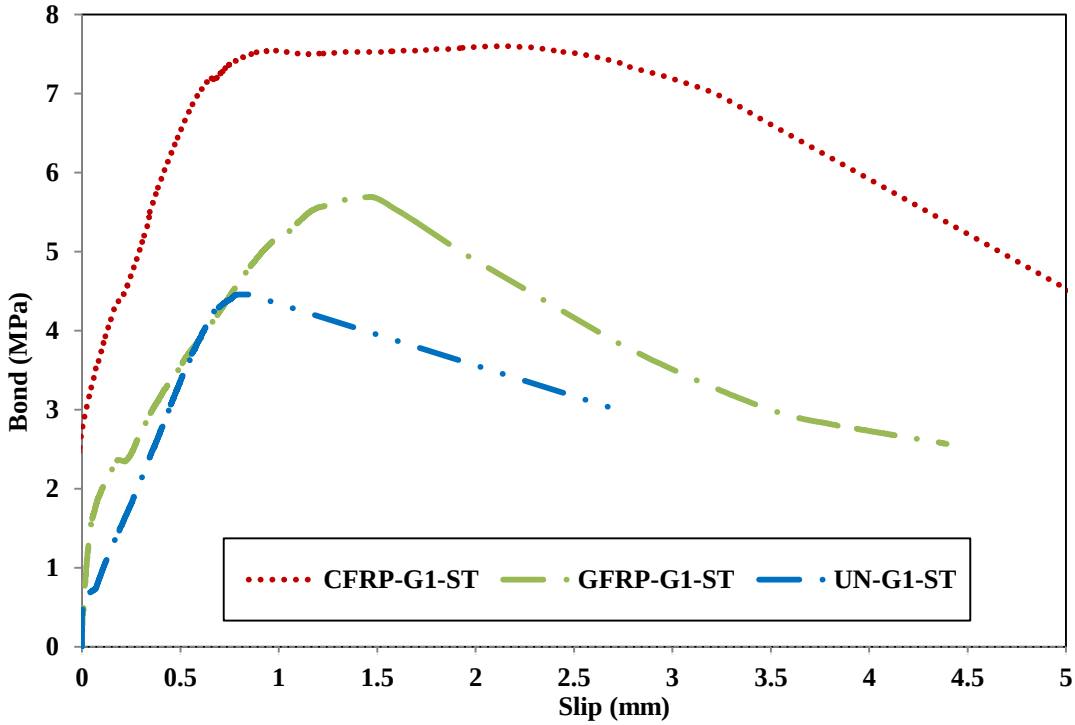

Figure 4.9 The local bond stress versus slip response for all beams tested under a monotonic loading for Group 1 (20 mm concrete cover)

Harajli et al. (2004) and Harajli (2009) proposed the following equations to predict the bond stress-slip responses for the unwrapped and FRP wrapped reinforced concrete beams:

$$u_m = 2.57\sqrt{f_c'} \tag{4.4}$$

$$u_{sp} = 0.78\sqrt{f_c'}\left(\frac{c + 56\frac{E_f\, n_f t_f}{E_s n_s}}{d_b}\right)^{2/3} \leq u_m \tag{4.5}$$

$$u_p = u_{sp}\left(0.5 + 46\frac{E_f\, n_f\, t_f}{E_s\, c\, n_s}\right) \leq u_{sp} \quad 4.6$$

$$s_{sp} = s_1 e^{3.3\, Ln\left(\frac{u_{sp}}{u_m}\right)} + s_o Ln\left(\frac{u_m}{u_{sp}}\right) \quad 4.7$$

Referring to **Error! Reference source not found.**: u_f *is 0.35* u_m *(MPa),* $_{s1}$ is 0.15 c_o (mm), s_2 s 0.35 c_o (mm), s_3 is c_o (mm) and s_o is 0.15 (mm) for the unwrapped and 0.2 (mm) for the FRP wrapped beam.

where u_1 is the *maximum* bond stress for a pullout failure (MPa), f_c' is the concrete compressive strength (MPa), u_{sp} is the maximum bond splitting failure stress (MPa), c is the clear concrete cover (mm), E_f is the modulus of elasticity of the FRP (MPa), n_f is the number of FRP layers, t_f is thickness of an FRP sheet (mm), E_s is the modulus of elasticity of steel (MPa), n_s is the number of bars being spliced, d_b is the steel bar diameter (mm) and c_o is the clear distance between the ribs of the steel. If the steel bar information is not available, Harajli (2009, 2006) suggested $s_1, s_2\ and\ s_3$ can be taken to be equal to 1.5, 3.5 and 10 mm, respectively, $\alpha\ is$ 0.7 and $\beta\ is$ 0.65. From the above equation, the type of the bond failure can be determined by calculating the value of the bond splitting strength u_{sp} then comparing it to the value of the maximum bond strength for a pullout failure (u_m). A splitting bond failure is expected to occur if the value of the bond splitting strength less than the value of the maximum bond strength and vice versa.

The actual and predicted bond stress-slip curves for unwrapped, GFRP wrapped and CFRP wrapped beams are shown in Figure 4.10. For the unwrapped beam, the figure shows that the predicted peak bond strength is slightly higher than the actual value, and the actual slip value at the peak bond stress is more than the predicted value. In contrast, the predicted peak bond strength for the GFRP wrapped beam is slightly lower than the test value and the slip at the peak bond stress is more than the predicted value. For the CFRP wrapped beam, the peak bond stress is almost identical to the predicted value. However, the slip at the peak bond

stress is more than the predicted value. Generally, the actual value of the peak bond stress falls close to the predicted value and the slip value at the peak stress is much higher than the predicted value. The FRP wrapping sheets led to an increase of the bond strength compared to the unwrapped beams. Also, the FRP wrapping sheets allowed more slip of the steel bar at the maximum bond compared to that for the unwrapped beam. The increase of the slip at failure gave a significant warning before failure for the wrapped beams unlike the sudden failure without warning of the unwrapped beam.

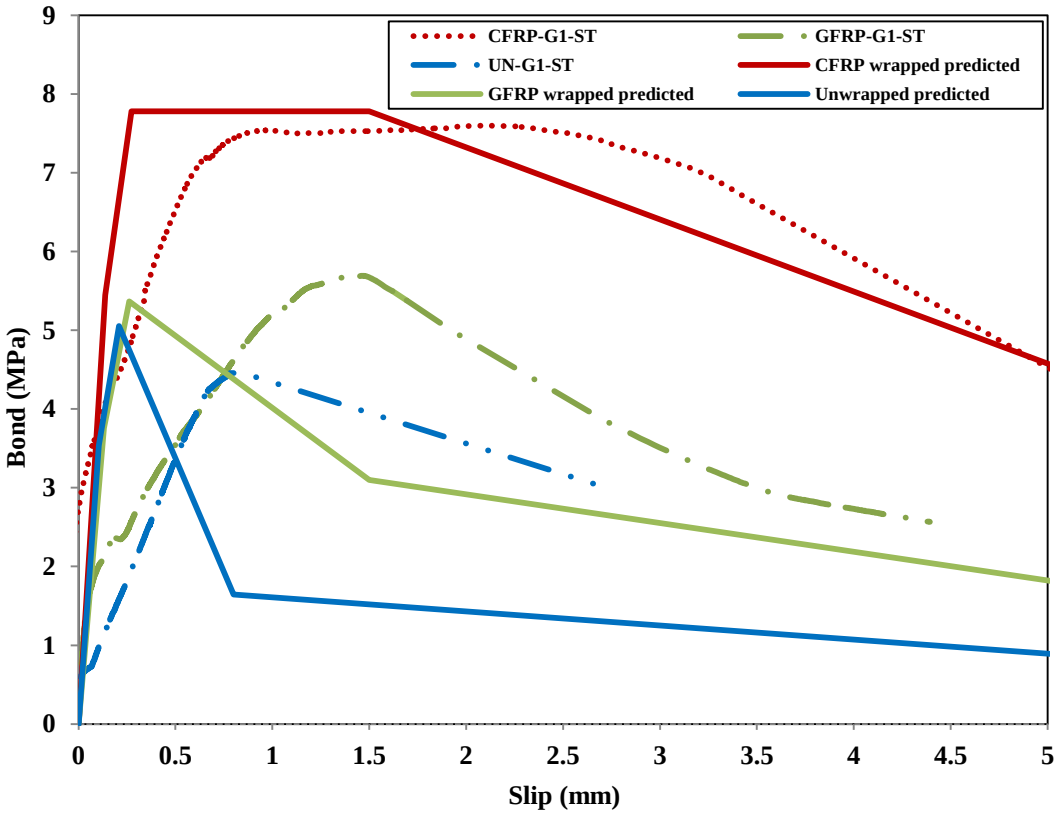

Figure 4.10 The actual and predicted bond stress versus slip for all beams tested under a monotonic loading

4.3 Monotonic Test Results Discussion

For all the unwrapped beams, the load deflection behaviour was the same for all different concrete covers. Also, for all the wrapped beams, the behaviour was same for all different

concrete covers. As the confinement (concrete cover or FRP sheet stiffness) increased, the bond strength increased. It is worth mentioning that, the 300 mm bonded length used in this study was less than the development length required to develop the ultimate stress of the reinforcing steel bar that would result in bar rupture failure for all beams tested under monotonic loading.

The load deflection curves for all wrapping conditions and for all the different concrete covers are shown in Figure 4.11. For all the unwrapped beams, the load dropped sharply right after the failure occurred. For the GFRP wrapped beams, after failure occurred, the load decreased with increasing deflection. Beyond the ultimate load, the CFRP wrapped beam maintained an almost constant load level during a significant amount of deflection before the load decreased at a much lower rate than that exhibited by the other beams.

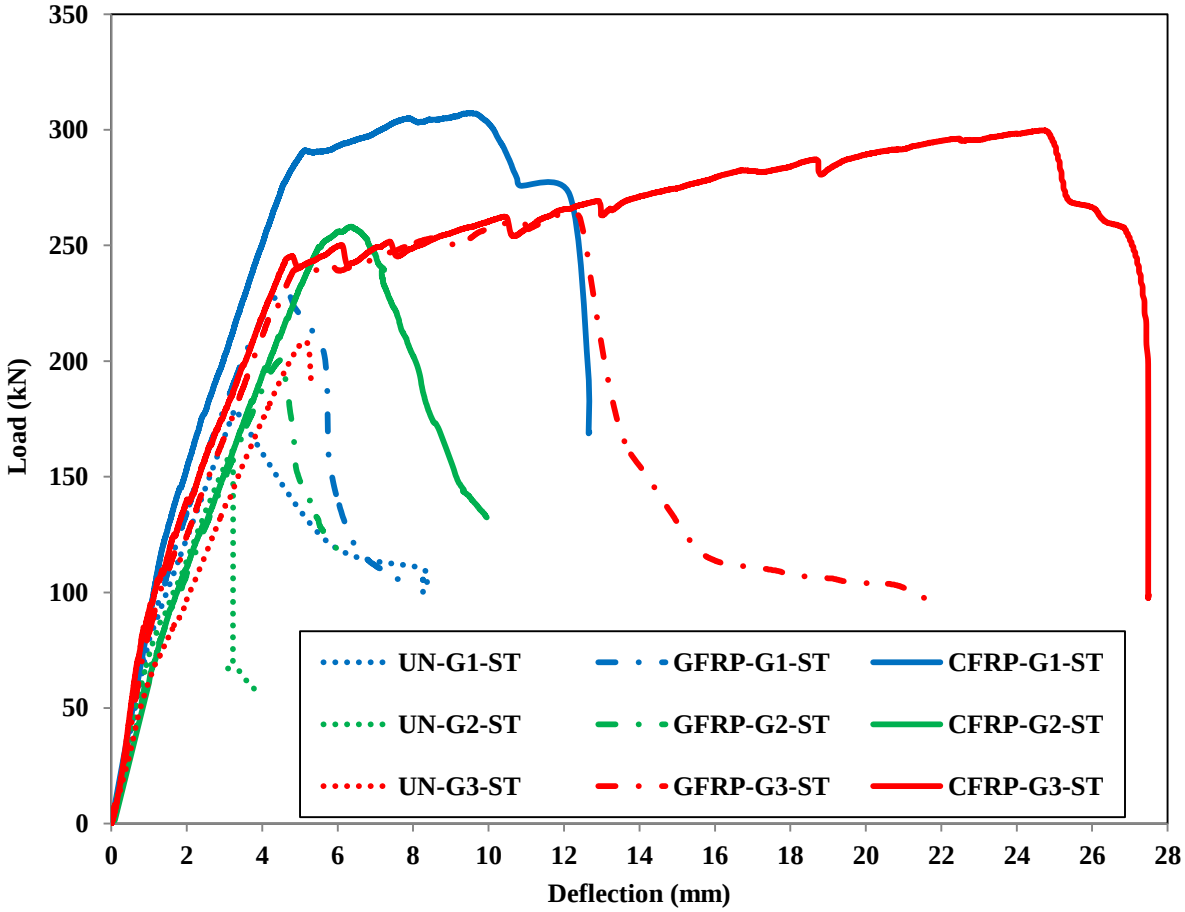

Figure 4.11 Load - deflection curves for all the unwrapped and the FRP wrapped beams

4.3.1 Bond Strength

Orangun et al. (1977) developed an analytical model to predict the average monotonic bond strength for various thicknesses of concrete cover, bar diameter, and concrete strength.

$$u = \left[0.10 + \frac{c}{4d_b} + \frac{4.2d_b}{l_d} + K_{tr's}\right]\sqrt{f'_c} \qquad 4.8$$

From the above equation, the factors affecting the bond strength by FRP wrapping was proposed by Hamad et al. (2004) as follows:

$$u = 0.10\sqrt{f'_c} + \frac{c}{4d_b}\sqrt{f'_c} + \frac{4.2d_b}{l_d}\sqrt{f'_c} + K_{tr\prime f}\sqrt{f'_c} \quad 4.9$$

The factor for the change in bond strength with concrete strength is $\sqrt{f'_c}$. The concrete compressive strength was different for all groups. The average concrete compressive strength was 42 MPa, 33 MPa and 35 MPa at the 28-day for Group 1, Group 2 and Group 3, respectively. The bond strength for Group 1 and Group 3 were normalized to the bond strength for Group 2. The bond strength was decreased by $\sqrt{\frac{33}{42}} = 0.88\ \%$ and by $\sqrt{\frac{33}{35}} = 0.97\ \%$ for a decrease in concrete strength from 42 to 33 MPa for Group 1 beams and a decrease in concrete strength from 35 to 33 MPa for Group 3 beams.

Table 4.3 gives the percentage decrease in monotonic bond strength due to a decrease in concrete strength from 42 to 33 MPa for Group 1 and from 35 to 33 MPa for Group 3 together with the measured values of monotonic bond strengths and an expected bond strength after normalization for Group 1 and Group 3. Table 4.4 shows the monotonic bond strength value for the Group 2 and the expected bond strength for Group 1 and Group 3 after normalization. Also, the table shows the predicted bond strengths for all Groups if they were made of 33 MPa concrete by using Orangun et al. (1977) and Hamad et al. (2004) equations and the ratio of the expected bond strength to the predicted bond strength. The ratio of the expected bond strength to the predicted value varies from 96% to 130%.

Table 4.3 Normalized monotonic bond strength for different concrete compressive strength

Group	Beam notation	Percentage ratio of normalized the bond strength	Actual bond strength (MPa)	Expected bond strength after normalization (MPa)
Group 1	UN-G1-ST	$\sqrt{\frac{33}{42}} = 0.88\ \%$	4.46	3.93
	GFRP-G1-ST		5.73	5.04
	CFRP-G1-ST		7.64	6.72
Group 2	UN-G2-ST	$\sqrt{\frac{33}{33}} = 100\%$	4.14	4.14
	GFRP-G2-ST		5.15	5.15
	CFRP-G2-ST		6.63	6.63
Group 3	UN-G3-ST	$\sqrt{\frac{33}{35}} = 0.97\ \%$	5.73	5.56
	GFRP-G3-ST		7.26	7.04
	CFRP-G3-ST		8.23	7.98

Table 4.4 The ratio of the expected to the prediceted bond strength after normalization for all Groups

Group	Beam notation	Expected bond strength after normalization (MPa)	Prediction of total bond for concrete strength 33 MPa (MPa)	Ratio of expected bond stress to predicted bond stress (%)
Group 1	UN-G1-ST	3.93	3.61	109
	GFRP-G1-ST	5.04	4.47	113
	CFRP-G1-ST	6.72	5.05	130
Group 2	UN-G2-ST	4.14	4.14	100
	GFRP-G2-ST	5.15	5.15	100
	CFRP-G2-ST	6.63	6.63	100
Group 3	UN-G3-ST	5.56	5.77	96
	GFRP-G3-ST	7.04	6.62	106
	CFRP-G3-ST	7.98	7.2	111

4.3.1.1 Effect of the FRP Wrapping on the Bond Strength

Table 4.5 shows the effect of the FRP wrapping on bond strength for the three different concrete covers. The increase of the bond strength due to the low stiffness GFRP 430 sheet was close to 126% for the three different concrete covers. The GFRP wrapping increased the normalized bond strengths for the 20 mm, 30 mm and 50 mm concrete cover beams by 128%, 124% and 127% compared to those of the unwrapped beams, respectively. However, for the CFRP wrapped beams, the rate of the increase of the normalized bond strength decreased as the concrete cover increased. The CFRP wrapping increased the normalized bond strengths for the 20 mm, 30 mm and 50 mm concrete cover beams compared to those of the unwrapped beams by 171%, 160% and 144%, respectively. The normalized bond strength of all concrete covers and wrapping conditions are shown in Figure 4.12.

Table 4.5 Effect of FRP wrapping to the bond strength

Group	Beam notation	Normalized bond strength (MPa)	Effect of wrapping %
Group 1	UN-G1-ST	3.93	100
	GFRP-G1-ST	5.04	128
	CFRP-G1-ST	6.72	171
Group 2	UN-G2-ST	4.14	100
	GFRP-G2-ST	5.15	124
	CFRP-G2-ST	6.63	160
Group 3	UN-G3-ST	5.56	100
	GFRP-G3-ST	7.04	127
	CFRP-G3-ST	7.98	144

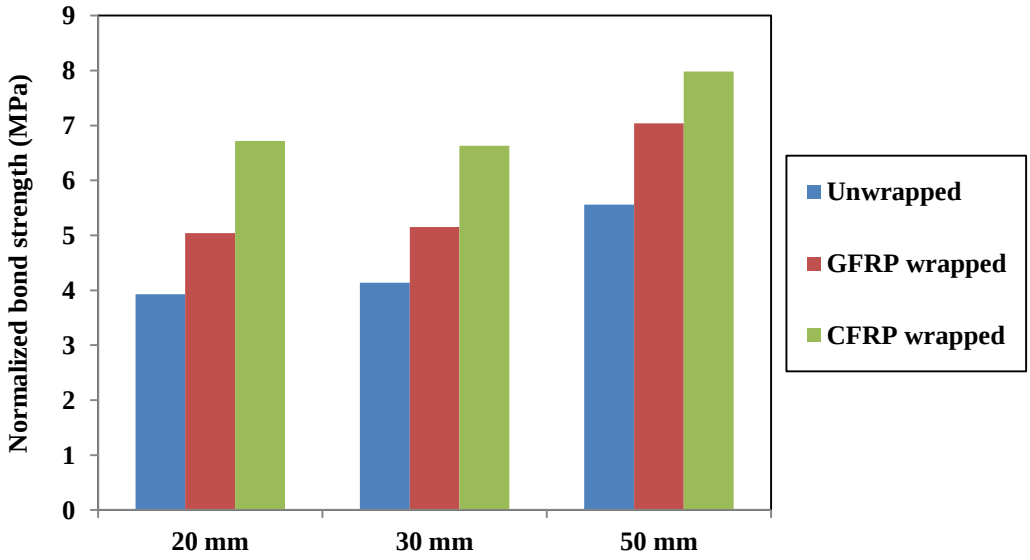

Figure 4.12 Effect of the FRP wrapped on normalized bond strength at different concrete covers

4.3.1.2 Effect of the Concrete Cover on the Bond Strength

Table 4.6 shows the effect of the concrete cover on the bond strength for the three different wrapping conditions. For the unwrapped beams, the normalized bond strength increased by 5% and 41% as the concrete cover increased from 20 mm, to 30 mm and 50 mm, respectively. For the GFRP wrapped beams, the increases in normalized bond strength with concrete cover were similar to those of the unwrapped beams. Also, the bond strength of the 50 mm concrete cover CFRP wrapped beam was 18% greater than that of the beam with a 20 mm concrete cover while the bond strength of the 30 mm cover beam was almost the same as that of the 20 mm cover beam. The normalized bond strengths of the beams for all wrapping conditions and concrete covers are shown in Figure 4.13.

Table 4.6 Effect of concrete cover thickness to the bond strength

Wrapping condition	Beam notation	Normalized bond strength (MPa)	Effect of the concrete cover %
Unwrapped	UN-G1-ST	3.93	100
	UN-G2-ST	4.14	105
	UN-G3-ST	5.56	141
GFRP wrapped	GFRP-G1-ST	5.04	100
	GFRP-G2-ST	5.15	102
	GFRP-G3-ST	7.04	140
CFRP wrapped	CFRP-G1-ST	6.72	100
	CFRP-G2-ST	6.63	99
	CFRP-G3-ST	7.98	119

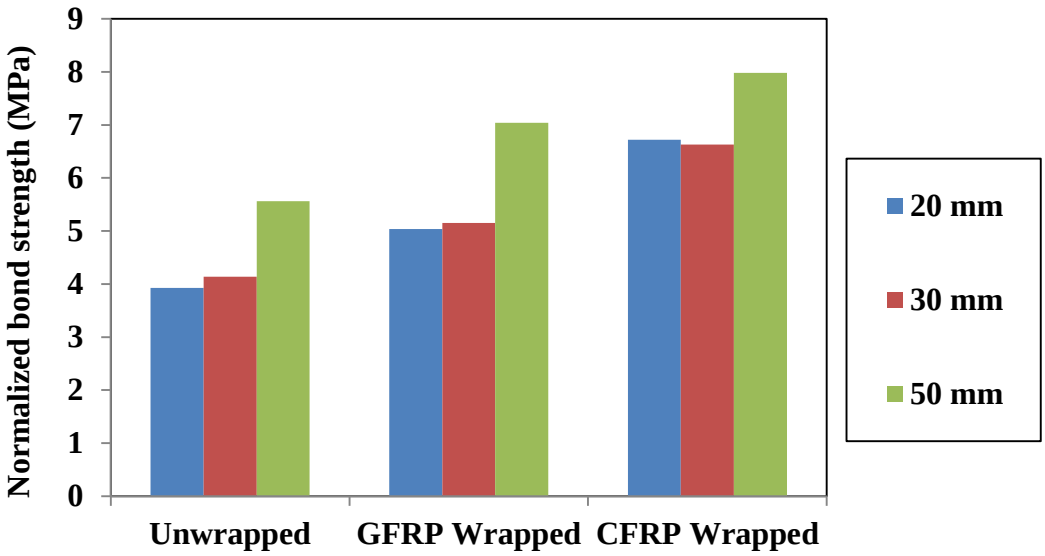

Figure 4.13 Effect of the different concrete cover on the normalized bond strength for all wrapping condition

4.4 Fatigue Results

A total of forty four beams were tested under fatigue loading divided into three groups. Group 1, Group 2 and Group 3 that consisted of 14 beams, 14 beams and 16 beams, respectively. Table 4.7 summarizes the minimum and the maximum loads, the load range as a percentage of the monotonic failure load, the stress range in MPa, the number of cycles to failure and the failure mode for all of the tests.

Table 4.7 Fatigue test results for all groups

Group	Wrapping Condition	Beam Notation	Load			Stress Range (MPa)	Number of Cycle	Failure Mode
			Min (kN)	Max (kN)	Load range* (%)			
Group 1 (20 mm concrete cover)	Unwrapped	UN-G1-83	18	168	83	223	57	Bond
		UN-G1-78	18	158	78	205	179	Bond
		UN-G1-75	18	153	75	200	42,086	Bond
		UN-G1-65	18	135	65	174	52,741	Bond
		UN-G1-55	18	117	55	147	1,000,000	Run Out
	GFRP wrapping	GFRP-G1-83	23	213	83	282	144	Bond
		GFRP-G1-78	23	203	78	267	296	Bond
		GFRP-G1-75	23	196	75	257	3,782	Bond
		GFRP-G1-65	23	173	65	223	49,086	Bond
		GFRP-G1-61	23	163	61	208	585,114	Bar Rupture
	CFRP wrapping	CFRP-G1-80	31	276	80	364	48	Bond
		CFRP-G1-73	31	256	73	334	1,689	Bond
		CFRP-G1-67	31	225	67	304	6,352	Bond
		CFRP-G1-65	31	230	65	297	18,623	Bond
		CFRP-G1-62	31	220	62	282	165,174	Bar Rupture
(30 mm conc	Unwrapped	UN-G2-80	16	145	80	200	300	Bond
		UN-G2-70	16	129	70	174	9,072	Bond

		UN-G2-63	16	117	63	155	22,168	Bond
		UN-G2-59	16	111	59	146	1,000,000	Run Out
		UN-G2-55	16	105	55	136	856,250	Bond
	GFRP wrapping	GFRP-G2-80	20	180	80	247	4,840	Bond
		GFRP-G2-75	20	170	75	231	1,125	Bond
		GFRP-G2-70	20	160	70	216	83,575	Bond
		GFRP-G2-63	20	146	63	194	356,800	Bond
		GFRP-G2-58	20	136	58	179	1,000,000	Run Out
	CFRP wrapping	CFRP-G2-80	26	232	80	318	471	Bond
		CFRP-G2-76	26	221	76	300	2,341	Bond
		CFRP-G2-71	26	209	71	282	5,713	Bond
		CFRP-G2-69	26	203	69	274	87,805	Bond
		CFRP-G2-63	26	189	63	251	137,950	Bond
		CFRP-G2-59	26	178	59	235	387,486	Bar Rupture
Group 3 (50 mm concrete cover)	**Unwrapped**	UN-G3-85	21	198	85	292	365	Bond
		UN-G3-83	21	192	83	283	12,002	Bond
		UN-G3-75	21	177	75	258	25,125	Bond
		UN-G3-70	21	166	70	240	1,982	Bond
		UN-G3-63	21	152	63	216	1,000,000	Run Out
	GFRP wrapping	GFRP-G3-82	27	243	82	357	482	Bond
		GFRP-G3-80	27	238	80	348	6,790	Bond
		GFRP-G3-73	27	219	73	318	1,352	Bond
		GFRP-G3-72	27	216	72	313	26,949	Bond
		GFRP-G3-67	27	203	67	291	199,250	Bar Rupture
		GFRP-G3-60	27	184	60	261	266,538	Bar Rupture
	CFRP wrapping	CFRP-G3-81	30	275	81	404	121	Bond
		CFRP-G3-76	30	259	76	377	1,324	Bond
		CFRP-G3-73	30	250	73	362	5,215	Bond
		CFRP-G3-66	30	230	66	330	26,317	Bond
		CFRP-G3-59	30	207	59	292	243,783	Bar Rupture
		CFRP-G3-53	30	189	53	263	425,147	Bar Rupture

*Percentage of static load

4.4.1 Mode of Failure

All beams tested under fatigue loading were first loaded manually up to the maximum load, and then the load was decreased to the mean load before load cycling commenced. For all the unwrapped beams, flexural cracks appeared at both ends of the lap splice and within the constant moment region during manual loading to the maximum load. Within a few cycles of loading, random flexural cracks appeared outside the constant moment region. The flexural cracks grew vertically and diagonally and stopped growing at about 80% of the beam depth. During the first cycle, splitting longitudinal cracks occurred on the bottom face at both ends of the lap splice. Then the cracks continued to grow with cycling until failure. The splitting cracks grew in width until failure occurred. The rate of growth of the splitting cracks increased as the applied load range increased. At the failure, the splitting cracks traversed the entire lap splice length as shown in Figure 4.14. The concrete in front of the steel bar lugs was clear without any abrasion as shown in Figure 4.15. The concrete chunks were larger for the small concrete cover than for the larger concrete covers as shown in Figure 4.16. The failure of all unwrapped beams was by a bond splitting failure between the concrete and the steel bar.

Figure 4.14 Flexural and splitting cracks on the unwrapped specimen

Figure 4.15 The interface of the concrete ahead of the steel bar ribs for the unwrapped beam

A: for Group 1 B: for Group 3

Figure 4.16 Size of chunk of concrete for different concrete cover

The presence of the FRP sheets prevented the visual monitoring of the splitting cracks in all the wrapped beams. During the initial manual loading to the maximum load, flexural cracks appeared outside the constant moment region in all the test beams and the FRP sheet split at both ends of the lap splice due to flexural cracks. A post-failure investigation was conducted for the GFRP and CFRP wrapped beams. The splitting cracks were finer in width compared to those in the unwrapped beam as shown in Figure 4.17. It is worth mentioning that the splitting cracks were finer in width and larger in number for the CFRP wrapped beams than for the GFRP wrapped beams. Also, as the concrete cover increased the chunks of broken concrete cover became smaller. Moreover, the concrete in front of the steel bar lugs was crushed and abraded for the FRP wrapped beams, as shown in Figure 4.18.

Figure 4.17 Typical failure mode for the FRP wrapped specimens

Figure 4.18 The interface of the concrete ahead of the steel bar ribs for the FRP wrapped specimens

4.4.2 Strain in a Steel Reinforcing Bar

Figure 4.19 shows typical strain distributions in a steel bar along the lap splice for an unwrapped beam. As the beam was loaded monotonically before starting the fatigue loading, random flexural cracks occurred at both ends of the lap splice and within the constant moment region. In the first cycle, the strain gauges located at 100, 200, 300 and 400 mm from the beginning of a bar at a lap splice recorded a sudden increase in the strain reading. From the first cycle to 85 percent of the fatigue life, all of the gauge readings slowly increased. During the last 5% of the fatigue life, the gauge readings at 200 mm from the beginning of the lap splice increased rapidly to high strains approaching those at the end of the lap splice. This flattening of the strain profile is a trend to a constant force in the bar

indicating a lack of shear stress and a partial de-ponding between the steel bar and the concrete from the loaded end of the lap splice to the location of the stain gauge.

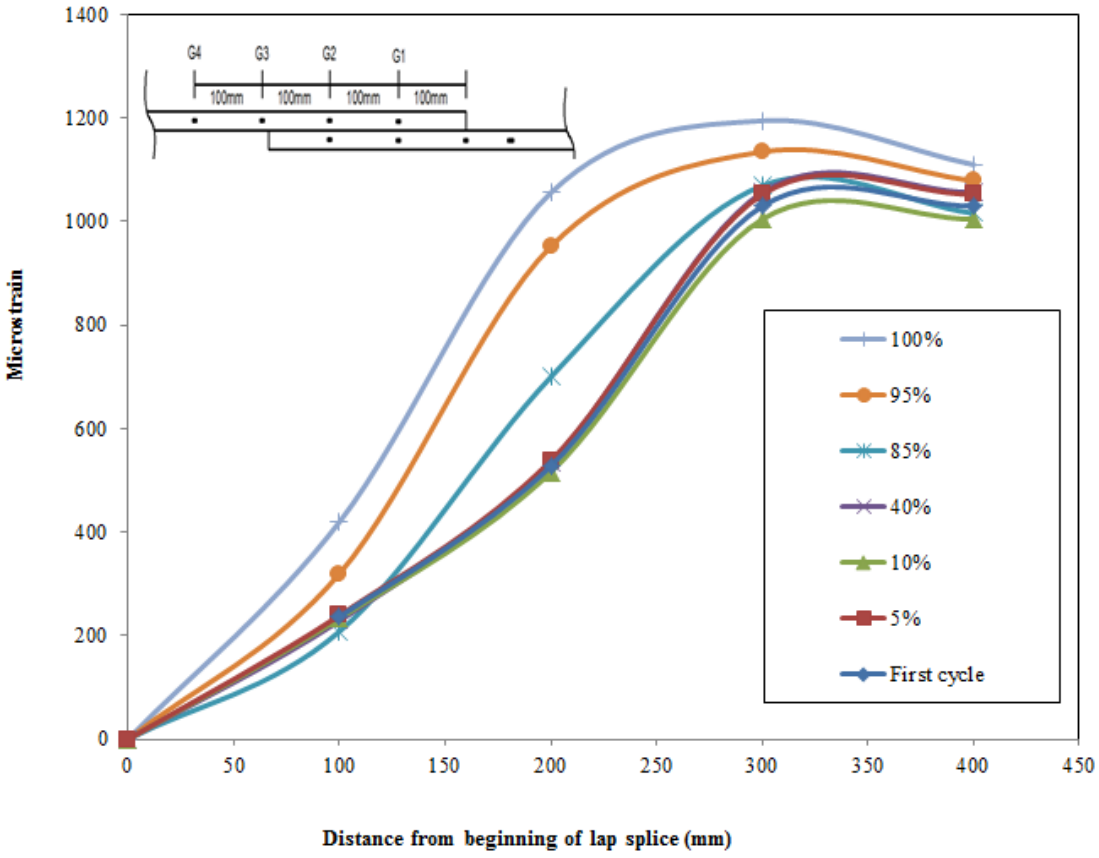

Figure 4.19 Strain distribution along the lap splice for beam UN-G1-75

Typical strain distributions along the lap splice under fatigue loading for an FRP wrapped specimen failed by bond are shown in Figure 4.20. As the number of cycles increased, the strain readings at 200 mm increased toward the level of the strain at the loaded end of the lap splice. This indicates that debonding between the steel bar and the concrete along the lap splice from 200 mm to the loaded end.

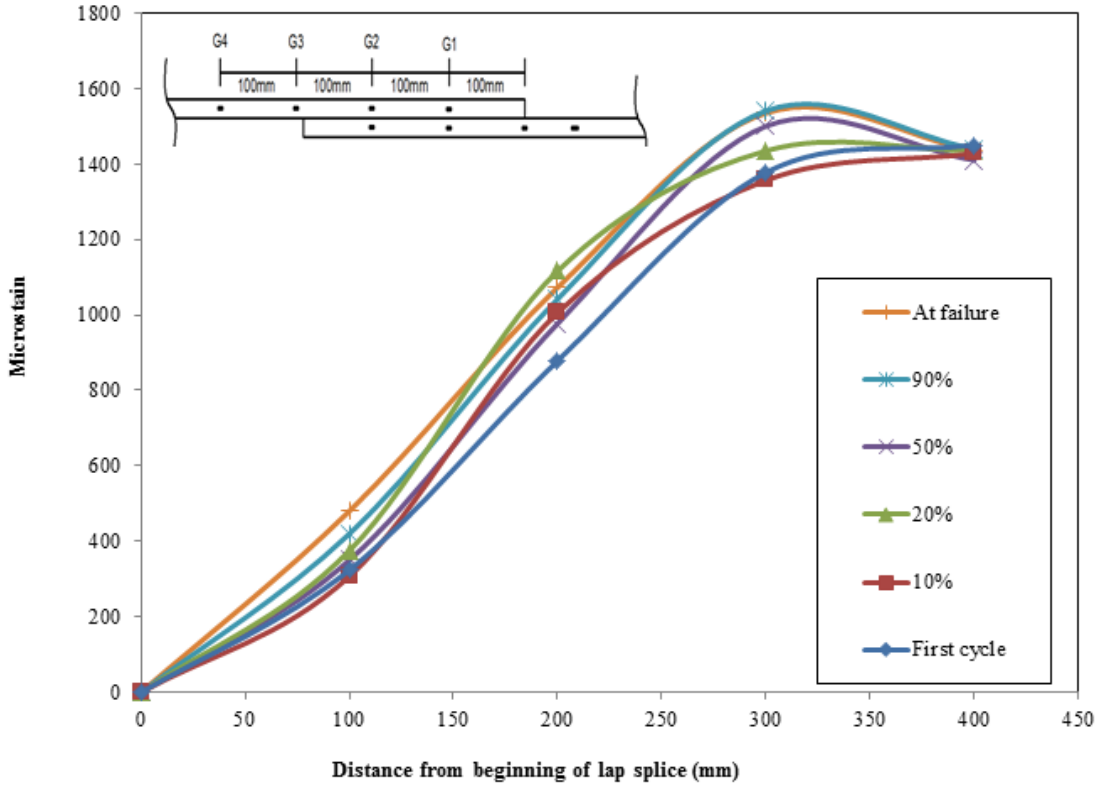

Figure 4.20 Strain distribution along the lap splice for beam GFRP-G1-75

4.4.3 Fatigue Life

As the load range increased, the fatigue life decreased linearly on logarithmic axes of the load range versus number of cycles to failure for all the unwrapped and FRP wrapped beams tested under fatigue loading, as summarized in Table 4.7. The mode of failure for all the unwrapped beams was a splitting bond failure. For all the FRP wrapped beams, the mode of failure was a splitting bond failure, except for those beams that exceeded the fatigue life limits for a longitudinal bar proposed by (Helgason and Hanson 1974) which failed by fatigue rupture of the longitudinal steel bars. Helgason and Hanson (1974) studied the fatigue of steel bars and proposed the following equation for the bar fatigue life:

$$log_{10}N = 6.696 - 0.0055f_r \qquad 4.10$$

where N is the fatigue life and f_r is the applied stress range in a steel rebar (MPa).

All the fatigue results obtained from the tests for Group 1, Group 2 and Group 3 are shown in Figure 4.21, Figure 4.22 and Figure 4.23, respectively. These figures show the load range in kN versus the fatigue life on logarithmic scales. The fatigue life of the beams varies linearly with the load range on the logarithmic scales used and the monotonic failure test results fall close to the best fit for the fatigue test data. For all the different concrete covers, the FRP sheet increased the fatigue bond strength and fatigue life compared to that of the unwrapped beams, with an incremental improvement that was higher for the CFRP sheet than for the GFRP sheet. Best fit linear curves fitted to the fatigue data are shown in the figures. For Group 1, the fatigue data shows a good correlation to the best fit curves with R^2 values of 0.90, 0.98 and 0.98 for the unwrapped, GFRP wrapped and CFRP wrapped beams, respectively. Also, the fatigue data for Group 2 fall close to their best fit curves with R^2 values that vary from 0.94 to 0.97. However, for Group 3, the scatter of the fatigue data for unwrapped beams and the GFRP wrapped gave larger R^2 values of 0.80 and 0.87, respectively. The R^2 value for the CFRP wrapped beams for Group 3 was 0.99.

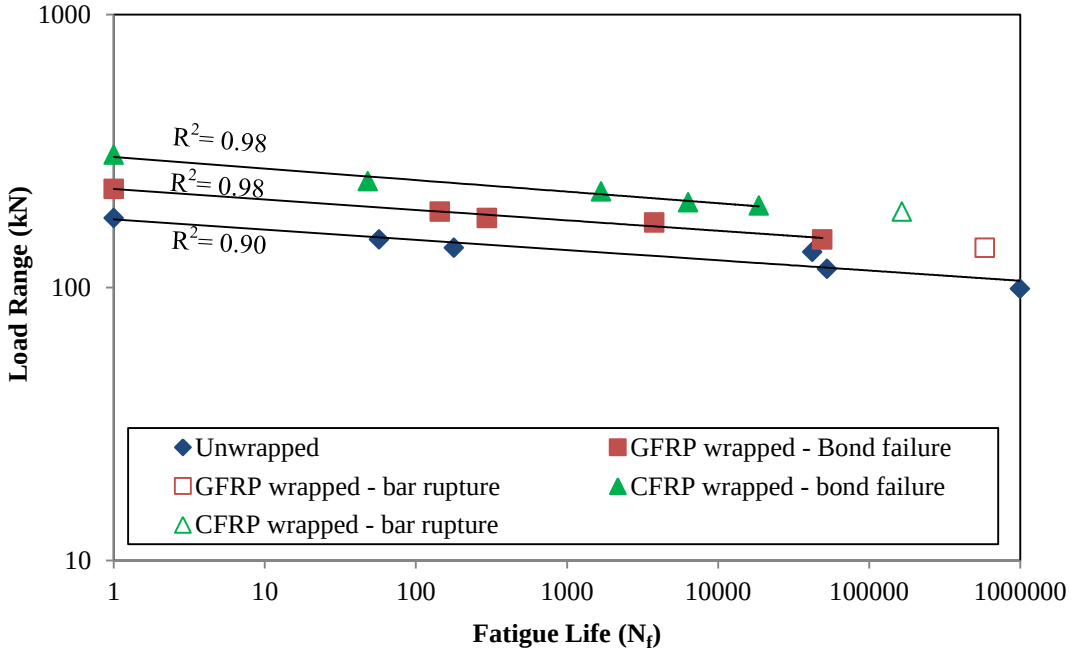

Figure 4.21 Fatigue test results for the unwrapped and FRP wrapped beams with best fit curves for Group 1 (20 mm concrete cover)

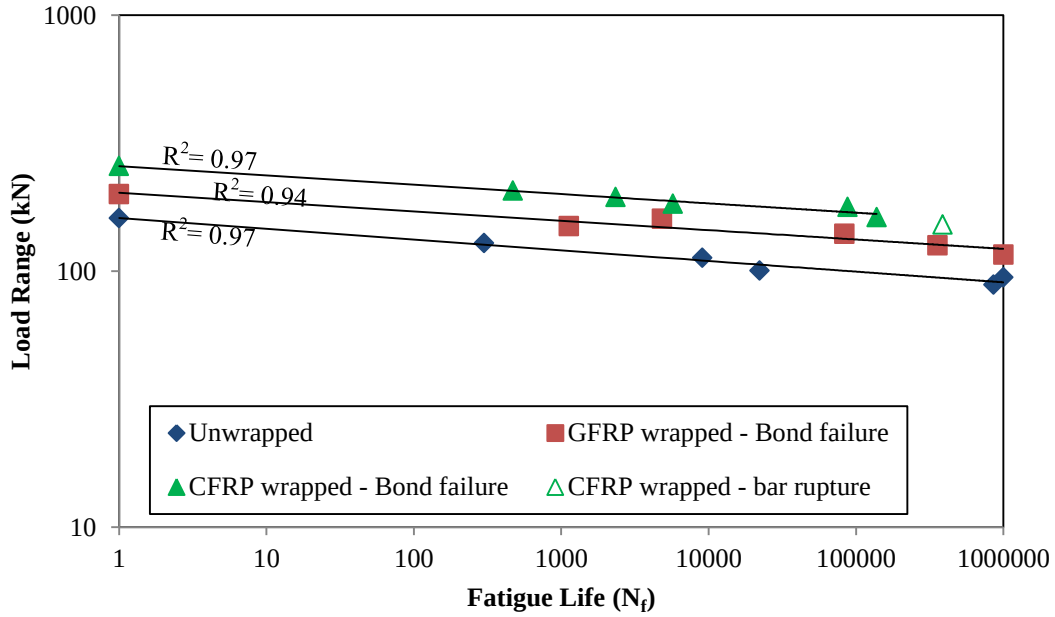

Figure 4.22 Fatigue test results for the unwrapped and FRP wrapped beams with best fit curves for Group 2 (30 mm concrete cover)

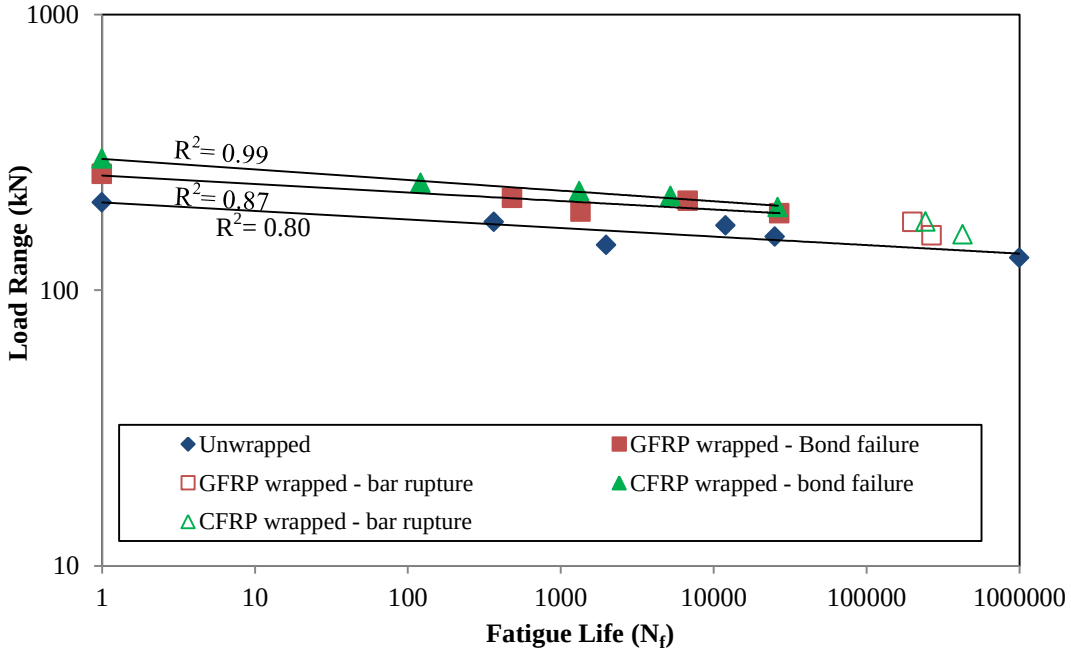

Figure 4.23 Fatigue test results for the unwrapped and FRP wrapped beams with best fit curves for Group 3 (50 mm concrete cover)

Fatigue data plots in terms of stress range versus fatigue life on logarithmic- logarithmic scales for Group 1, Group 2 and Group 3 are shown in Figure 4.24, Figure 4.25 and Figure 4.26, respectively. For all the groups, the bond fatigue strengths were lowest for the unwrapped beams, higher for the GFRP wrapped beams and highest for the CFRP wrapped beams. For each group, a minimum of one beam exceeded the fatigue life limits for a longitudinal bar proposed by Helgason and Hanson (1974) and failed by bar rupture as shown in Figure 4.24, Figure 4.25 and Figure 4.26for Group 1, Group 2 and Group 3, respectively. In each group, one unwrapped beam tested at a low load range did not fail within the one million cycles chosen as an endurance fatigue limit and was retested at a higher load range. The endurance fatigue limit for the unwrapped beams was 55%, 59% and 63% of the monotonic failure load for Group 1, Group 2 and Group 3, respectively.

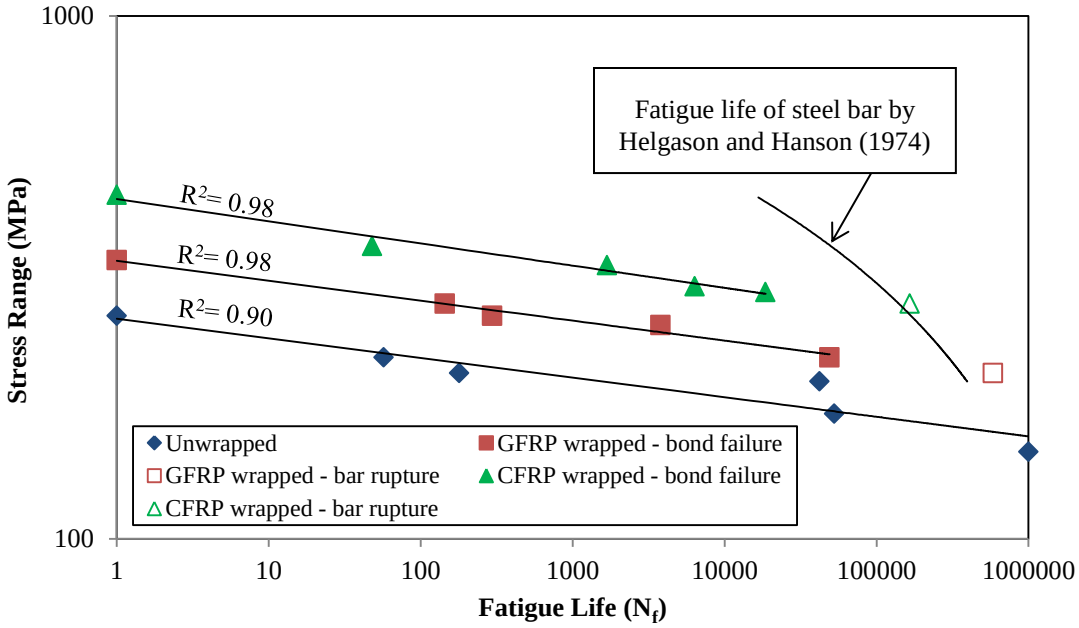

Figure 4.24 Stress range versus fatigue life for the test data with the bar fatigue limit for Group 1 (20 mm concrete cover)

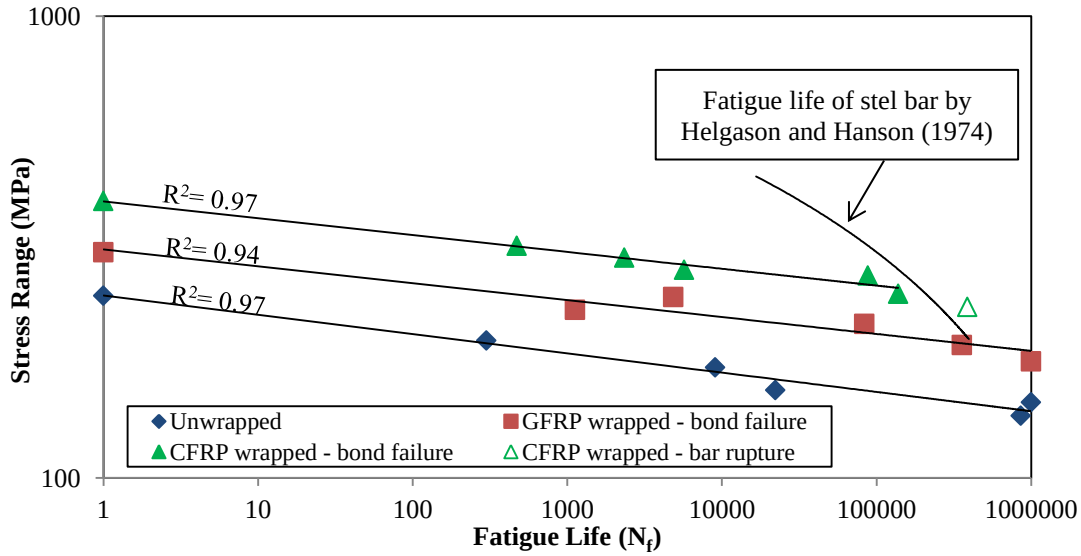

Figure 4.25 Stress range versus fatigue life for the test data with the bar fatigue limit for Group 2 (30 mm concrete cover)

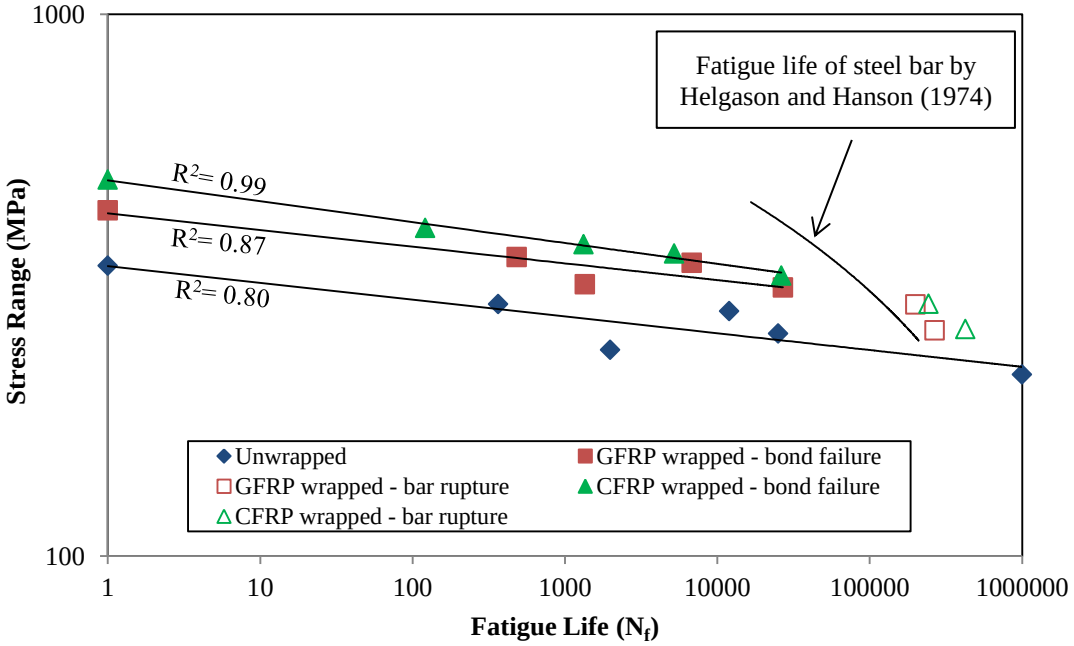

Figure 4.26 Stress range versus fatigue life for the test data with the bar fatigue limit for Group 3 (50 mm concrete cover)

For each group, the fatigue results were normalized to the ultimate load under the monotonic test and the normalized load range versus fatigue life data are shown in Figure 4.27, Figure 4.28 and Figure 4.29 for Group 1, Group 2 and Group 3, respectively. For each group, best fit curves were fitted to the normalized experimental fatigue data that failed by bond using an Excel least squares program and the fatigue data for the unwrapped, GFRP wrapped and CFRP wrapped beams show a good correlation to the best fit curves. The normalized data shows a good correlation to the best fit curves and the R^2 values were 0.92, 0.95 and 0.85 for Group 1, Group 2 and Group 3, respectively. This suggests that a single mechanism is responsible for the monotonic and fatigue failures for all wrapping conditions and all different concrete covers.

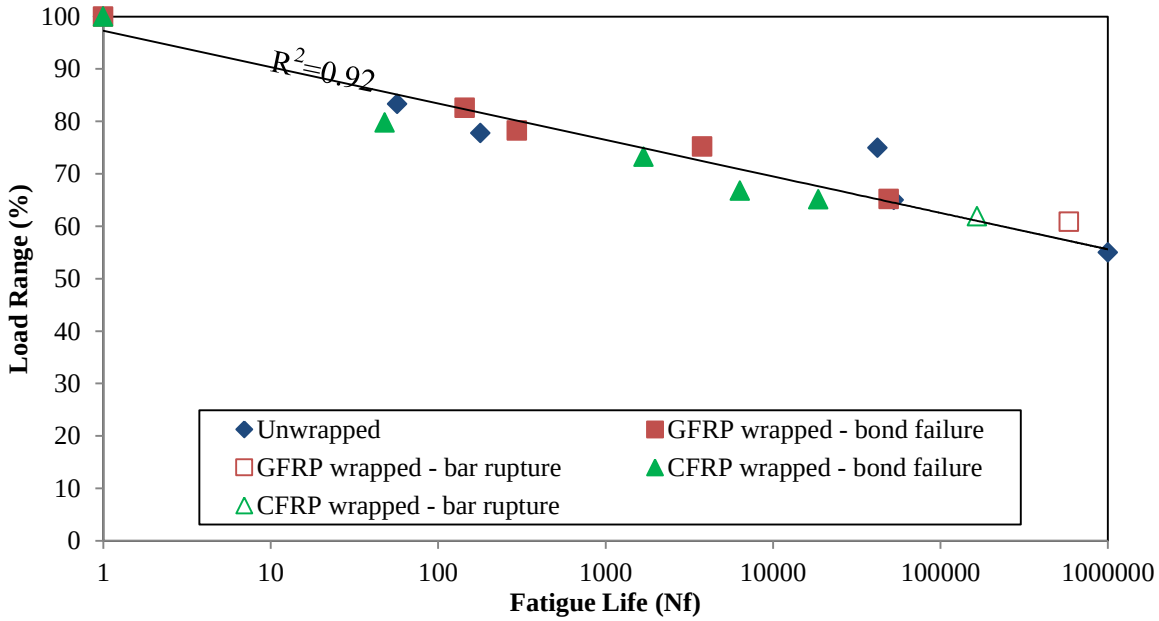

Figure 4.27 Normalized data of the fatigue results for unwrapped and FRP wrapped beams of Group 1 (20 mm concrete cover)

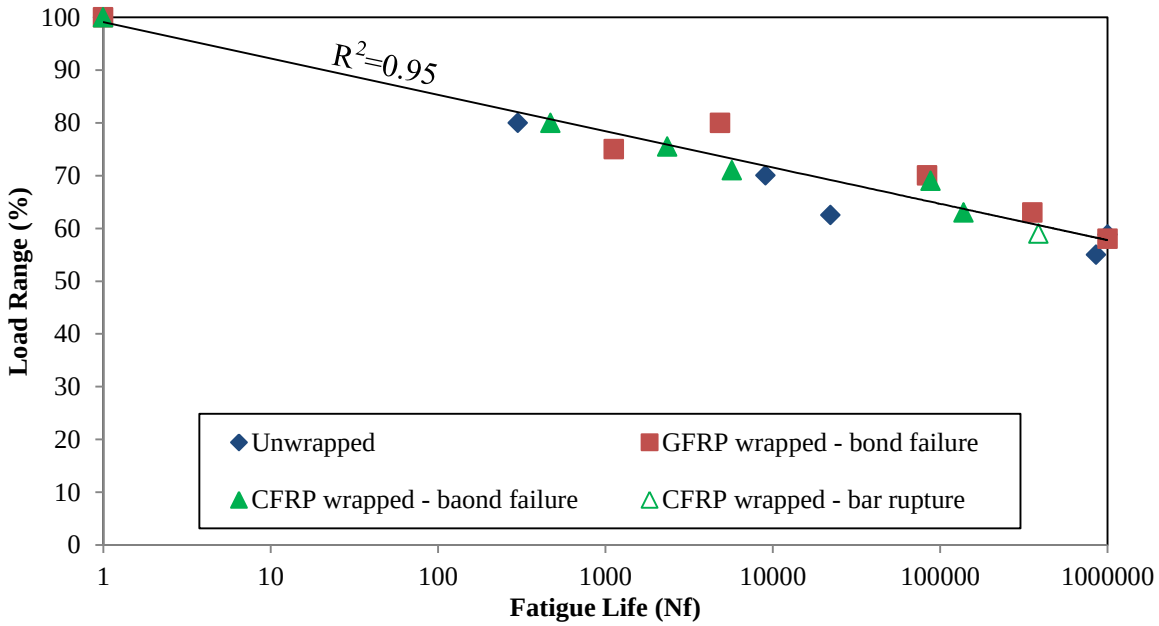

Figure 4.28 Normalized data of the fatigue results for unwrapped and FRP wrapped beams of Group 2 (30 mm concrete cover)

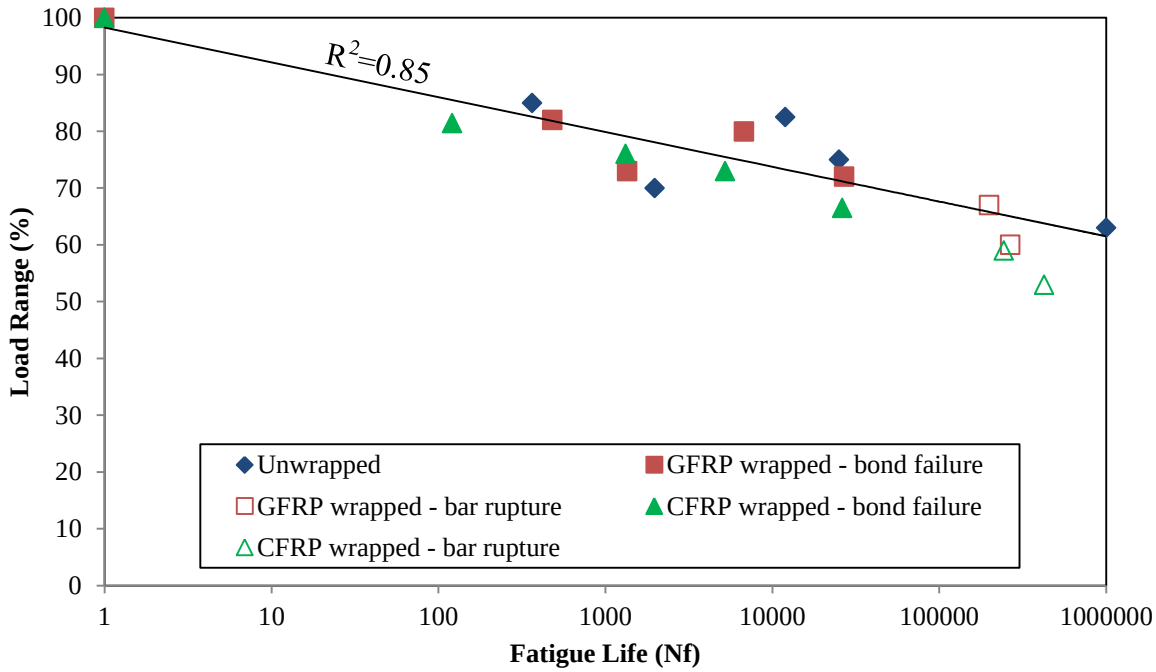

Figure 4.29 Normalized data of the fatigue results for unwrapped and FRP wrapped beams of Group 3 (50 mm concrete cover)

The fatigue data for all different concrete covers, thicknesses and wrapping conditions were normalized to their ultimate monotonic load as shown in. One single best fit curve was used to fit all the fatigue data that failed by bond strength. The R^2 value for this best fit curve was 0.91. This suggests that, a single mechanism is responsible for the bond failure for all monotonic and fatigue beams.

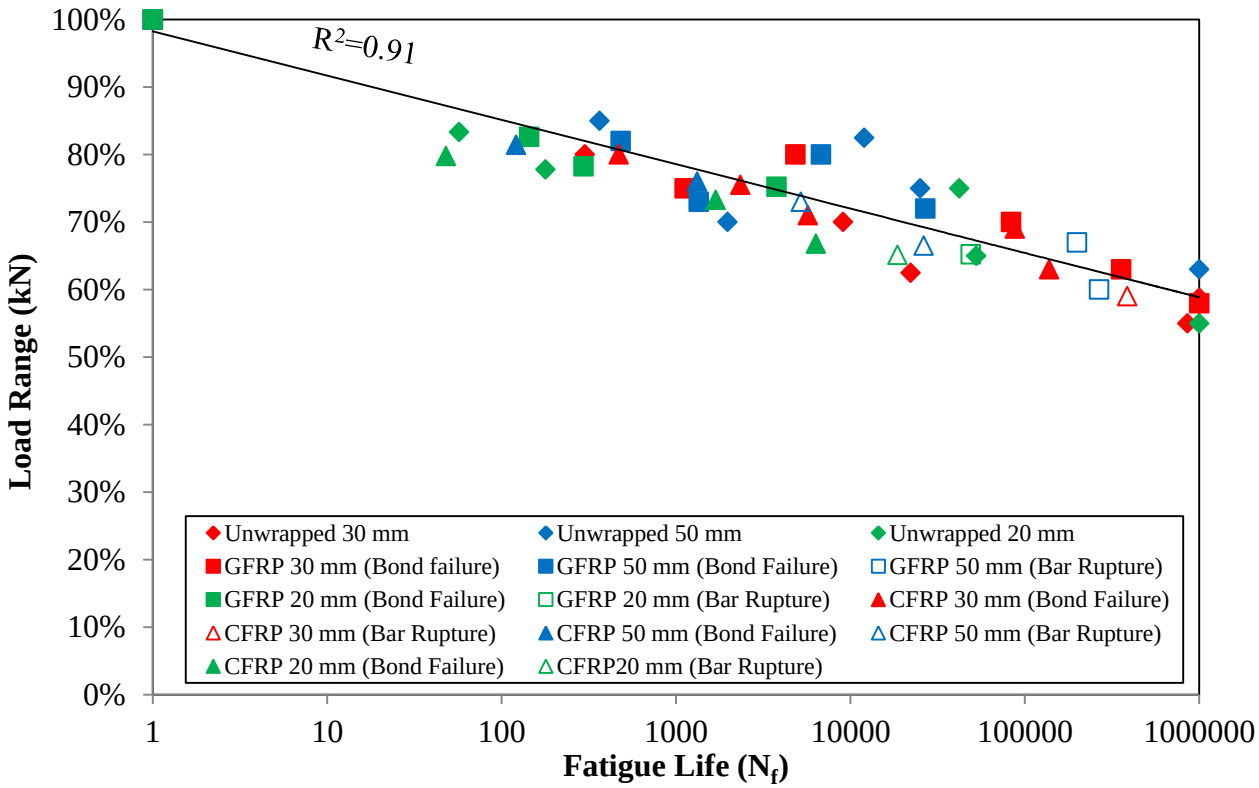

Figure 4.30 Normalized fatigue results for unwrapped and FRP wrapped beams for all different concrete cover with a best fit curve for all data

4.4.4 Increase in Beam Deflection with Number of Cycles

Typical deflection versus load cycles plotted as cycles and as a percentage of the fatigue life for the beams tested at the highest applied load range for each of the unwrapped, GFRP wrapped and CFRP wrapped beams are shown in Figure 4.31, Figure 4.32, Figure 4.33, Figure 4.34, Figure 4.35 and Figure 4.36 for Group 1, Group 2 and Group 3, respectively. At the beginning of each test, the deflection increased rapidly as the steel bars started to move breaking the adhesion and friction forces and then deforming the concrete ahead of the ribs to activate a resisting bearing force. For all the unwrapped beams under fatigue loading, the deflection showed only a small change from 10% to 95% of the fatigue life and then increased rapidly during the last 5% of the fatigue life and the failure happened suddenly

without warning. For all the GFRP wrapped beams, the deflection behaviour was similar to the unwrapped beams with a slow increase from the beginning of a test until 90% of the fatigue life; however, during the last 10% of the fatigue life the deflection increased continuously providing a warning before failure. The deflection of all the CFRP wrapped beams is characterized by a rapid initial deflection followed by a phase of slower deflection, but more rapid than for the other two types of beams, and finally a rapid deflection in the last ten percent of the fatigue life. The rapid deflection at the end of the fatigue life again provided a warning of failure.

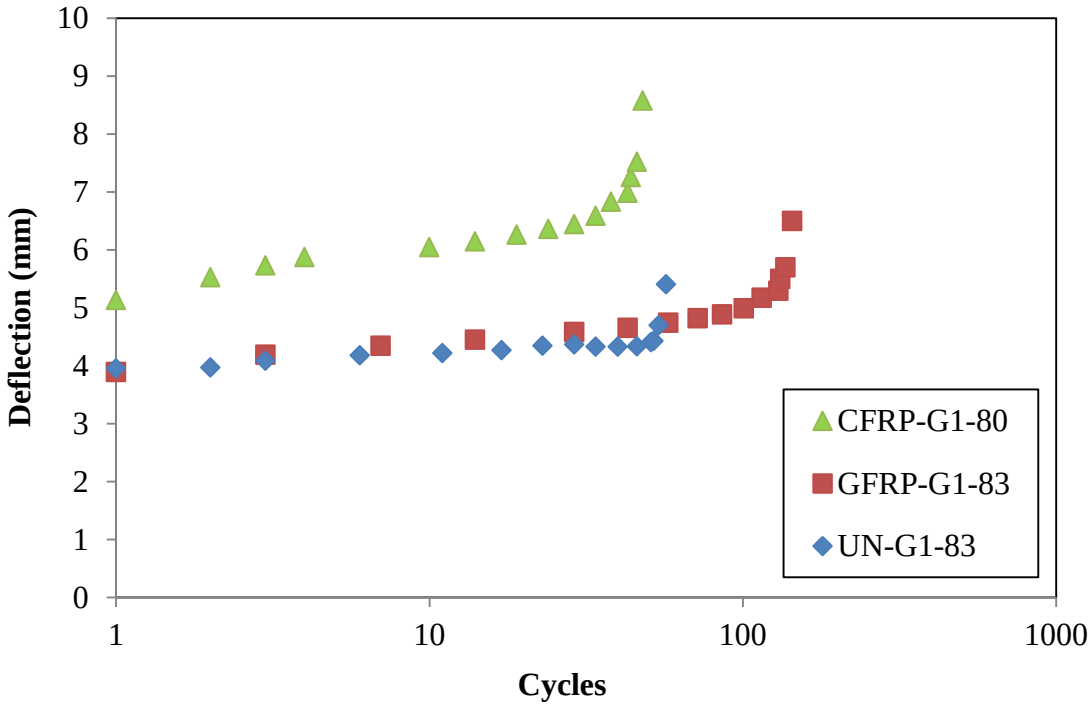

Figure 4.31 Deflection versus load cycles for Group 1 (20 mm concrete cover)

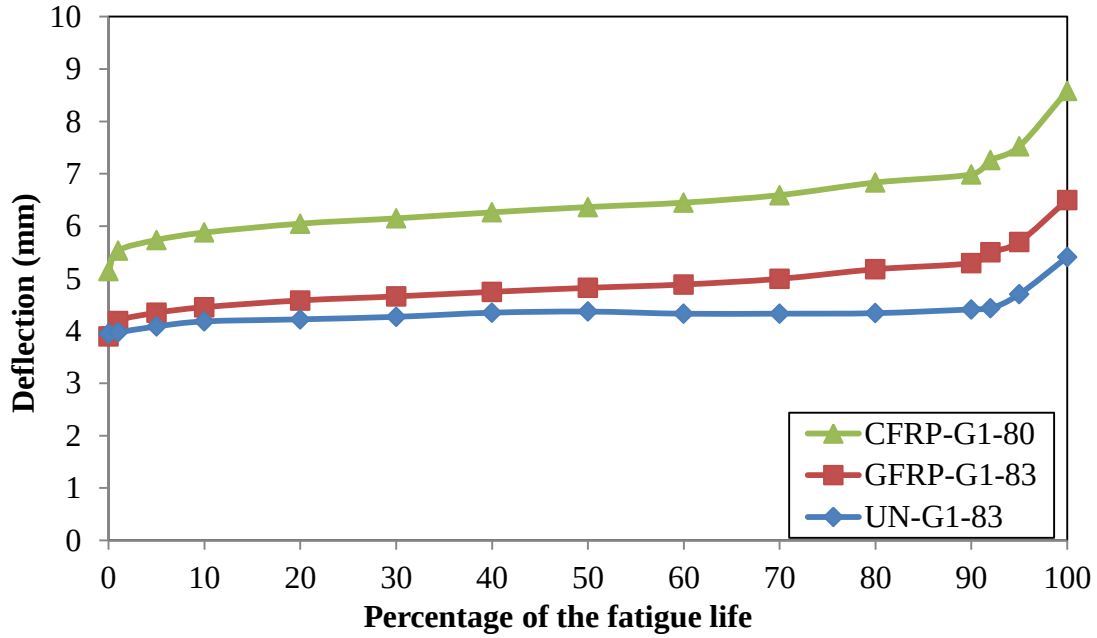

Figure 4.32 Deflection versus load cycles as percentage of the fatigue life for Group 1 (20 mm concrete cover)

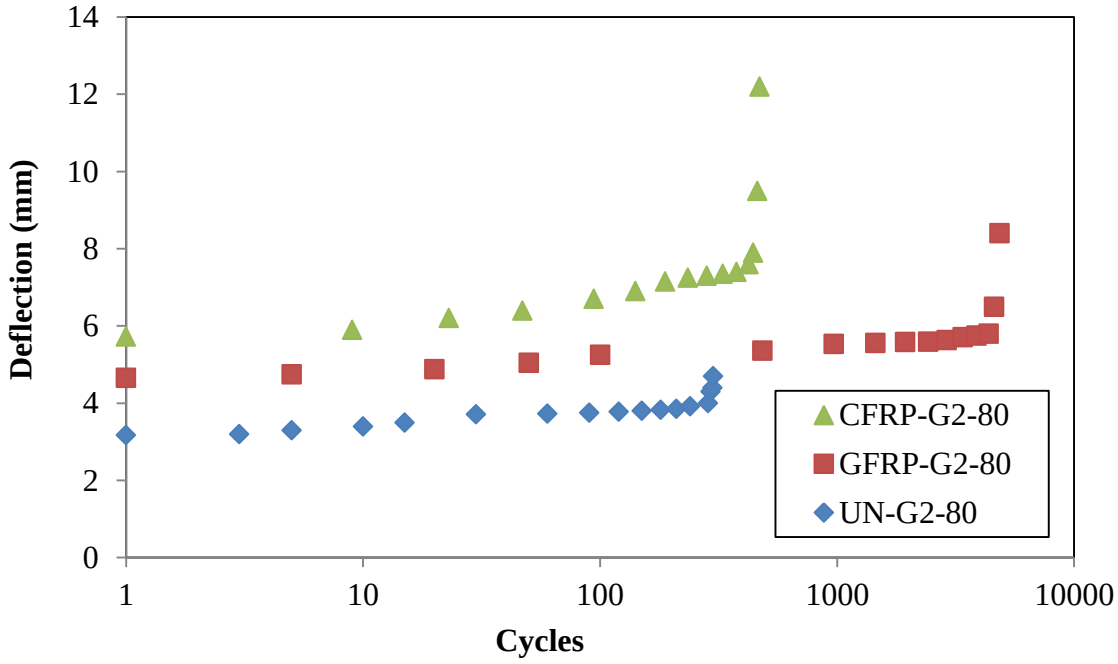

Figure 4.33 Deflection versus load cycles for Group 2 (30 mm concrete cover)

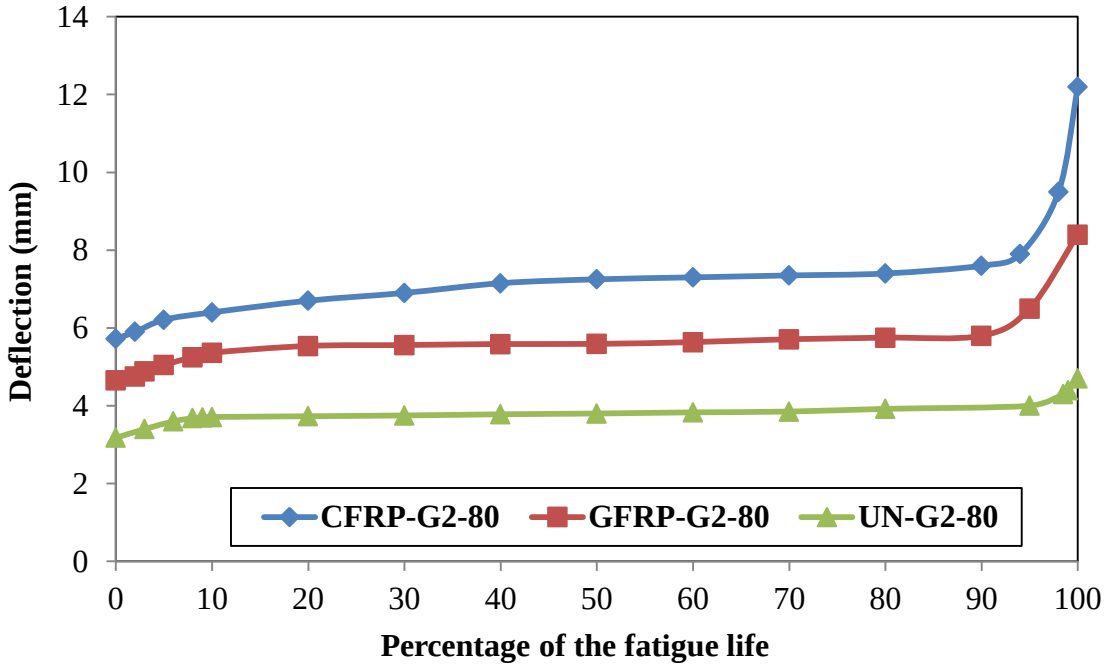

Figure 4.34 Deflection versus load cycles as a percentage of the fatigue life for Group 2 (30 mm concrete cover)

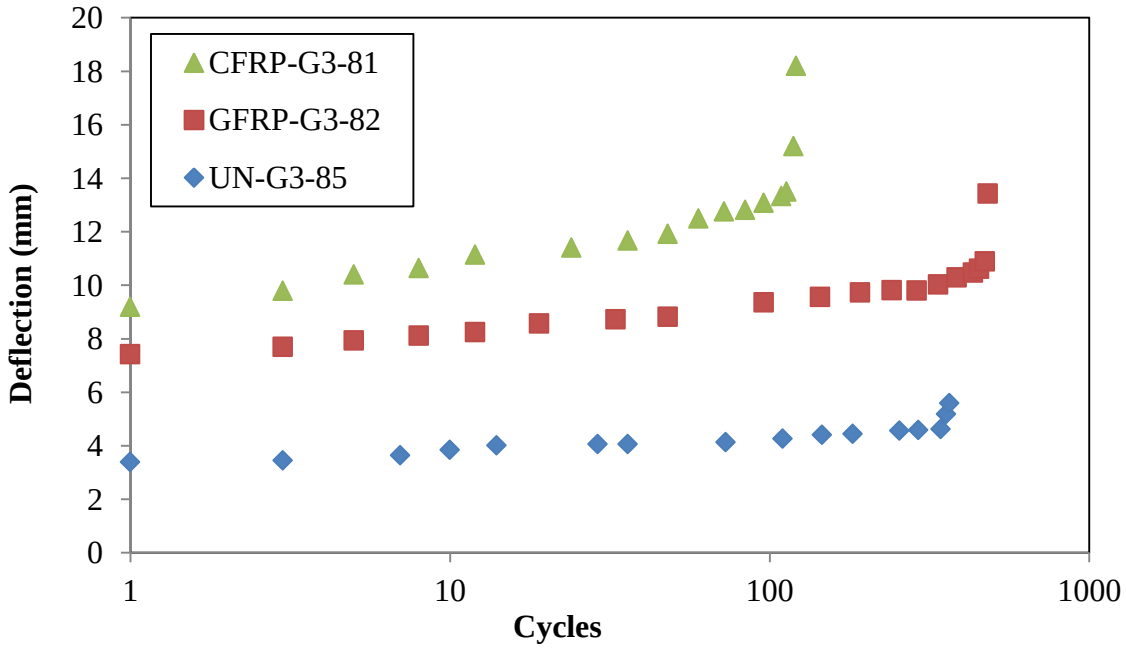

Figure 4.35 Deflection versus load cycles for Group 3 (50 mm concrete cover)

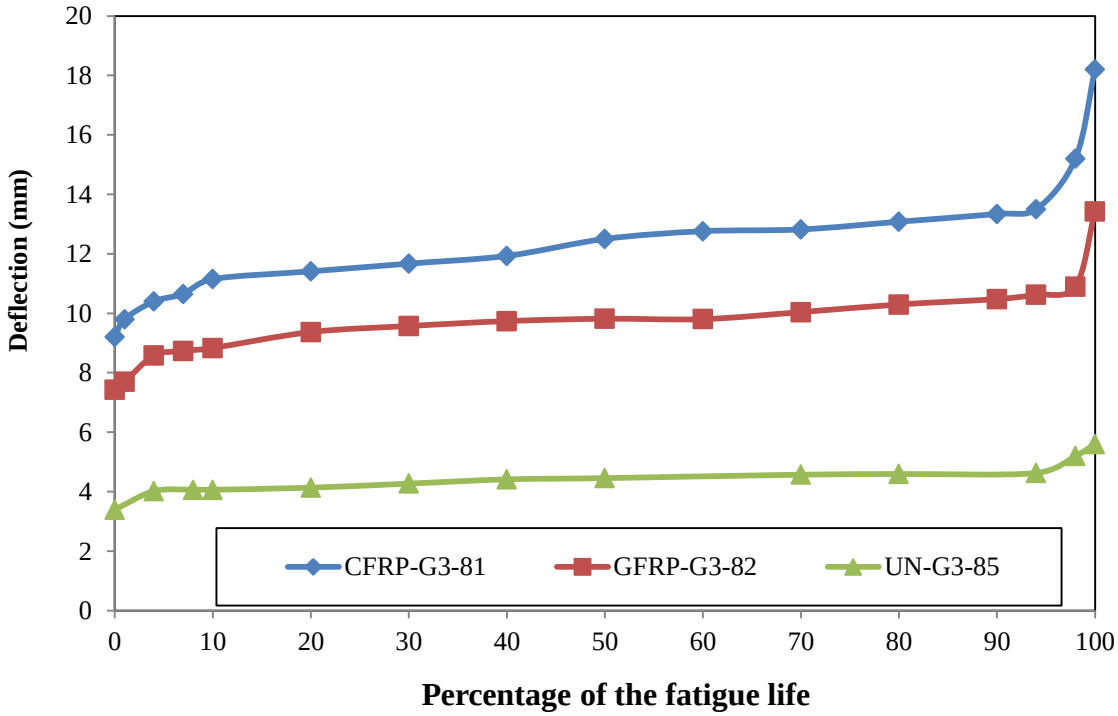

Figure 4.36 Deflection versus load cycles as percentage of the fatigue life for Group 3 (50 mm concrete cover)

4.4.5 Slip Behaviour

Only for Group 1 was the slip measured during the test. Load versus slip data were recorded only at the minimum and maximum applied loads of loading cycles. The cyclic load versus slip behaviour for the highest load range tested under fatigue load and the slip behaviour under monotonic load are shown in Figure 4.37, Figure 4.38, Figure 4.39 for the CFRP wrapped, GFRP wrapped and unwrapped beams, respectively. The stress at the applied maximum loading for all wrapping conditions was higher than the concrete tensile strength. At the beginning of each fatigue test, the load was increased manually using the set point of the controller to reach the desired maximum load. Then the load was decreased manually to the mean load. During the manual loading in cyclic tests, the slip behaviour was expected to follow the monatomic slip behaviour until the maximum load. On the return to the mean

load, the slip was expected to be higher than the corresponding slip during monotonic loading due to a decreased stiffness. For each wrapping condition, the expected load versus slip behaviour during the initial manual loading is given by a dashed red line. For the wrapped beams, the slip value at the maximum load for the first cycle was close to the value for the monotonic slip curve; however, for the unwrapped beam the slip after the initial loading was slightly greater than for the monotonic curve. As the number of cycles increased, the slope of the slip versus load curves increased due to the deterioration of the concrete surrounding the lap spliced bars. The slope of the load versus slip curves was highest for the CFRP wrapped beams and lowest for the unwrapped beams.

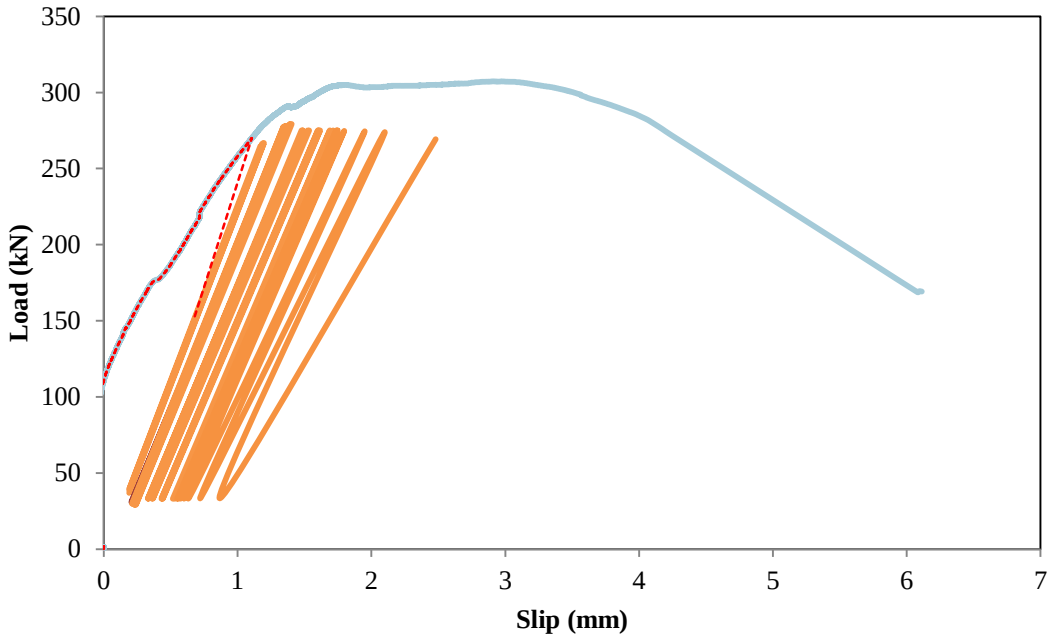

Figure 4.37 The slip behaviour of the monotonic CFRP wrapped beam and the fatigue CFRP-G1-80 beam

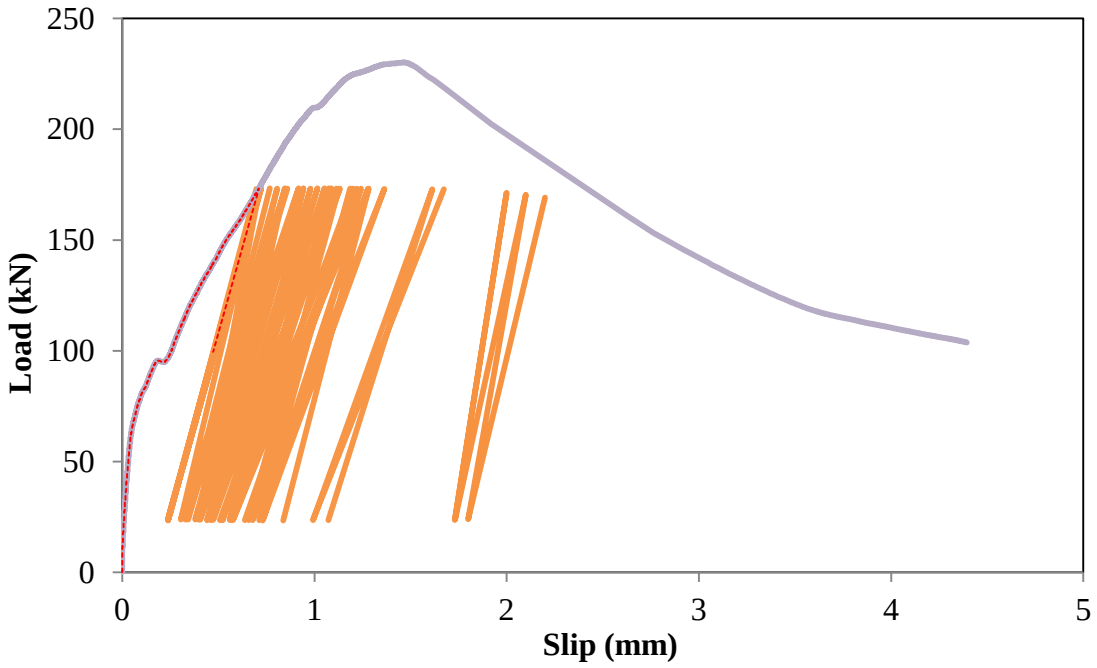

Figure 4.38 The slip behaviour of the monotonic GFRP wrapped beam and the fatigue GFRP-G1-83 beam

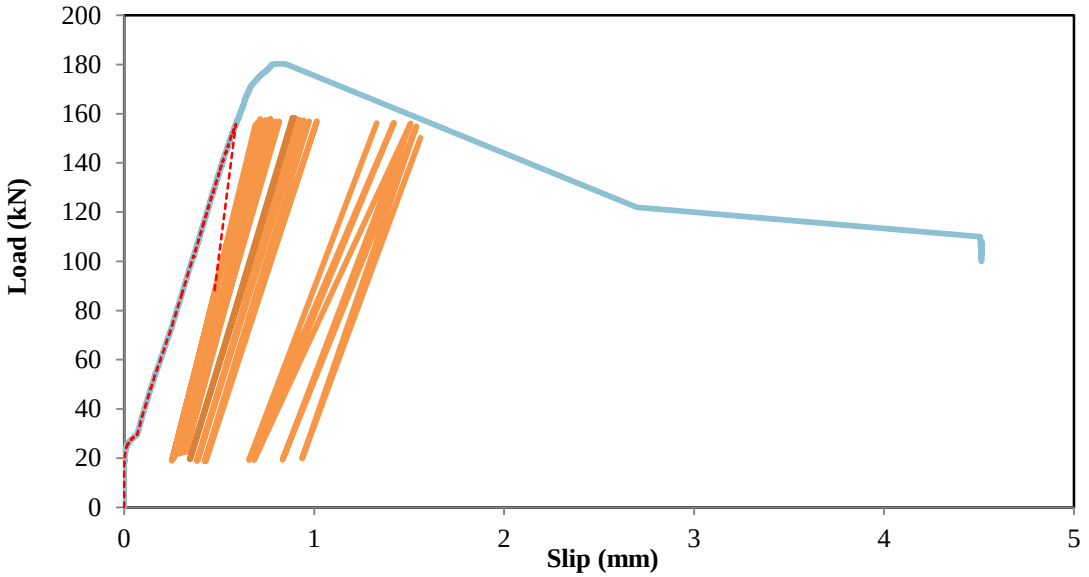

Figure 4.39 The slip behaviour of the monotonic unwrapped beam and the fatigue UN-G1-83 beam

The slip increased with the number of cycles, taken here as a fraction of the fatigue life. Figure 4.40 and Figure 4.41 show the slip behaviour for the beams tested at the highest applied load for the unwrapped, GFRP wrapped and CFRP wrapped beams respectively. During the first few cycles of fatigue loading, the slip of the steel bar increased significantly as the chemical adhesion and friction forces were broken and a resisting bearing force was activated by deforming the concrete in front of the steel bar ribs. For the unwrapped beams, the slip then increased slowly from 5% to 90% of the fatigue life followed by a rapid increase in the last 5% of the fatigue life. The slip behaviour for the GFRP and CFRP wrapped beams was characterized by a more rapid increase between 5% and 90% of the fatigue life. During the last 10% of the fatigue life, there was a rapid increase in slip similar to that seen for the unwrapped beams. This rapid increase in slip near the end of the fatigue life provided a corresponding increase in beam deflection and a warning of failure.

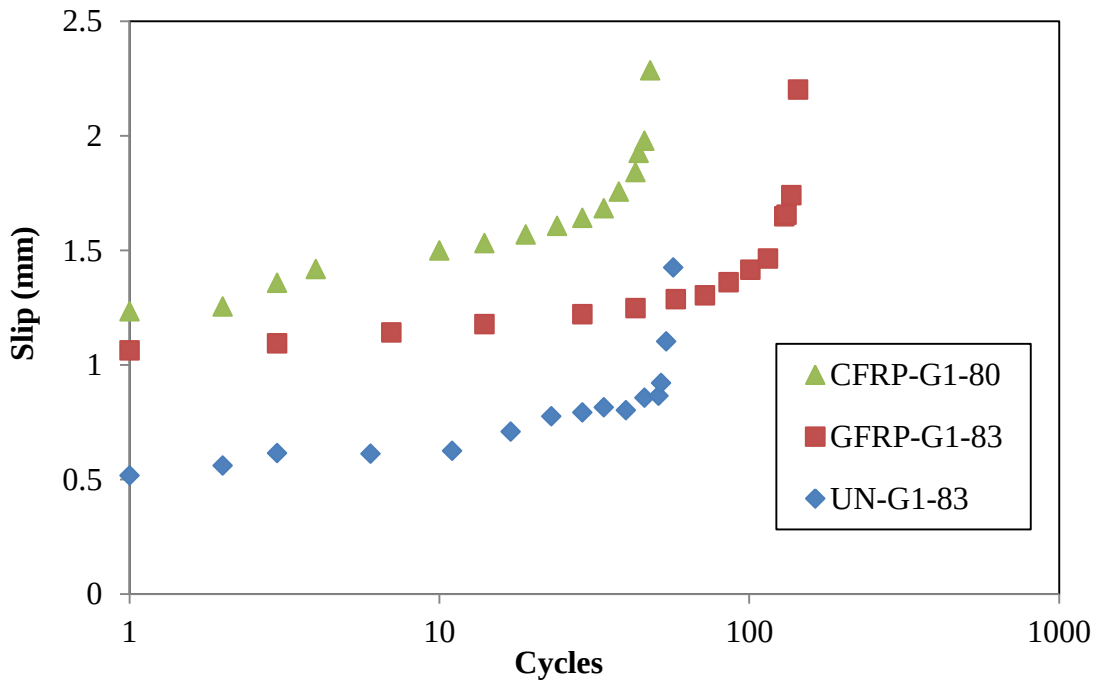

Figure 4.40 Typical slip versus number of cycles as a fraction of the fatigue life curves

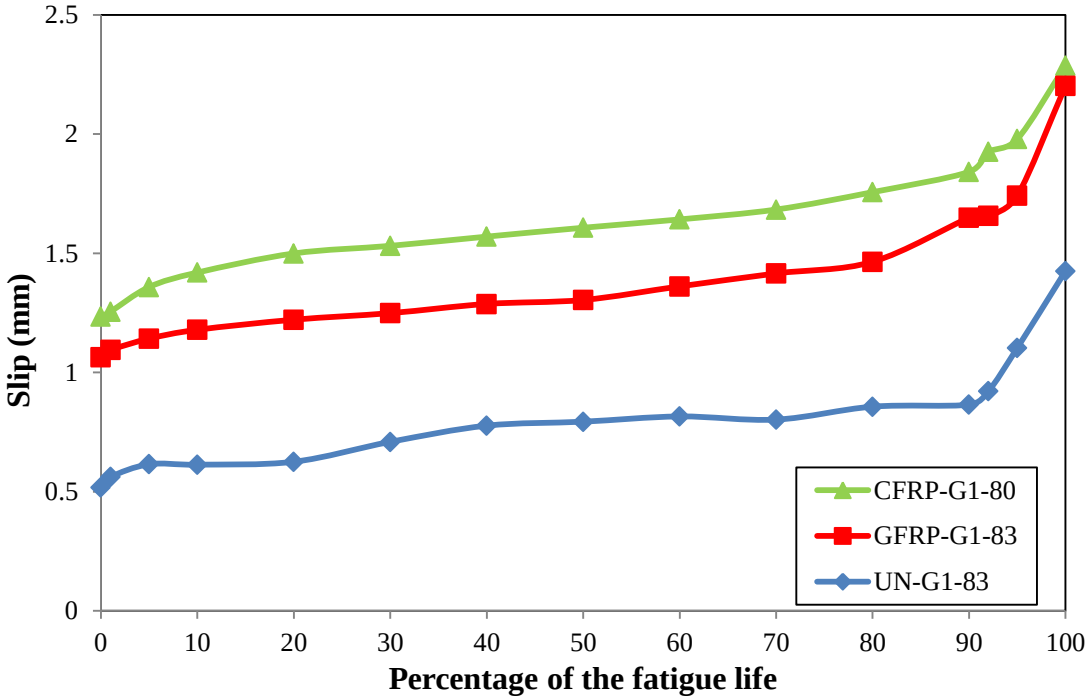

Figure 4.41 Slip versus cycles as percentage of the fatigue life for Group 1 (20 mm concrete cover)

4.4.6 Deflection versus Slip

For all Group 1 beams, the slip of the steel bar was monitored; there was a linear relationship between the slip and the inelastic deflection (total deflection minus the calculated elastic deflection) behaviour for all different wrapping conditions as shown in Figure 4.42. Also, the figure shows that at the beginning of a fatigue test, the rate of increase of deflection with slip was higher than later in the test. After that, the relationship became linear.

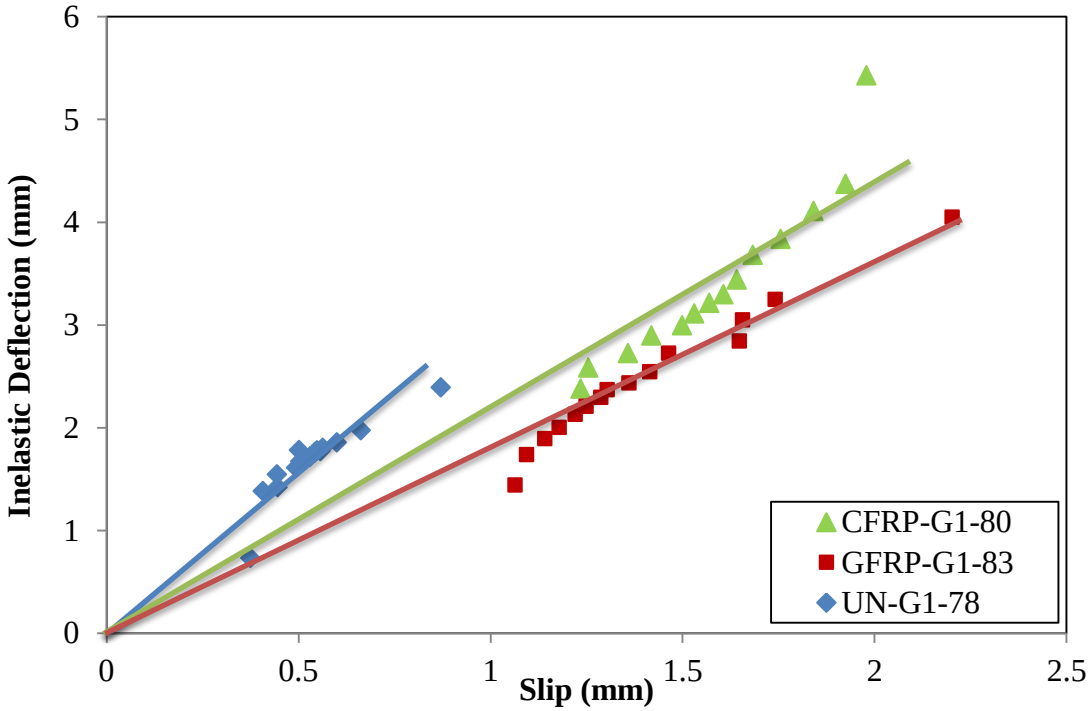

Figure 4.42 Typical slip versus deflection (subtract the elastic deflection) for Group 1 (20 mm concrete cover) for different wrapping conditions

4.5 Discussion of the Fatigue Test Results

For the unwrapped beams, for all different concrete covers, flexural cracks grew at both ends of the lap splice and within the constant moment region during the initial manual loading. After a few cycles, random flexural cracks appeared within and outside the constant moment region. As the number of cycles increased, the splitting longitudinal cracks initiated and propagated from one end of the lap splice to the other.

For the wrapped beams of all concrete cover thicknesses, flexural cracks appeared outside the constant moment region and the FRP sheets split at both ends of the lap splice during fatigue tests. The failure of all the FRP wrapped beams was by bond splitting failure except for those beams that exceeded the fatigue life limits for a longitudinal bar proposed by Helgason and Hanson (1974). These beams failed by fatigue rupture of the longitudinal steel bars. The splitting cracks were finer in width and larger in number for large concrete covers than for

small concrete covers. For all different concrete cover thicknesses, the concrete in front of the steel lugs of the rebars was crushed and abraded.

4.5.1 Fatigue Life

The concrete compressive strength was different for each group. The concrete compressive strength was 42 MPa, 33 MPa and 35 MPa for Group 1, Group 2 and Group 3, respectively. To allow a comparison, the applied fatigue load range was normalized for Group1 and Group 3 by 88% and 97%, respectively, as discussed in section 1.3.1.

Figure 4.43, Figure 4.44 and Figure 4.45 show the normalized fatigue data for all concrete covers with their best fit curves for the normalized data for the unwrapped, GFRP wrapped and CFRP wrapped beams, respectively. The slopes for the best fit curves for the fatigue load range versus fatigue life curves for all different concrete covers were almost the same for the unwrapped beams and the GFRP wrapped beams as shown in Figure 4.43 and Figure 4.44, respectively. However, for the CFRP wrapped beams, the slope of the best fit curve for the normalized data for Group 2 (50 mm concrete cover) was higher than the other groups as shown in Figure 4.45.

All the monotonic test results for all different concrete covers and different wrapping conditions fell close to their fatigue life curves. This suggests that a single mechanism is responsible for the monotonic and fatigue failures for all wrapping conditions and concrete cover thicknesses and that the percentage changes in fatigue strength with changes in wrapping condition and cover thickness are the same as those found in the monotonic tests. As the concrete cover increased, the endurance fatigue limit increased for the unwrapped beams.

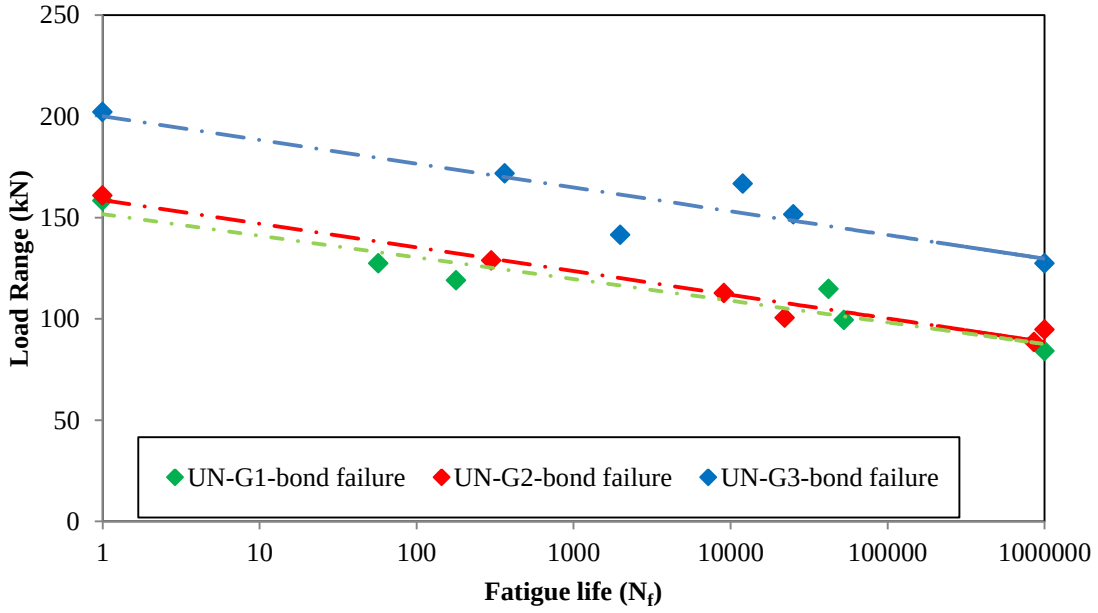

Figure 4.43 Fatigue test results for the unwrapped beams for all concrete covers with the best fit curves for the normalized data

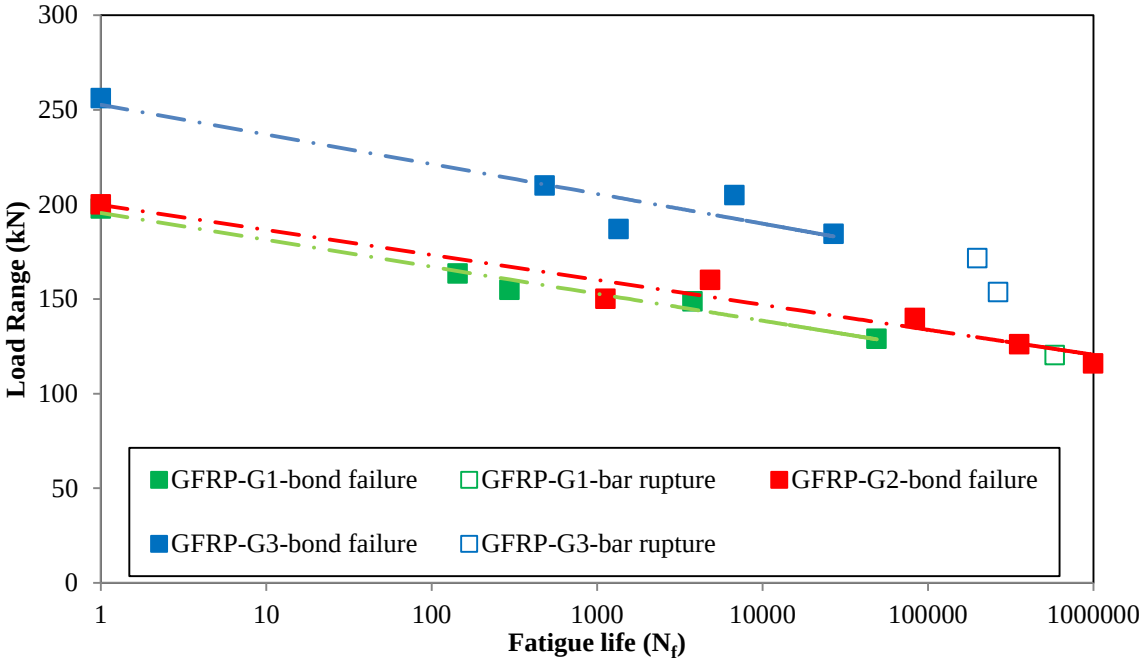

Figure 4.44 Fatigue test results for the GFRP wrapped beams for all concrete cover with the best fit curves for the normalized data

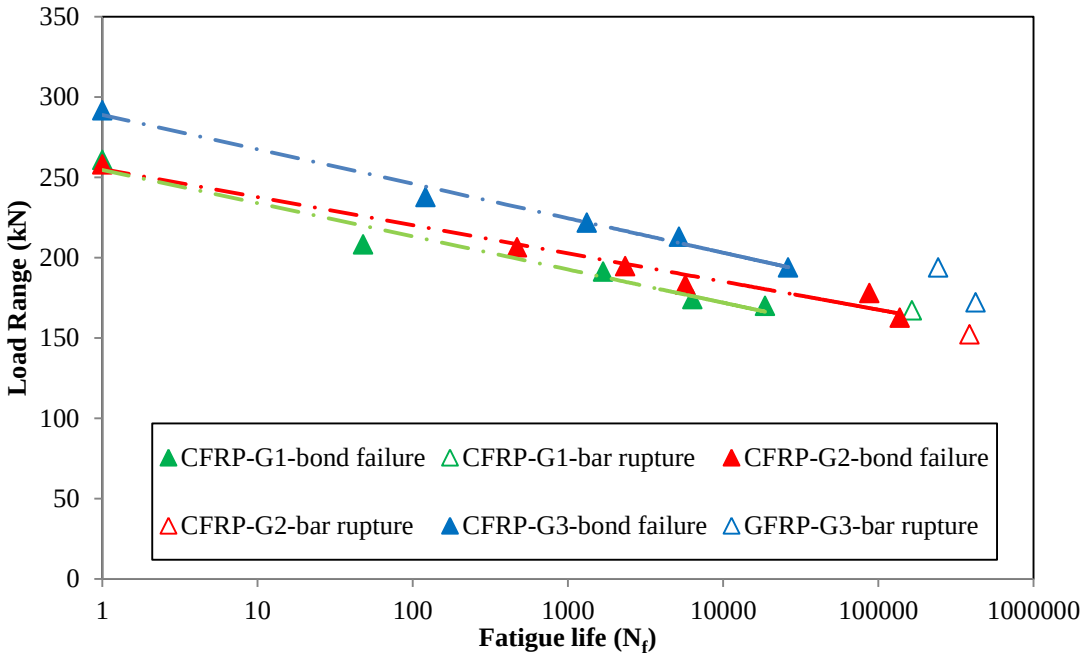

Figure 4.45 Fatigue test results for the CFRP wrapped beams for all concrete covers with the best fit curves for the normalized data

The fatigue test results for all different concrete cover beams in each of the three wrapping conditions tested were normalized to the ultimate loads of their respective monotonic tests and the resulting normalized stress range versus fatigue life data on logarithmic scales are shown in Figure 4.46. One single best fit curve was used to fit the fatigue beams data for all different concrete covers and all different wrapping condition that failed by bond using an Excel least squares program. The R^2 value for the best fit curve was 0.91. The data for the various wrapping options fall into a compact band in the normalized presentation of the figure. This suggests that a single mechanism is responsible for the monotonic and fatigue failures for all wrapping condition and all different concrete covers.

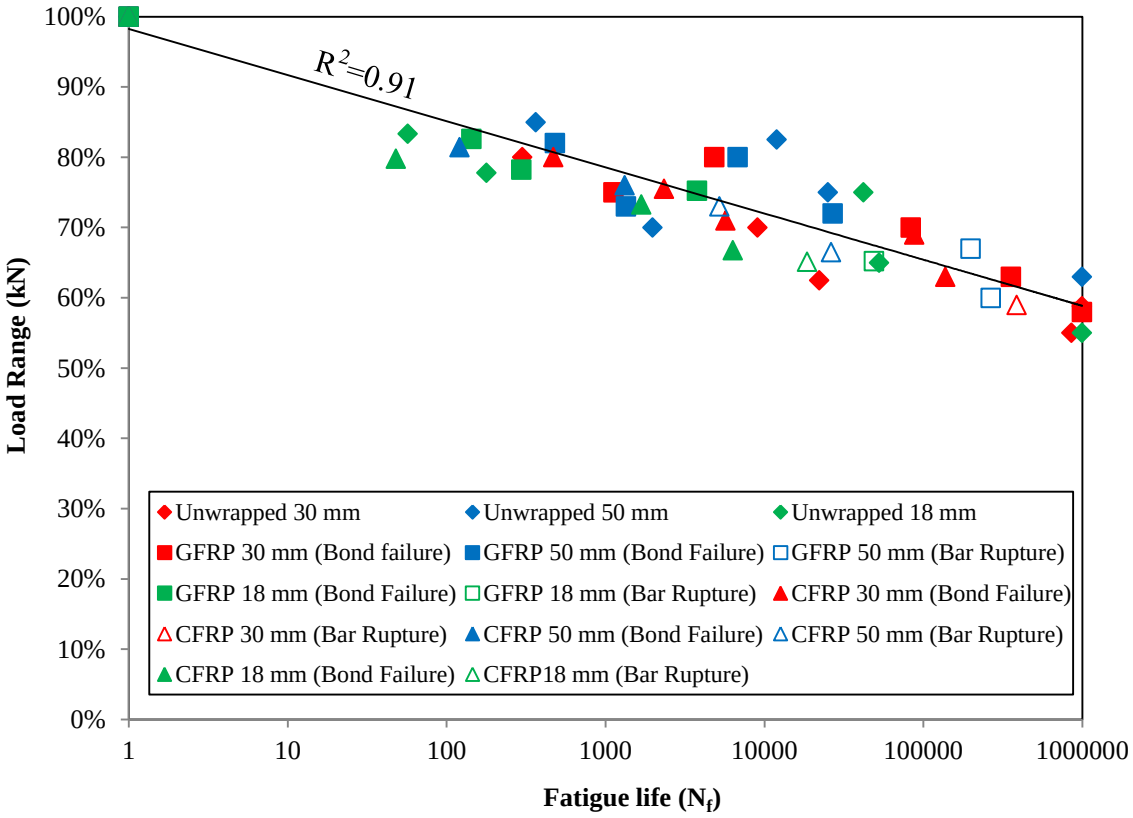

Figure 4.46 Normalized fatigue results for unwrapped and FRP wrapped beams for all different concrete covers together with a best fit curve for all the data

Chapter 5 Modeling of Experimental Results

5.1 Introduction

A mechanism model used to describe the experimental data are presented in this chapter. First, the shear stress distribution and the associated crack growth model used in a previous study by Wahab et al., 2015 will be presented followed by the shear stress distribution and crack growth model used for this study. Then the parameters of the crack growth model will be derived from the fatigue life versus shear stress curve. Finally, a comparison will be made between the observed fatigue life, slip and deflection behaviour and the model results.

5.2 Mode of Failure

A single mode of bond failure was observed for all beams tested under fatigue loading namely: splitting bond failure. This bond failure was characterized by longitudinal splitting cracks that resulted in a partial debonding of the reinforcing steel bar from the surrounding concrete in the lap splice region. For the unwrapped beams, longitudinal splitting cracks occurred on the bottom face at both ends of the lap splice at the beginning of the fatigue tests. As the number of cycles increased, the splitting cracks propagated at both ends of the lap splice. The cracks grew in length and width until failure occurred. The rate of growth of the splitting cracks increased as the applied load range increased.

It was noticed that, in the lap splice beam confined with stirrups, splitting cracks initiated at the beginning of the fatigue test from both ends of the lap splice and propagated toward the other end as load cycling continued Rezansoff et al., (1993); Tocci, (1981) and Tepfers, (1973). For the lap splice beams confined with FRP sheets, the presence of the FRP sheets prevented the visual monitoring of the splitting cracks.

5.3 Shear Stress Distribution and Crack Growth Model (Wahab et al., 2015)

Wahab et al., 2015 studied the shear stress distribution and crack growth in the bond of near surface mounted prestressed FRP bars. It was found that, during a fatigue test, the bond length can be divided into two regions: a fully bonded region and a partially or fully debonded region as shown in Figure 5.1. Also, the shear stress distribution was exponentially distributed along the fully bonded region.

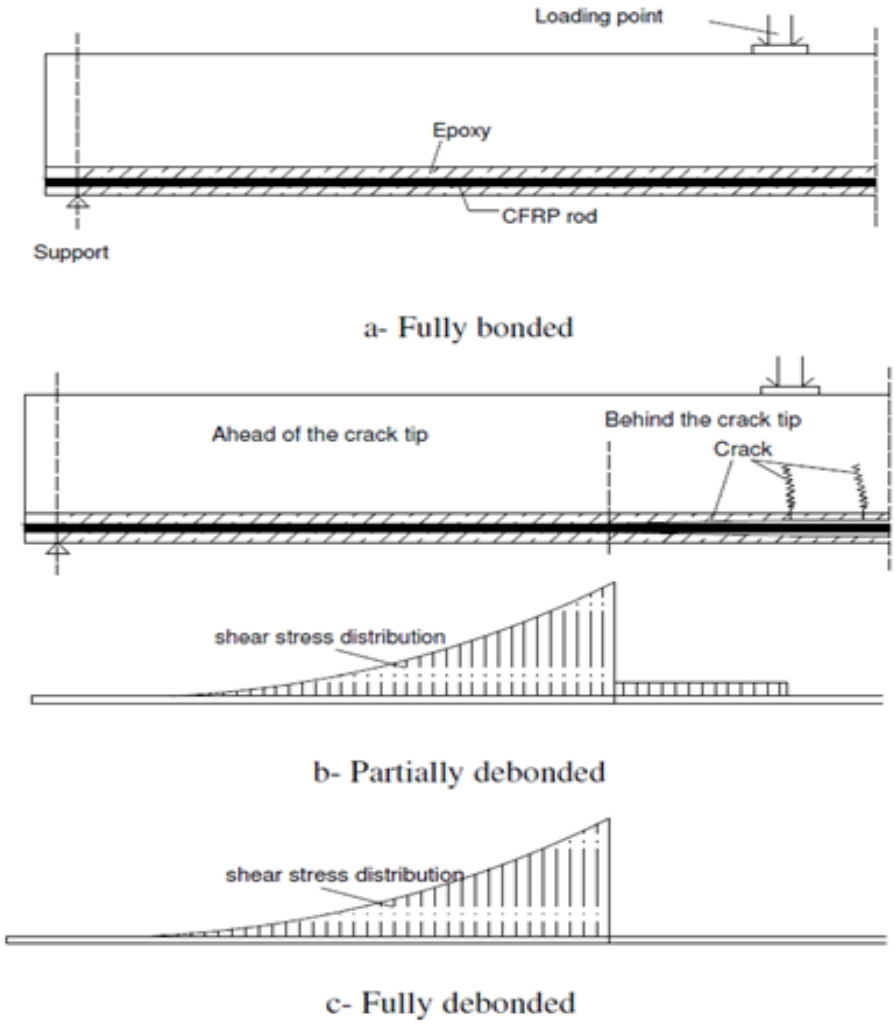

Figure 5.1 Bonded regions and shear stress distribution (Wahab et al., 2015)

5.3.1 Shear Stress Distribution Parameters

Wahab et al., 2015 used enough strain gauges along the bonded length to deduce the form of the shear stress distribution and its changes during their fatigue tests. It was reported that the value of the shear stress in the partially bonded region varied from 1 MPa to 2.25 MPa. The following exponential equations were used to describe the force distribution:

$$F(x) = Fexp^{(-C*x)} \quad 5.1$$

The *C* value was constant for each beam type but varied from 0.004 to 0.012 for the various beam types they tested.

5.3.2 Crack Growth Model

Figure 5.2 shows the crack growth curve used by Wahab, 2011 and Wahab et al., 2015. The following equation was used for the rate of the crack growth:

$$\frac{da}{dn} = \alpha F^{\beta} \quad 5.2$$

where

da is the incremental increase in crack length (mm), *dn* is the incremental number of cycles (cycles), *F* is the force in the CFRP rod at the crack tip which was proportional to the local shear stress driving the crack (kN), β is a constant that depended on the rod type and α is a constant that depended on the rod type, the presence or absence of internal steel and the prestressing force in the CFRP rod.

The β and α are different for each beam type.

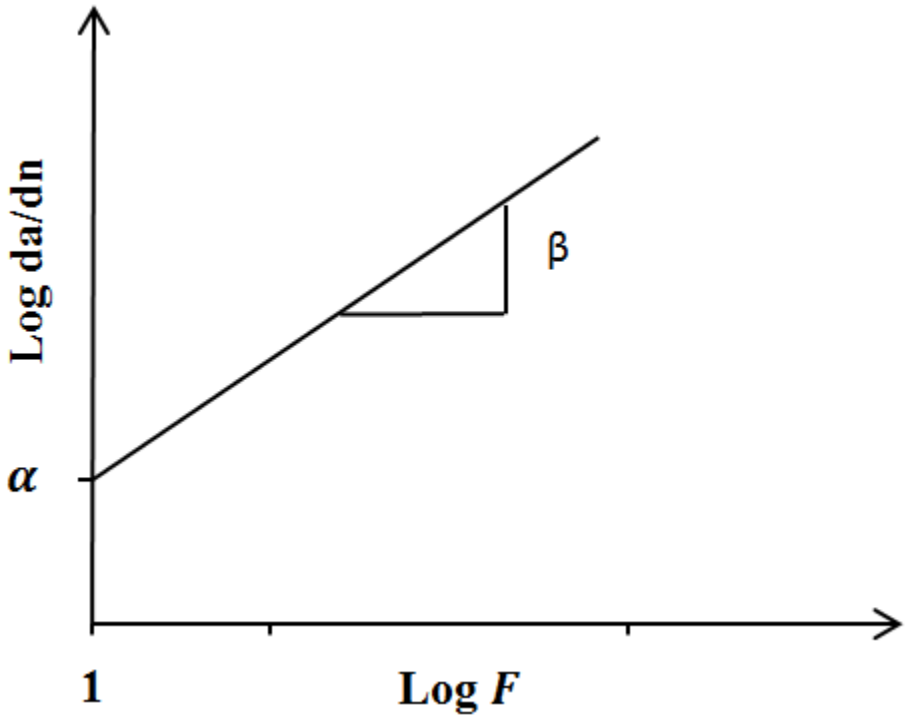

Figure 5.2 Rate of crack growth versus force in the reinforcing bar on a log-log scale Wahab, 2011 and Wahab et al., 2015

5.3.2.1 The procedure to find α and β

Wahab et al., 2015 determined the values of α and β from the fatigue life curves plotted in terms of load range versus fatigue life. The intercept (α) of the best fit load versus fatigue life curves at one cycle was different for each set of beams for a given rod type. Also, the slope of the fatigue life curve for beams of a given rod type was almost constant and that a single value of β for each rod type gave a good fit to the experimental data.

5.4 Shear Stress Distribution and the Crack Growth Model Used in the Current Study

5.4.1 Crack Growth Model

The crack growth model used in the current study was similar to that used by Wahab et al., 2015; however, the average shear stress τ_{avg} has been used instead of the force in the steel bar at the crack tip as shown in Figure 5.3 and the following equation:

$$\frac{da}{dn} = \alpha\, \tau^{\beta} \qquad 5.3$$

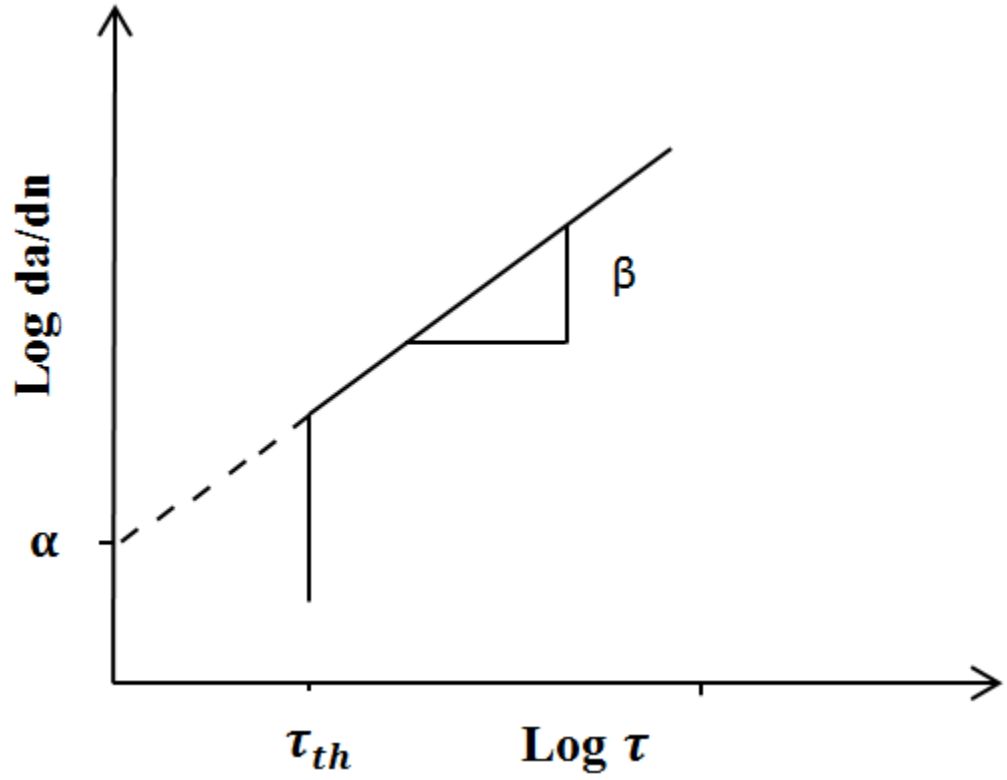

Figure 5.3 The rate of the crack growth versus the average shear stress on log- log scales

5.4.1.1 Procedure to find α and β in the current study

The procedure used to determine the constants α and β in the crack growth model in current study was the same as the one used by Wahab et al., 2015 except that the fatigue life curves used were of the average shear stress versus fatigue life instead of the load range versus fatigue life. The derivation of the shear stress at the crack tip as the crack advances is given in the next section. Figure 5.4 shows the type of fatigue life curve that was used to calculate the α and β.

Deriving the crack growth curve from the fatigue life curve is solved as an inverse problem. A crack growth curve is constructed by trial and error that gives the observed fatigue life curve shown on log-log linear scales of average shear stress versus fatigue life in Figure 5.4. The assumed power function crack growth of Equation 5.3 shown in Figure 5.3 is derived from the log-log linear curve of average shear stress range versus fatigue life shown in Figure 5.4 by calculating values of α and β that result in a correct prediction of the fatigue life curve. The procedure starts with assumption of initial values of the $\boldsymbol{\alpha}$ and β to define the crack growth versus average shear stress curve. The initial values of $\boldsymbol{\alpha}$ and β were assumed to be equal to those found by Wahab et al., 2015. Then, the fatigue life was calculated at a long fatigue life (the fatigue limit shear stress level was used). If the calculated fatigue life was shorter than $N_{f,1}$, then the rate of the crack growth (da/dn) was too high and $\boldsymbol{\alpha}$ was reduced to increase the calculated number of cycles to failure (if the calculated fatigue life was too long $\boldsymbol{\alpha}$ was increased). This step is repeated until a value of $\boldsymbol{\alpha}$ is found for which the calculated fatigue life matches the observed fatigue life. This value of $\boldsymbol{\alpha}$ and the initially assumed value of β are used to calculate the fatigue life at a high shear stress and short fatigue life (the shear stress corresponding to a fatigue life of 1,000 cycles was used). At this level β was varied until the calculated fatigue life matched the observed value. The values of $\boldsymbol{\alpha}$ and β were further modified by repeated adjustments to match calculated and actual fatigue life at the chosen stress levels respectively until changes in their values were negligible.

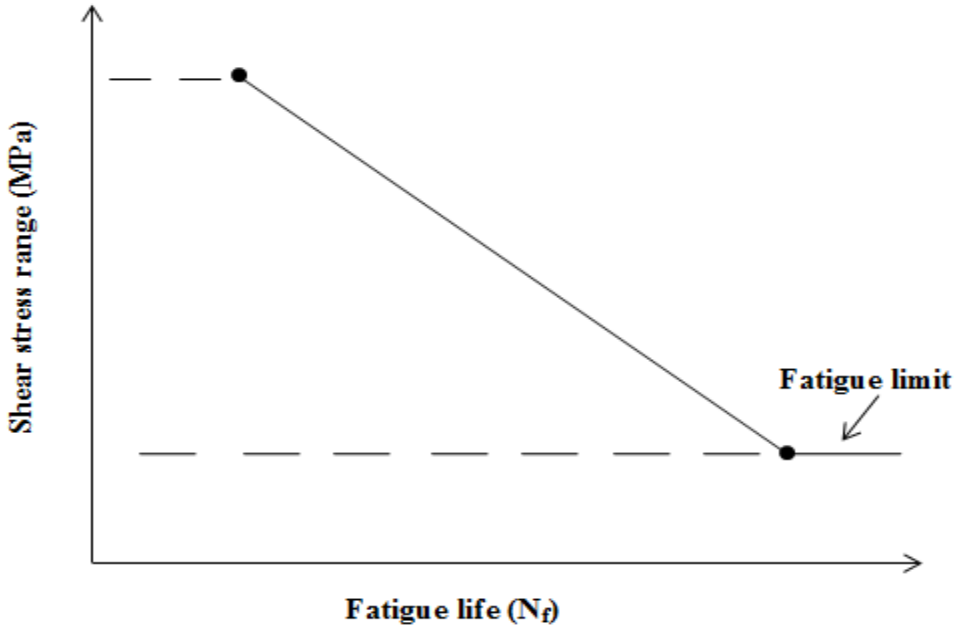

Figure 5.4 The fatigue life curve used to determine the α and β showing the shear stress ranges used in the iterative calculations

5.4.2 Shear Stress Distribution along the Lap Splice as a Crack Advances

In this study, the length of the lap splice was small and we did not want to affect the bond strength of the lap splice by using many strain gauges. As a result we did not have a sufficient number of strain measurements in the reinforcing bar to describe the bond shear stress distribution and its changes during fatigue. The shear stress distribution was assumed to follow the exponential distribution with a partly debonded region having a uniform stress behind the advancing crack tip found by Wahab et al., 2015.

The initial shear stress distribution along the lap splice before cracking is shown in Figure 5.5a. As the applied load increased in a monotonic test or as the number of cycles increased in a fatigue test, cracks in the concrete between the bars accompanied by splitting cracks propagated from each end of the lap splice toward the other end. The shear stress distribution was divided into two regions partially debonded regions and a fully bonded region as shown in Figure 5.5b.

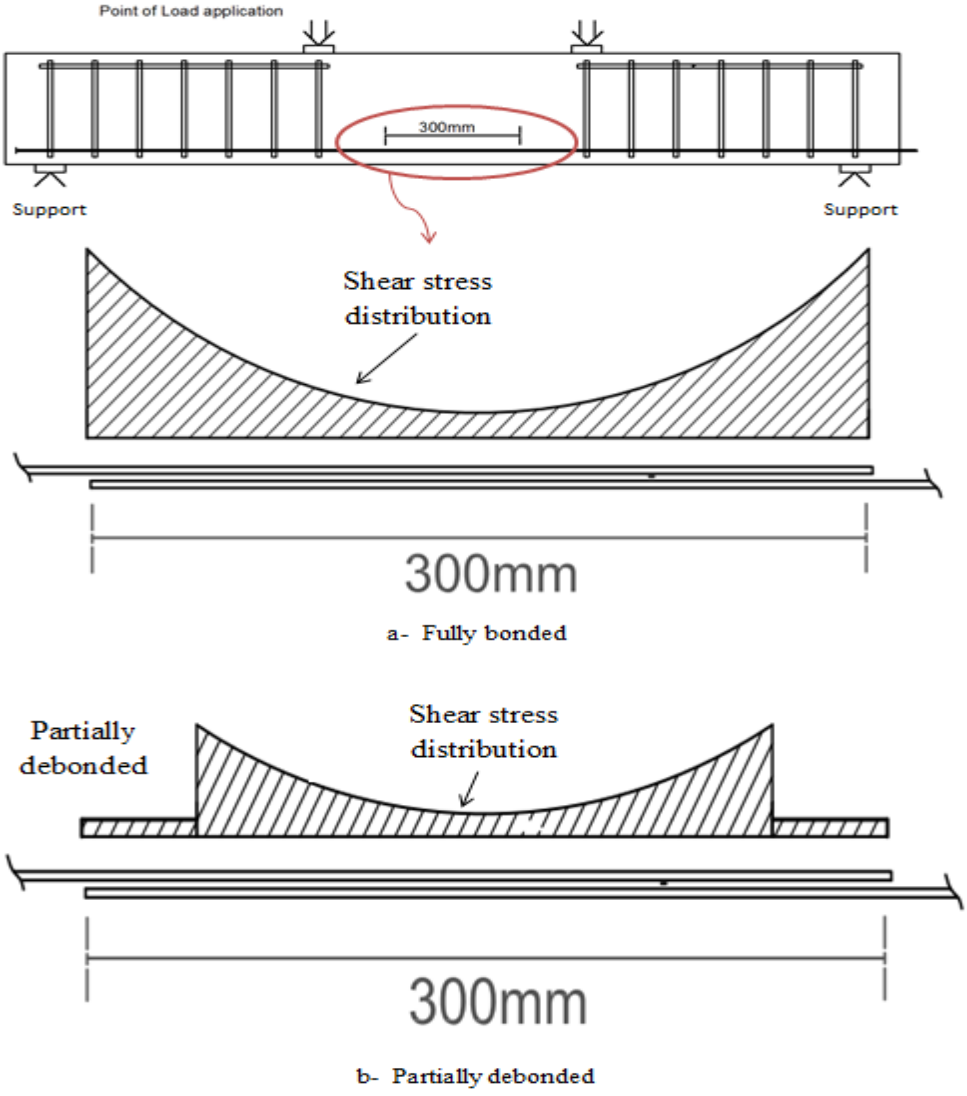

Figure 5.5 Fully bonded and partially debonded regions along the lap splice

5.5 Shear Stress Distribution

The exponential steel force distribution curve of Wahab et al., 2015 is replaced by the shear stress distribution described by the following equation:

$$\tau(x) = \tau_0 exp^{(-C*x)} \quad 5.4$$

where:

$\tau(x)$ is the shear stress along the lap splice at any distance *x* (MPa)
τ_0 is the peak shear stress at zero distance before the splitting cracks took place
C is a constant that describes of the shape of the shear stress distribution
x is the distance from the beginning of the lap splice (mm)

As noted above it was assumed that, since the peak load of the cycles in a fatigue test remains constant, the elastic component of the peak deflection will remain constant and increases in deflection will be due to slip (and, at very high loads, inelastic cyclic creep strains in the highly stressed region of the concrete). The slip as measured in these tests has three components: delta steel $\boldsymbol{\delta}_s$ an increase in steel bar length in the cracked region where force is transferred from the concrete to the steel as debonding occurs resulting in an increase in steel stress and strain, delta concrete $\boldsymbol{\delta}_c$ a decrease in concrete length in the cracked region where force is transferred from the concrete to the steel as debonding occurs resulting in a decrease in concrete stress and strain and delta lug embedment $\boldsymbol{\delta}_l$ the translation of a steel bar as the lugs on the bar break the chemical bonds with the surrounding concrete and deform the concrete ahead of them to resist the applied shear stresses. Figure 5.6 shows the shear stress and bar force distributions for one of the bars of a lap splice before and after a splitting crack occurs.

$$Total\ slip = \delta s + \delta c + \delta l$$

$$\delta s = \frac{\Delta f_s}{E_s} * a, \delta c = \frac{\Delta f_c}{E_c} * a \quad 5.5$$

Where:

δs = steel elongation, δc = decrease in concrete elongation, δl = deformation of the concrete in front of the rebar lugs, Δf_s and Δf_c = change in steel and concrete stress due to cracking respectively, E_s= steel modulus elasticity, E_c= concrete modulus elasticity and a= crack length.

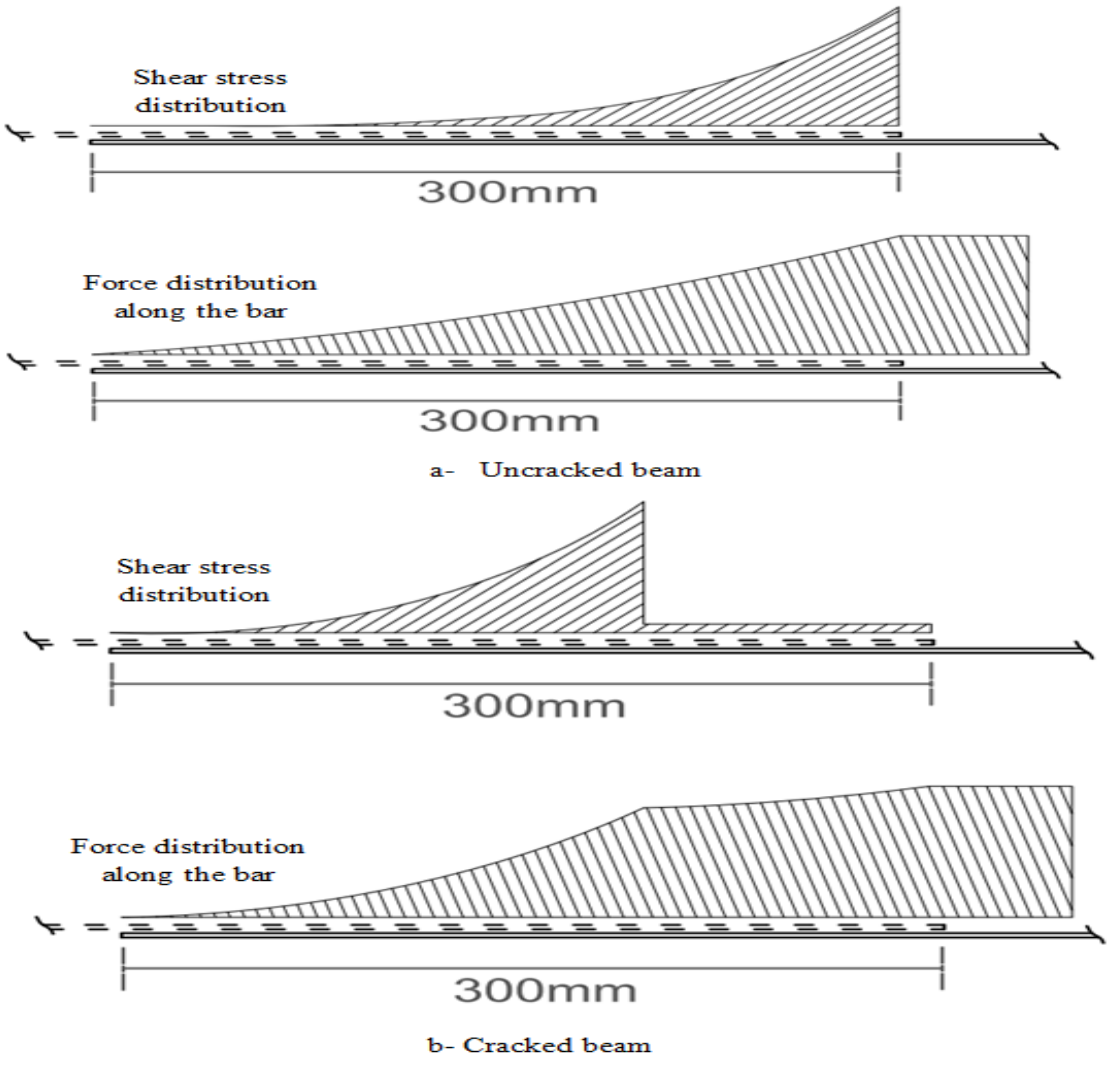

Figure 5.6 The shear stress and the force on the bar distributions along one bar of a lap splice for a cracked and uncracked beam

5.5.1 Derivation of the Shear Stress Distribution as a Crack Advances

Wahab et al., 2015 used a constant value of *C* in equation 5.1, a measured value of the residual shear stress after debonding and the equilibrium condition that the total shear force remain constant as the crack advances under constant amplitude loading to describe the variation of the shear stress distribution as the crack advances. In the present case, the short bonded length of the lap splice led us to expect the bond shear stress would become more uniform and the value of *C* would decrease as the crack advanced. For simplicity, this reduction was assumed to be linear as shown in Figure 5.7. The condition imposed to determine the three variables governing the evolution of the shear stress distribution as the crack advances where: the equilibrium condition of a constant total shear force, matching of the crack advance during the first cycle with the measured value for the load level as shown in Figure 4.2 and a calculated value of the fatigue life equal to that given by the best fit of the fatigue life curve. It was hoped that single values of the initial value of *C*, the rate of decrease of *C* with crack length and the residual of bond stress expressed as a fraction of the average of the bond stress would apply to all the beam configurations. Values of the shear stress distribution parameters where arrived at by trial and error calculations using the crack growth model calibrated as described in the next section. They are C_0 of 0.037, a linear decrease of *C* to zero at a crack length of 135 mm and the residual shear stress (τ_r) of 0.3 times the initial average shear stress τ_{avg}. The shear stress distributions at various crack length and the locus of the maximum of shear stress values are shown in Figure 5.8 and Figure 5.9, respectively. Equation 5.6 describe this locus,

$$\tau(x) = \tau_{avg}\left(\frac{x^4}{1.22 * 10^7} - \frac{x^3}{6.81 * 10^4} + \frac{x^2}{9.45 * 10^2} - \frac{x}{13.5} + 5.54\right) \quad 5.6$$

The residual stress behind the crack decreases the shear force on the uncrack ligament and initially its average shear stress. This together with the decrease in *C* reduces the peak shear stress (and slows crack growth). As the crack advances and the un-cracked ligament becomes smaller, the average and peak shear stress increase and the crack growth rate increases.

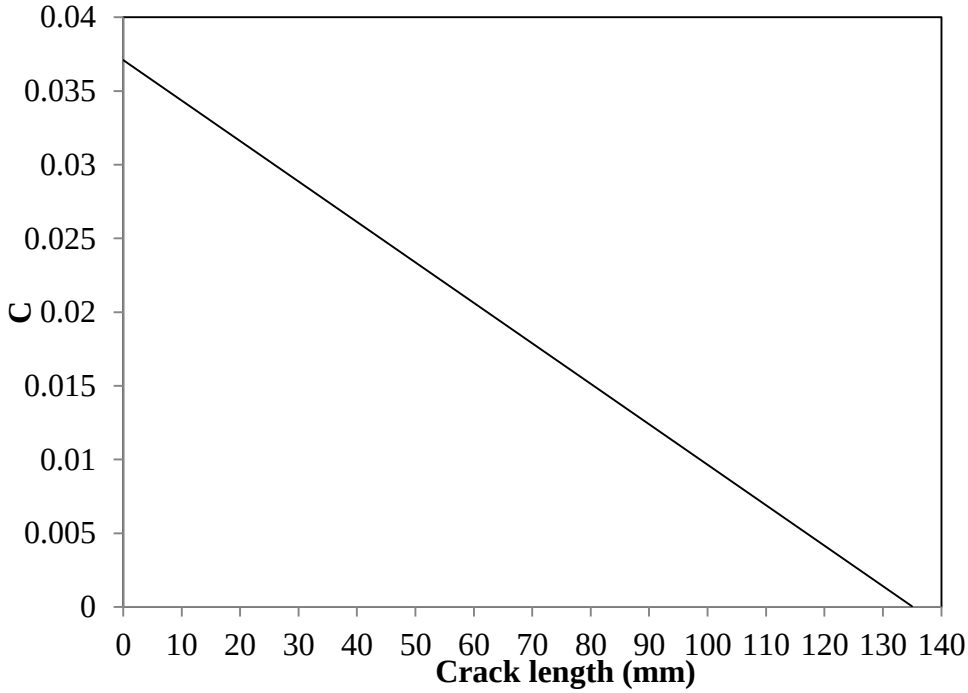

Figure 5.7 The C versus the crack length curve used for all beams

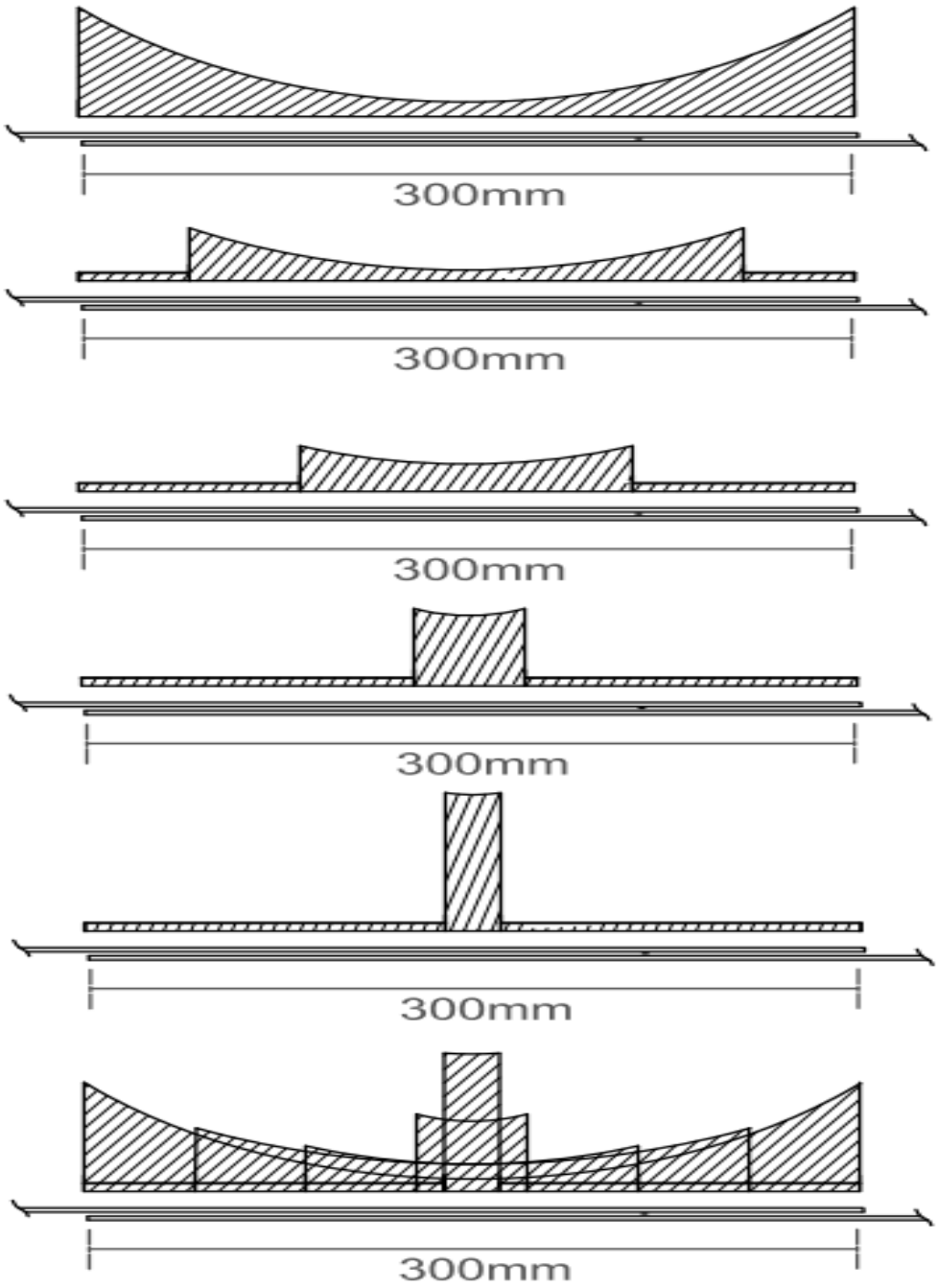

Figure 5.8 The summations shear stress distributions for both bars along the lap splice as a crack progresses

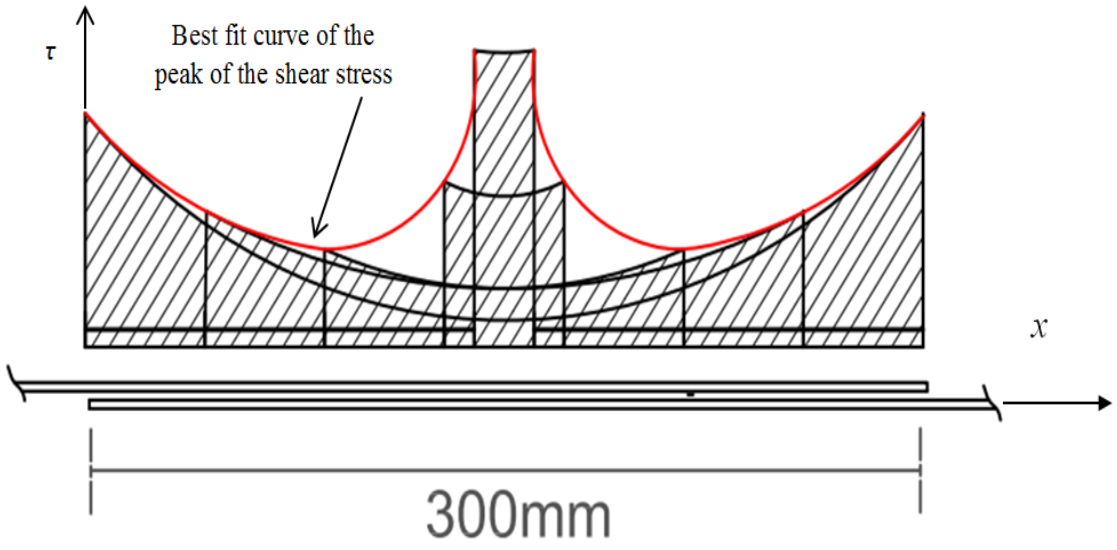

Figure 5.9 The shape of the best fit curve to the peak shear stress values from the summation of the stresses contributed by both bars

5.5.2 Values of the Constants α and β

The value of the constants α and β for the three cover thicknesses of CFRP wrapped beams determined and used to calibrate the model. Then, the model was used to predict the fatigue life for the unwrapped and the GFRP wrapped beams.

The fatigue life data for the CFRP wrapped beams for three different concrete cover thicknesses are shown in Figure 5.11. From the figure, the intercept of the fatigue curves at one cycle fell close to the monotonic failure stress which was plotted at that point. When values of **α** (shown in Table 5.1) were plotted against the monotonic failure stresses as shown in Figure 5.10, a linear relationship was obtained.

The value of the constant **α** can be calculated for each set of beams by using the following equation as shown in Figure 5.10:

$$\tau(monotoic\ shear\ stress\ for\ each\ set) = -0.572 * Ln(\alpha) - 11.954 \qquad 5.7$$

$$\alpha = e^{-\left(\frac{\tau+11.954}{0.572}\right)}$$

Table 5.1 Value of α and monotonic shear stress for CFRP wrapped beam for each cover

Wrapping condition	Concrete cover thickness	Alpha (α)	The average monotonic shear stress (τ)
CFRP	20 mm	3.96E-16	7.64
	30 mm	2.83E-15	6.63
	50 mm	1.26E-16	8.23

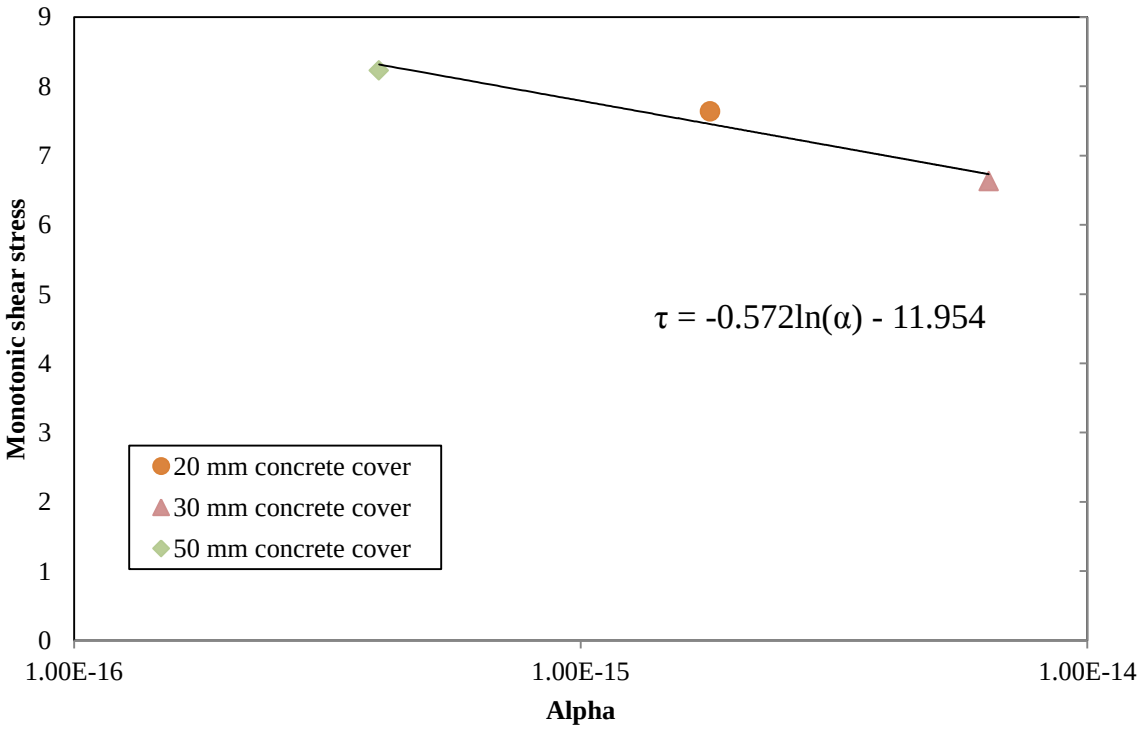

Figure 5.10 The monotonic shear stress at failure versus α for each set of beams different concrete cover thicknesses of CFRP wrapped beams

The values of β which are determined by the slopes of the shear stress versus life curves were almost the same for all different concrete cover thicknesses of CFRP wrapped beams. This single β value taken from the CFRP wrapped beams were used to predict fatigue lives of all other wrapping conditions and concrete cover thicknesses. The values of **α** for all concrete cover thicknesses for GFRP wrapped beams and unwrapped beams were estimated using equation 5.7. Table 5.2 shows the values of the **α** and β for each of the combinations.

Table 5.2 Value of α and β for each combination of concrete cover and wrapping condition

Group	Wrapping condition	Beta	Alpha
Group 1 20 mm	Unwrapped	10.84	3.44E-13
	GFRP		3.74E-14
	CFRP		1.3E-15
Group 2 30 mm	Unwrapped	10.84	6.03E-13
	GFRP		1.03E-13
	CFRP		7.76E-15
Group 3 50 mm	Unwrapped	10.84	3.74E-14
	GFRP		2.58E-15
	CFRP		4.73E-16

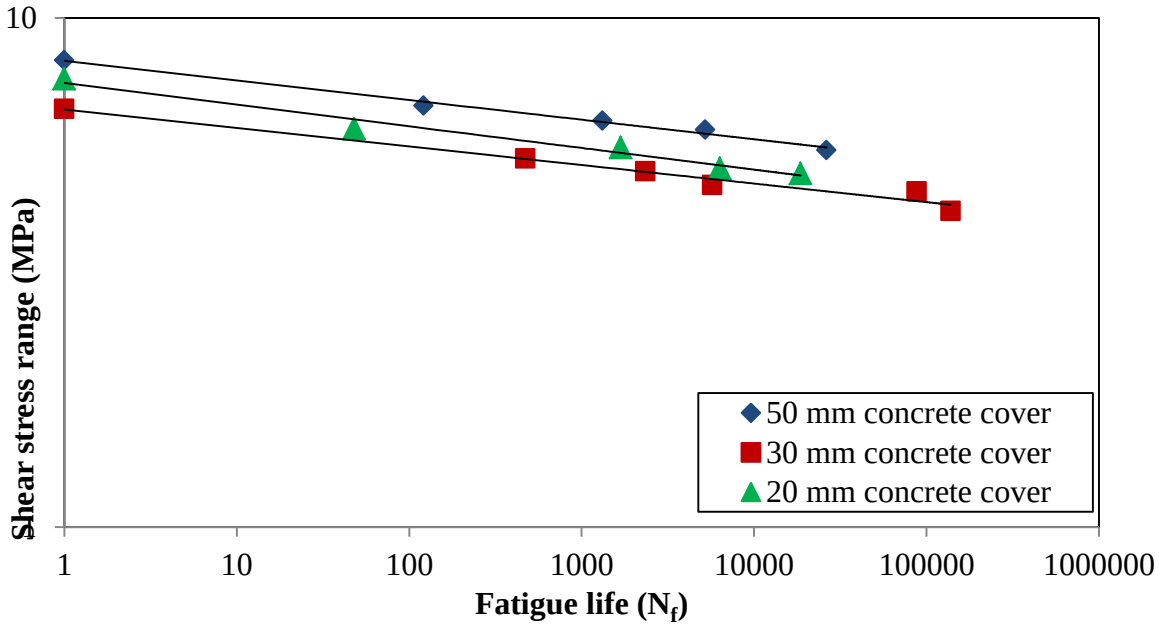

Figure 5.11 The average shear stress versus fatigue life for the test data on log-log scales with best fit curves for CFRP wrapped beams (20 mm, 30 mm and 50 mm concrete covers)

5.5.3 Review of the Crack Growth Calculation Procedure

The fatigue life of a given beam can be calculated using the following steps:

1. The monotonic bond strength for a beam with a given wrapping and concrete cover can be calculated by using the Orangun et al. (1977) and Hamad et al. (2004) equations as follows:

$$u = \left[0.10 + \frac{c}{4d_b} + \frac{4.2d_b}{l_d} + K_{tr,f}\right]\sqrt{f'_c} \qquad 5.8$$

2. The value of the crack growth parameter **α** for each cover and wrapping condition can then be calculated from its linear relationship with the monotonic maximum shear stress by using the following equation:

$$\alpha = e^{-\left(\frac{\tau+11.954}{0.572}\right)} \quad 5.9$$

3. The peak of the exponential shear stress distribution at a given length may be calculated from the following equation:

$$\tau(x) = \tau_{avg}\left(\frac{x^4}{1.22*10^7} - \frac{x^3}{6.81*10^4} + \frac{x^2}{9.45*10^2} - \frac{x}{13.5} + 5.54\right) \quad 5.10$$

4. The increment of the crack growth (da) for a given cycle (dn_1) is then given by :

$$\boldsymbol{\delta} a(n_i) = \frac{da}{dn} = \alpha\, \tau^{\beta} \longrightarrow da(n_i) = \alpha\, \tau^{\beta} \quad 5.11$$

And the crack length is obtained by summing successive increments of crack growth $\boldsymbol{\delta} a(n_i)$until one of the following failure criteria are met.

1) When $a \geq 150$ mm (the half of the lap splice length) the beam has failed.

If the $a < 150$ mm, then the next condition is checked.

2) When the peak average shear stress is greater than the 5.5 times the average shear stress at monotonic failure the beam is assumed to have failed. If neither of the failure

criteria is met the above procedure is repeated for subsequent cycles. The number of cycles at failure is the value of N_i when one of the two failure criteria is met.

5.6 Comparison between the Experimental Results and the Model

5.6.1 Fatigue Life

Figure 5.12, Figure 5.13 and Figure 5.14 show the actual fatigue life data and curves calculated using the calibrated model on log-log scales of shear stress versus fatigue life for Group 1(20 mm concrete cover), Group 2 (30 mm concrete cover) and Group 3 (50 mm concrete cover), respectively. The calculated number of cycles was in good agreement with the actual fatigue data for all different wrapping condition and all different concrete cover thicknesses.

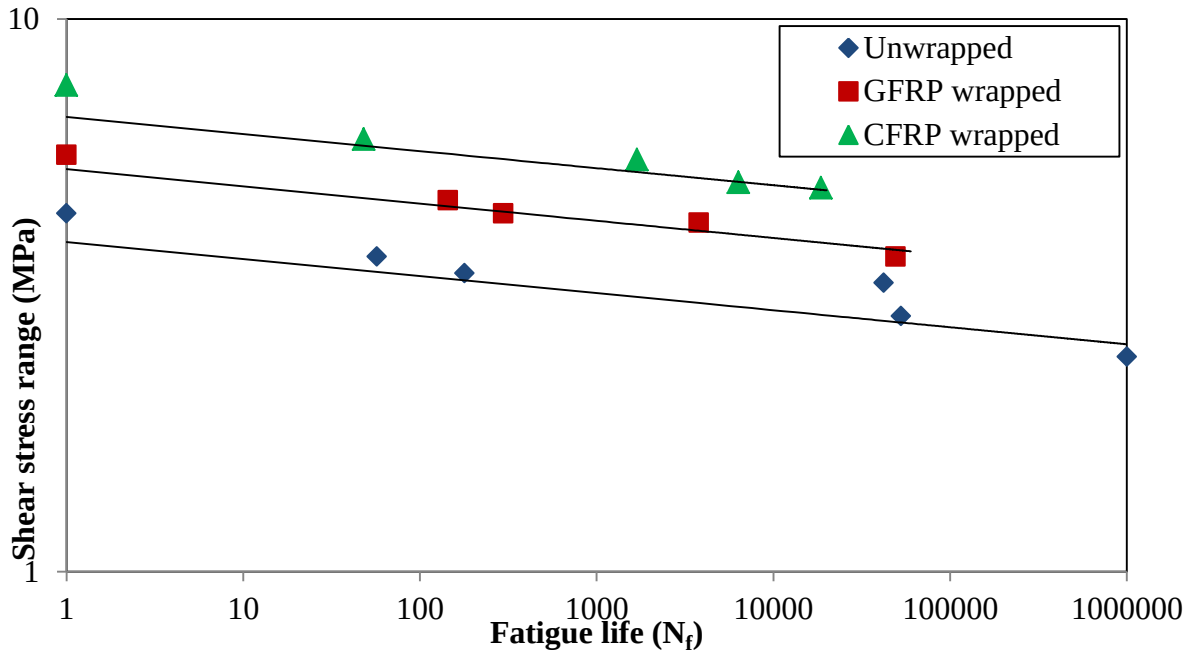

Figure 5.12 The actual fatigue test results for the unwrapped and FRP wrapped beams with fit curves of the calculated number of cycles for Group 1 (20 mm concrete cover)

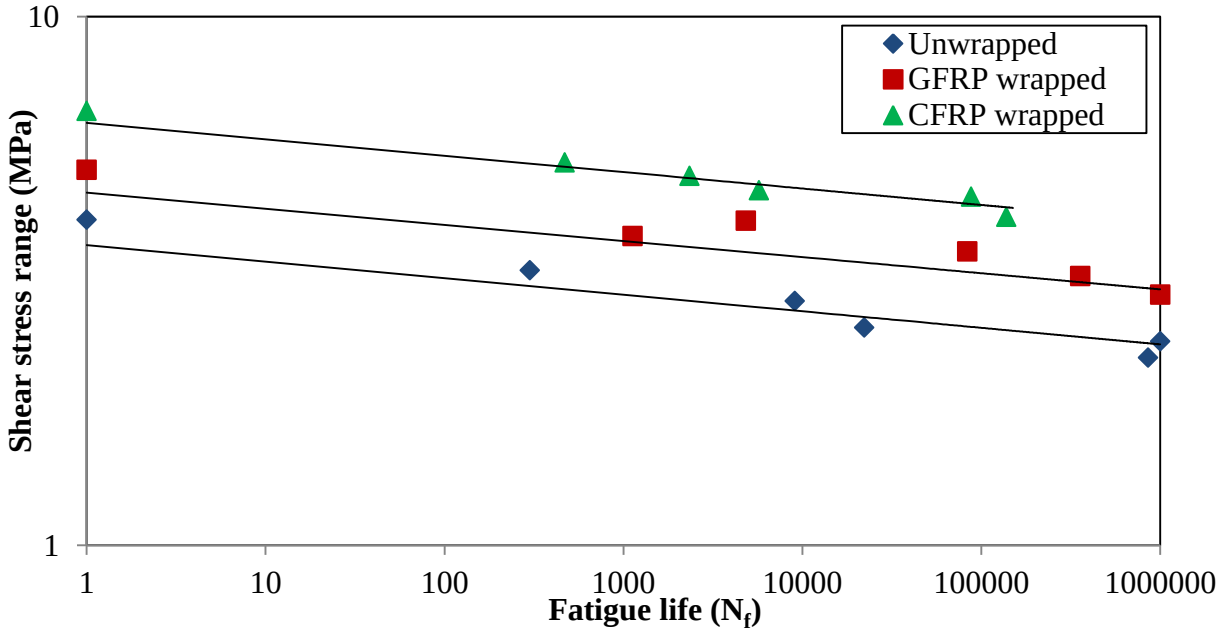

Figure 5.13 The actual fatigue test results for the unwrapped and FRP wrapped beams with fit curves of the calculated number of cycles for Group 2 (30 mm concrete cover)

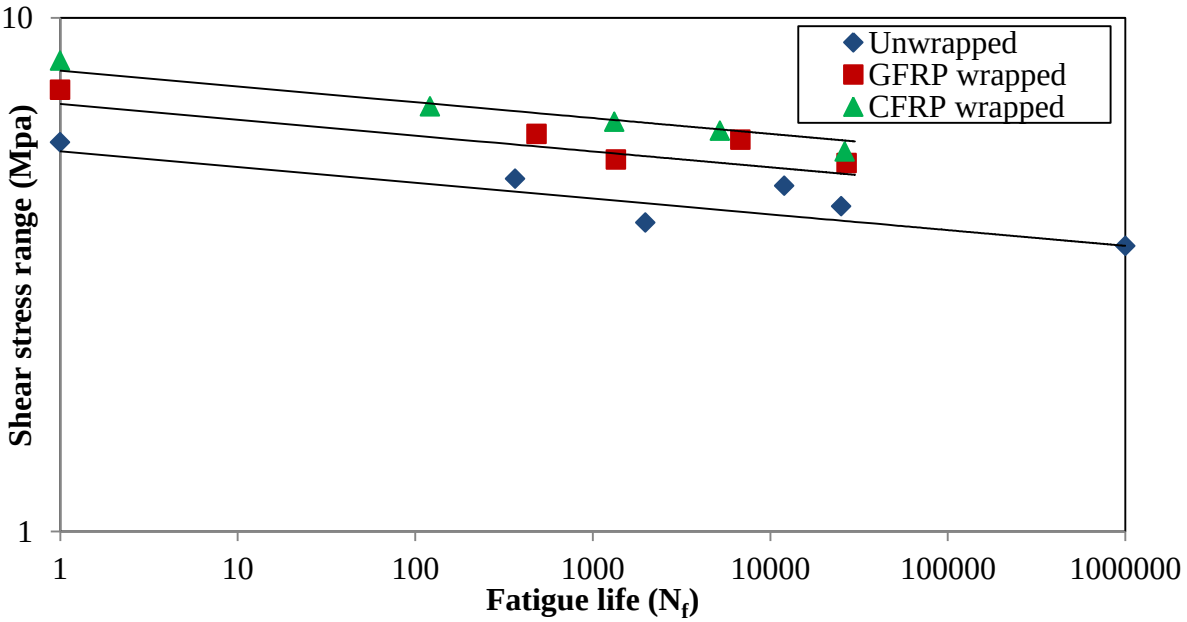

Figure 5.14 The actual fatigue test results for the unwrapped and FRP wrapped beams with fit curves of the calculated number of cycles for Group 3 (50 mm concrete cover)

5.6.2 Inelastic Slip and Deflection Due to Changes in Steel and Concrete Strains and Total Slip and Deflection as a Crack Advances

Figure 5.15 shows typical curves of crack length versus cycles expressed as a percentage of fatigue life. Figure 5.16, Figure 5.17 and Figure 5.18 show calculated values of inelastic slip due to stress changes in the steel and concrete due to cracking together with measured values of total slip versus cycles expressed as a percentage of the fatigue life to failure. It can be seen that only a small amount of the inelastic slip is due to the stress changes in the steel and concrete. The remaining slip which is due to deformation of the concrete in front of the steel rebar lugs is much larger.

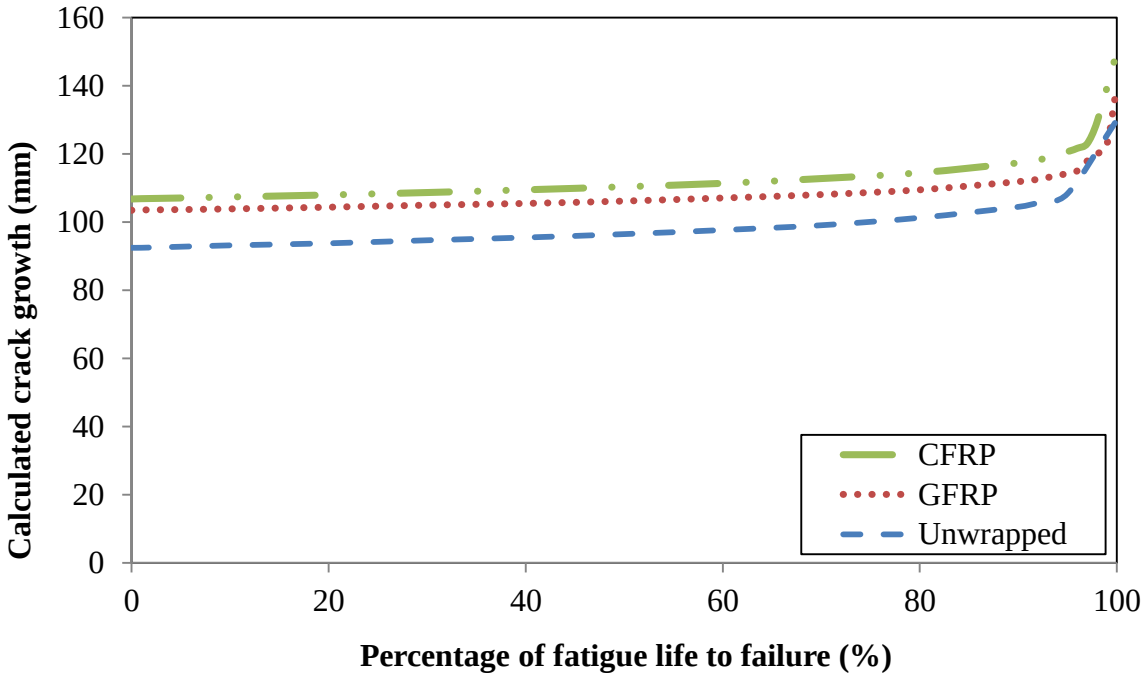

Figure 5.15 Typical crack growth curve for the three different wrapping conditions

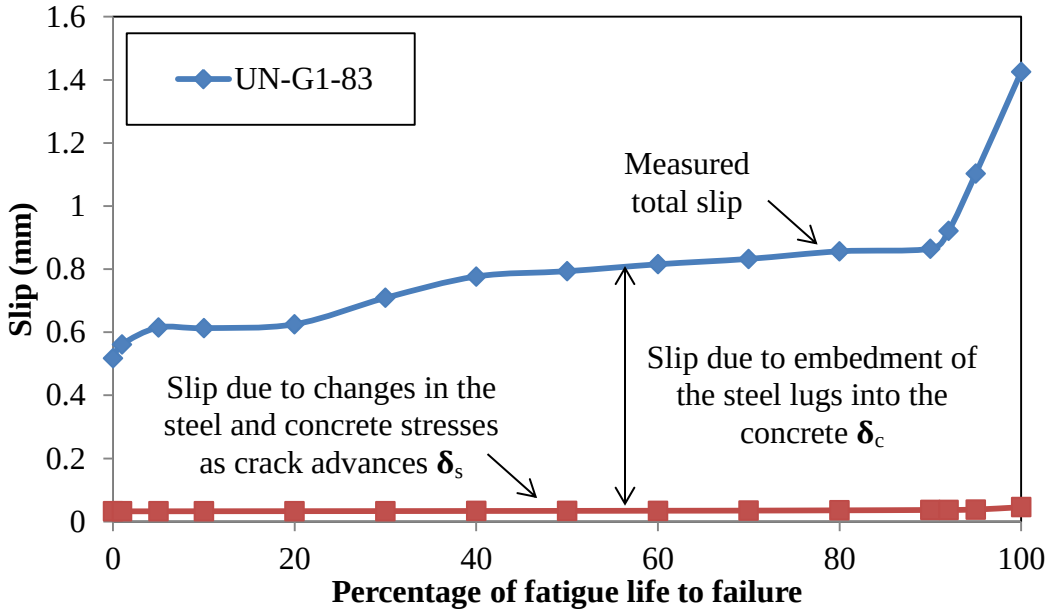

Figure 5.16 The measured total slip and the slip due to changes in the steel and the concrete strains due to crack advance for the unwrapped beam with a 20 mm concrete cover

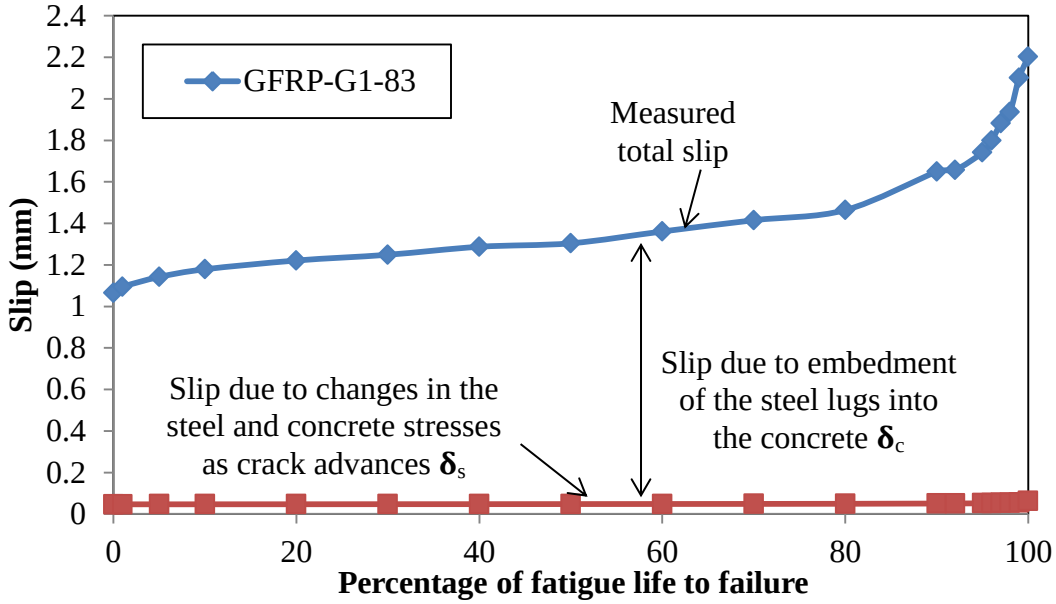

Figure 5.17 The measured total slip and the slip due to changes in the steel and the concrete strains due to crack advance for the GFRP beam with a 20 mm concrete cover

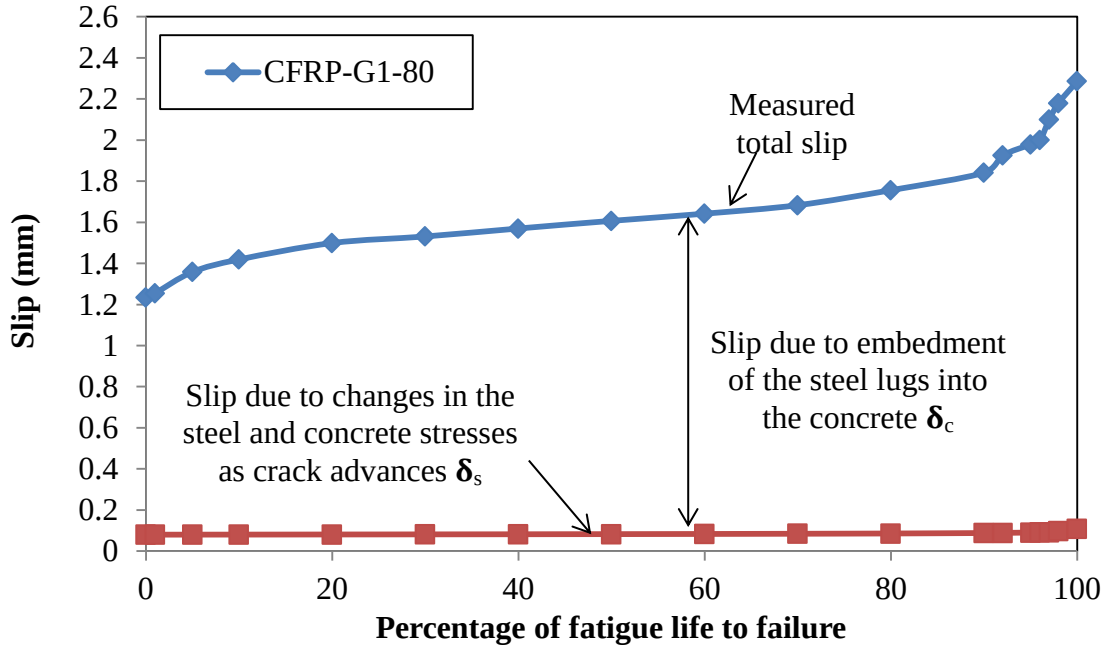

Figure 5.18 The measured total slip and the slip due to changes in the steel and the concrete strains due to crack advance for the CFRP beam with a 20 mm concrete cover

Figure 5.19, Figure 5.20 and Figure 5.21 show calculated values of the inelastic deflection due to stress changes in the steel due to cracking together with measured values of inelastic deflection versus cycles expressed as a percentage of the fatigue life to failure. It can be seen that only a small amount of the inelastic deflection is due to the stress changes in the steel and concrete. The remaining inelastic deflection which is due to deformation of the concrete in front of the steel rebar lugs is much larger.

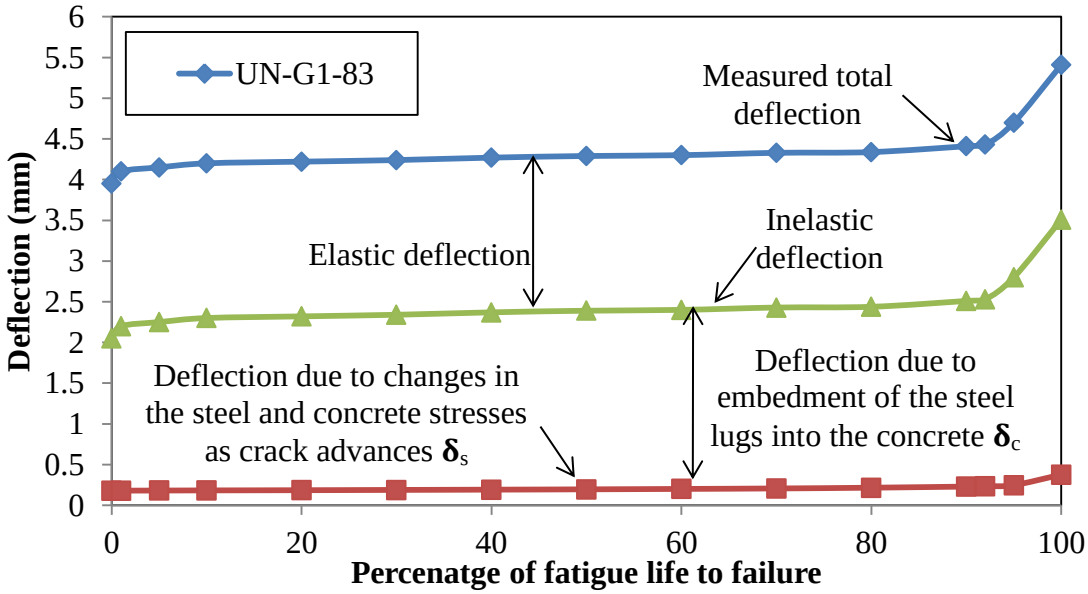

Figure 5.19 The measured total deflection and the deflection due to changes in the steel and the concrete strains due to crack advance for the unwrapped beam with a 20 mm concrete cover

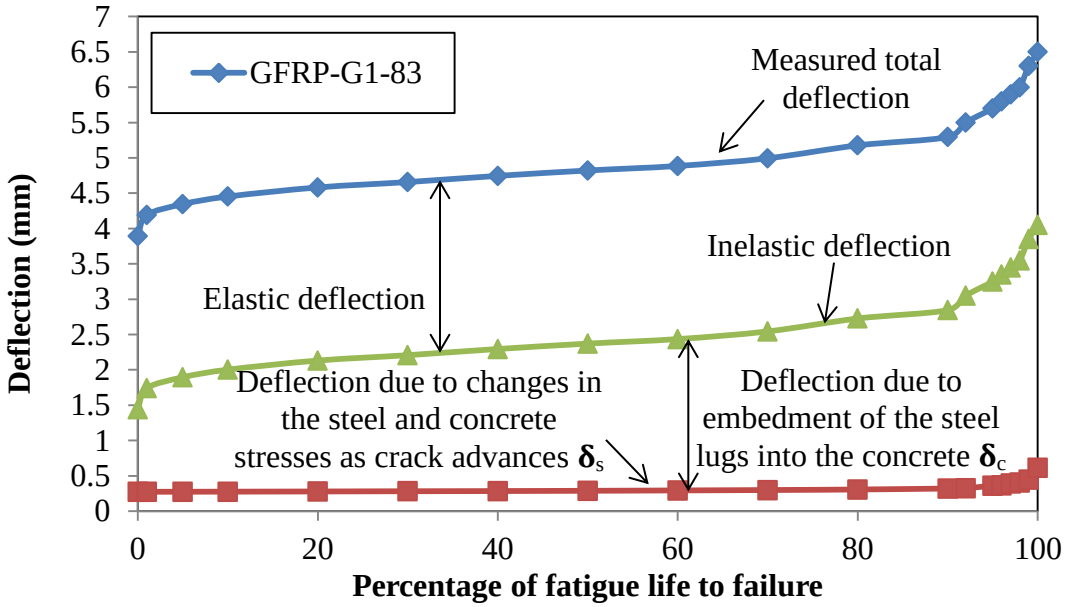

Figure 5.20 The measured total deflection and the deflection due to changes in the steel and the concrete strains due to crack advance for the GFRP beam with a 20 mm concrete cover

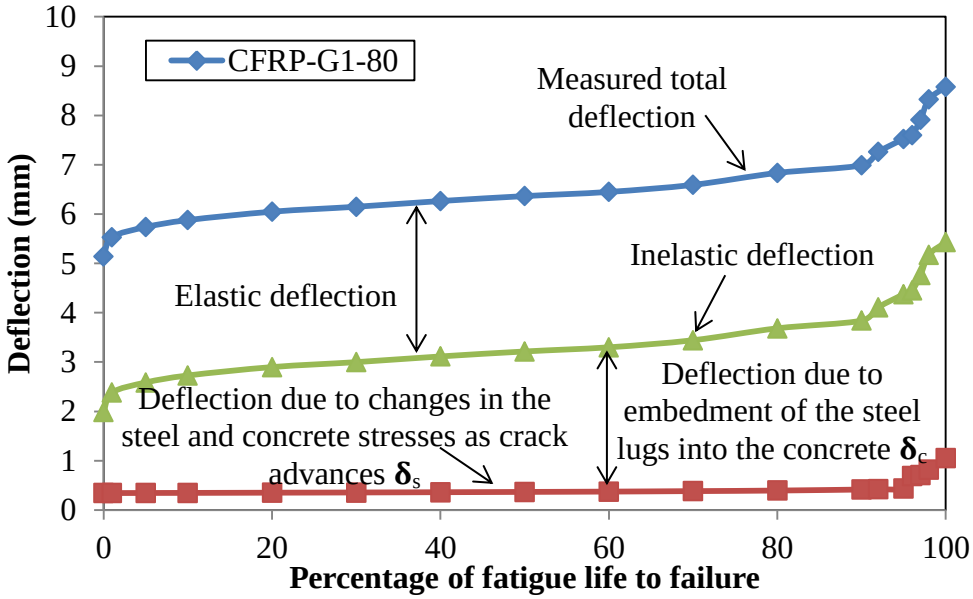

Figure 5.21 The measured total deflection and the deflection due to changes in the steel and the concrete strains due to crack advance for the CFRP beam with a 20 mm concrete cover

Figure 5.22 presents typical curves of inelastic deflection versus crack length. The deflection as expected increases as the crack length increases. The relationship is almost linear throughout most of the fatigue life. At the beginning of a test there is an increase in the slip as the rebar lugs deform the concrete ahead of them until an equilibrium is achieved and slip slows.

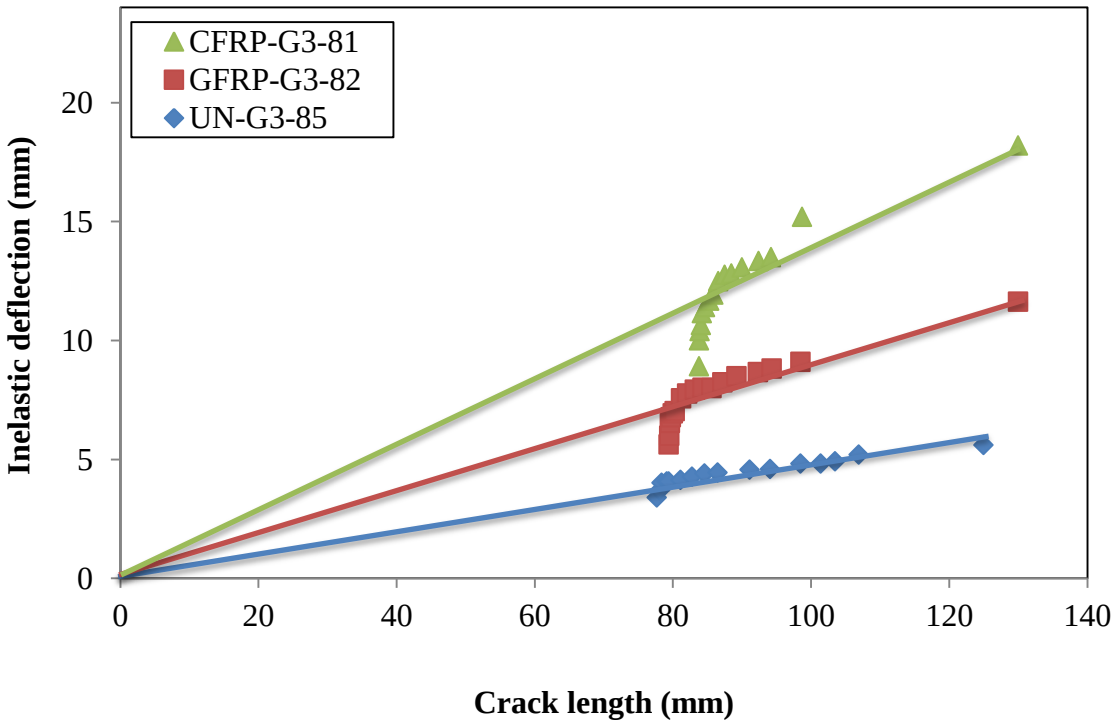

Figure 5.22 Inelastic deflection versus calculated crack length for different wrapping condition for Group 3 (50 mm concrete cover)

5.7 Discussion

5.7.1 Crack Growth versus Slip and Deflection Curves

There was a large amount of slip during the first cycle together with a large predicted crack growth. The slip due to the crack growth can be estimated as the sum of the elongation in the steel due to its increased stress as the stress is transferred from the debonded concrete and the decrease in the elongation of the concrete as its stress is decreased due to debonding. However, an elastic calculation of the slip due to these factors indicates that they are responsible for only a small amount of the observed slip. The remainder is presumed to come from the movement of the rebar in the uncracked region as it breaks the bond with the concrete and embeds itself in the concrete to a depth sufficient to develop the necessary bond force to support the shear force.

This process of deforming the concrete to produce the force in the lugs to resist the shear force would explain the increase in slip shown at the beginning of a test (see the circled region of Figure 5.23).

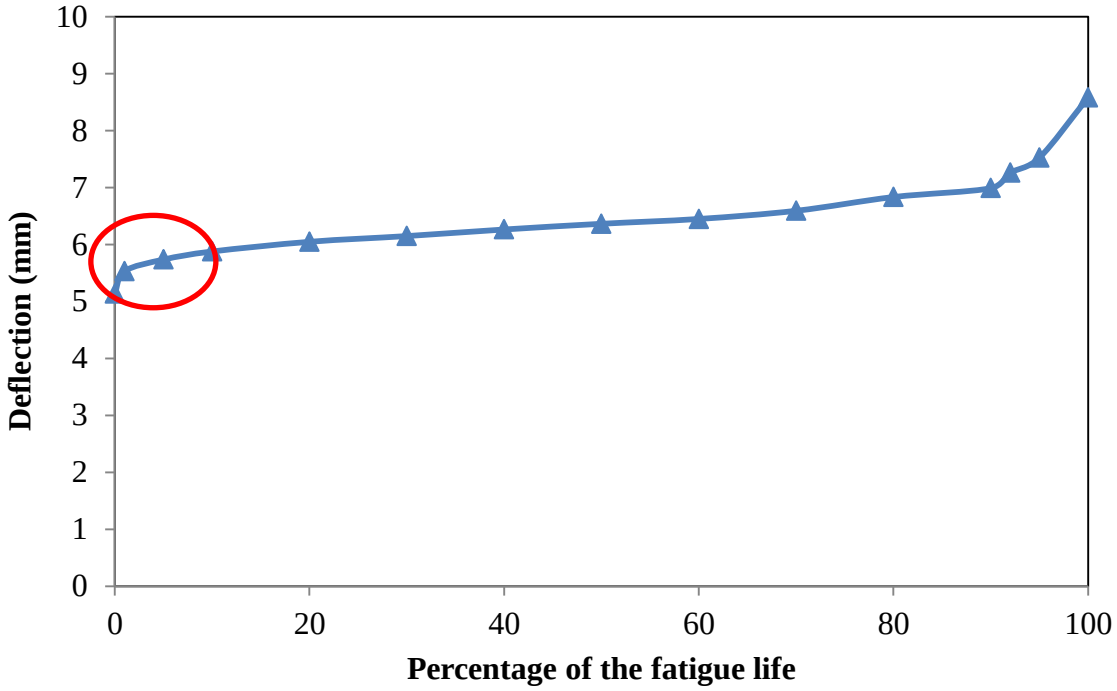

Figure 5.23 The actual deflection and the calculated cracks growth versus fatigue life as percentage CFRP-G1-80

Chapter 6 Non-Destructive Test (NDT)

6.1 Non-Destructive Test (NDT)

6.1.1 Introduction

Nondestructive test methods have become more popular and are now used to evaluate the condition of existing structures such as the bridges, buildings, deep foundations and many other reinforced concrete structures (Breysse, 2012). The NDT methods are more economical and faster than the traditional destructive testing. The ACI 228.2R (2013) listed four primary uses of NDT for dealing with concrete members:

1. Determining the quality of new construction
2. Troubleshooting problems for new and the existing construction
3. Evaluation of the condition of old concrete for rehabilitation purposes
4. Determining the quality of concrete repairs

There are several non-destructive test methods that are used to assess the condition of reinforced concrete members including surface wave methods and ultrasonic methods. The surface wave testing method was used in this study to evaluate the changes in the condition of chosen beams with fatigue cycling.

6.1.2 Techniques of Using the Wave Testing Method for NDT Evaluation

There are three techniques that use the wave testing method. They are direct, semi direct and indirect transmission ultrasonic testing as shown in Figure 6.1. The direct technique should be used when it is possible because it is the most accurate of the three methods. The semi direct technique method is more accurate than the indirect technique. The indirect technique is the least accurate but the most easily used technique (Breysse, 2012).

A: Direct transmission ultrasonic testing

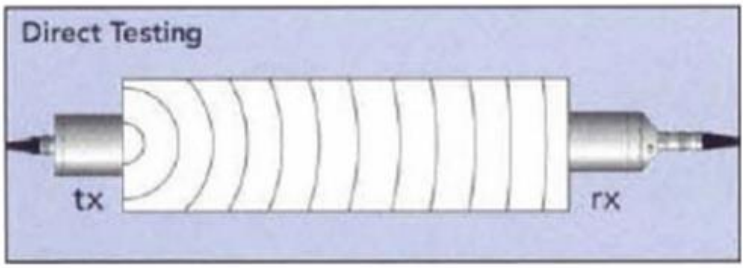

B: Semi direct transmission ultrasonic testing

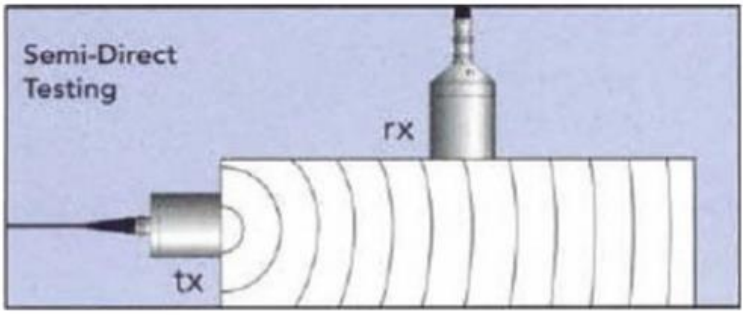

C: Indirect transmission ultrasonic testing

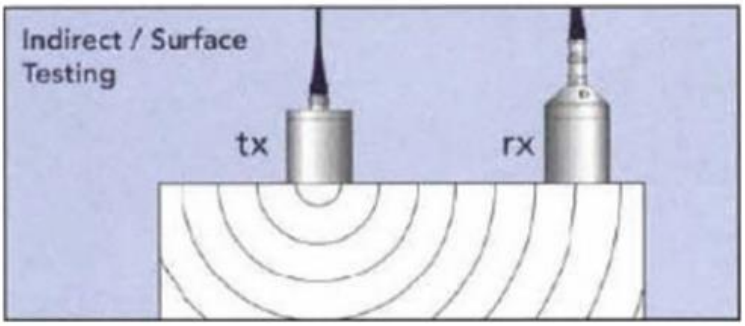

Figure 6.1 Three techniques can be used for the transmission ultrasonic testing (Breysse, 2012)

In the indirect technique used in this study, the transducers and the receivers must be mounted on same line with a minimum of four receivers as shown in Figure 6.2. The minimum distance between the receivers should be greater than five times the average concrete aggregate size. The distance between the transducers and the receivers is measured from center to center. The direct wave velocity is faster than the indirect wave velocity by about 15%.

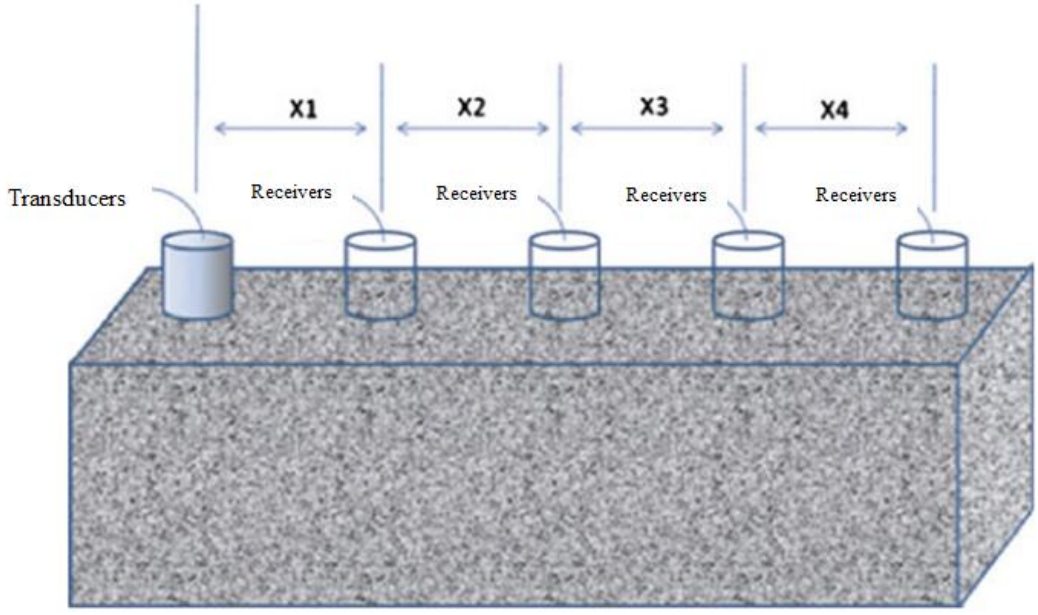

Figure 6.2 Indirect method principle (Breysse, 2012)

6.1.3 Surface Wave Testing

The surface wave method is usually used for reinforced concrete structures when the geometry allows propagation of the wave through body of a component. The surface wave method uses Rayleight waves (R-waves) that propagate through solid materials. The R-waves propagate through the concrete and provide information about the condition of a concrete member (Hevin et al., 1998). The dispersion of the R-waves varies with concrete stiffness, leading to a variation in velocity of the R-waves termed phase velocity. Also, a change in frequency of the R-wave results in a change in wave velocity. The main characteristics of the surface wave are the wave propagation velocity and the amount of wave energy that reflect from the interface between two distance media. These characteristics are a function of the Young's modulus of elasticity, the Poisson's ratio, the density and the geometry of a member (ACI 228.2R, 2013). The surface wave method has been used to measure the crack depth (Goueygou et al., 2008; Yang et al., 2009), to evaluate the condition of repaired concrete (Aggelis et al., 2009) and to assess amount of concrete damage (Kirlangic, 2013).

6.2 Experimental Program

6.2.1 Instrumentation of NDT

Nondestructive testing was used to evaluate the deterioration of our concrete lap splice due to fatigue loading. Five beams were tested under fatigue loading to evaluate the usefulness of the nondestructive test method. One beam was unwrapped and four beams were wrapped with FRP sheets.

The surface wave testing method used consists of a wave generating transducer (this can be a hammer) and receivers as shown in Figure 6.3. The hammer was used to send waves and the receivers were used to record the arrival times of the waves. As the number of receivers increases the quality of the results increases and we can draw the phase velocities curves. The hammer generates an R-wave by impacting the surface. The typical wave frequency range used with concrete varies from 20 kHz to 300 kHz (ACI 228.2R, 2013). The most commonly used transducers operate between 24 kHz and 54 kHz.

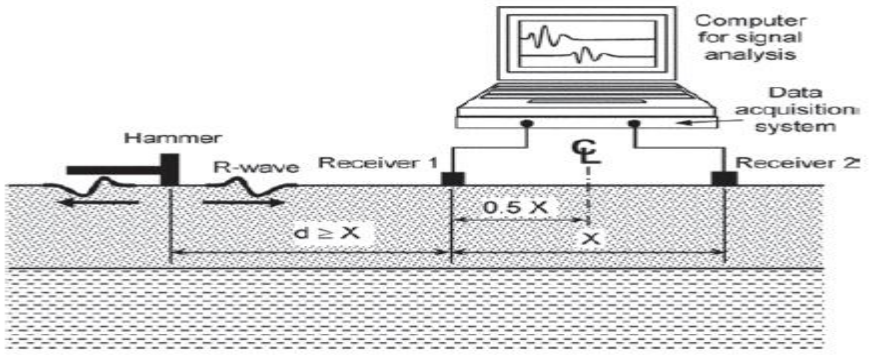

Figure 6.3 Surface method configuration

6.2.2 Test Setup

For all the five beams, the first NDT test measurement which was taken before the initial manual loading to the peak of the following fatigue loading recorded the condition of the undamaged beam for use as baseline. Then, during the manual loading, the NDT

measurement was taken at the mean and the maximum load before switching to the automatic cycling of the remainder of a fatigue test. Then NDT data were collected at regular intervals throughout a fatigue test. Figure 6.4 shows the setup of the NDT test equipment.

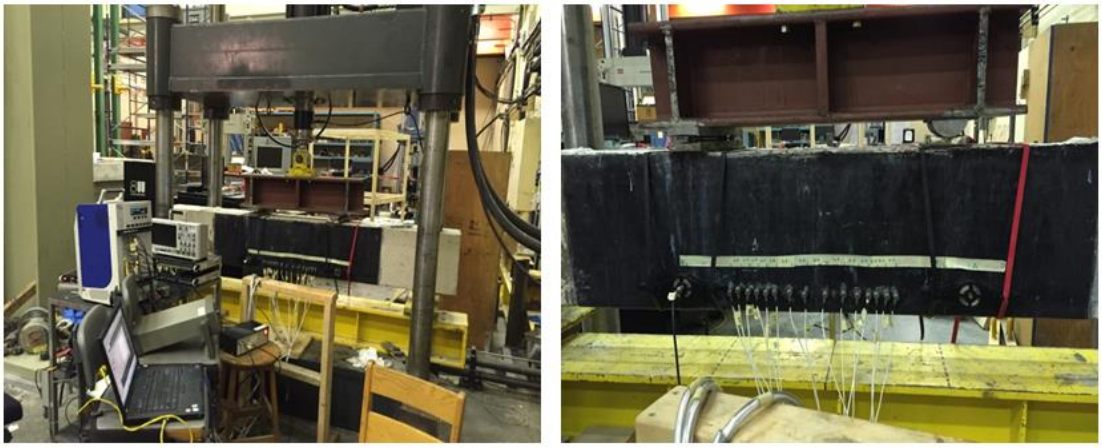

Figure 6.4 NDT test setup

6.3 Test Results

6.3.1 NDT Test Results

Figure 6.5 and Figure 6.6 show the changes in wave velocity with frequency in the lap splice region after various numbers of cycles for the CFRP wrapped beam with a 20 mm concrete cover and for the unwrapped beam with 50 mm concrete cover. As the number of cycles increased, the wave velocity decreased at all frequencies. The change in the velocity is attributed to damage to the concrete providing the bond between the lap splice bars and the concrete. For each set of NDT measurements the wave velocity versus frequency curves initially decrease with increasing frequency and then become flat. These curves become flatter and the decrease of velocity with frequency decreases as the number of cycles in a fatigue test increase.

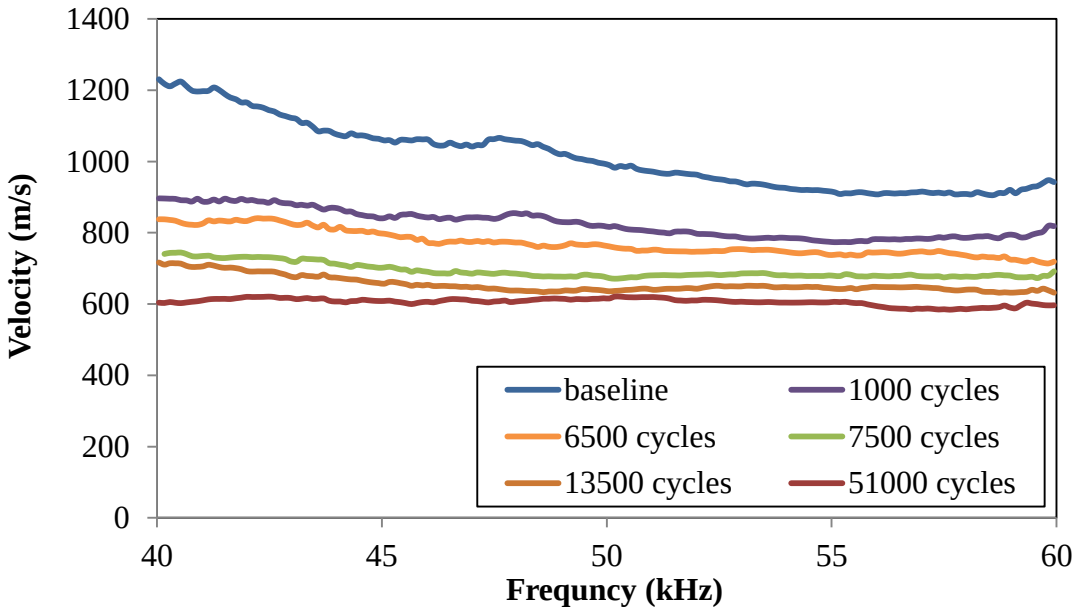

Figure 6.5 Change of wave velocity for CFRP-G2-69 beam at different stage of fatigue life

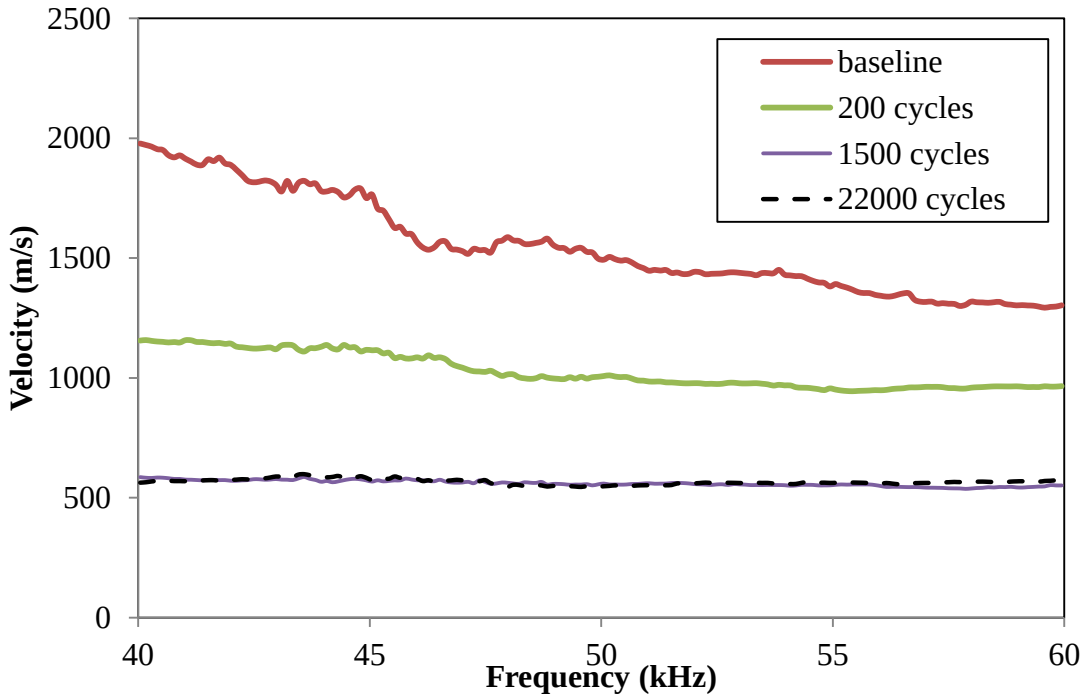

Figure 6.6 Change of wave velocity for UN-G3-75 beam at different stage of fatigue life

Figure 6.7 shows wave velocity versus the number of cycles as a fraction of the fatigue life curves on logarithmic scales for both the CFRP wrapped beam and the unwrapped beam at three frequencies. The initial undamaged velocity was arbitrarily plotted at one cycle. The same data is plotted on linear scales in Figure 6.8. The initial wave velocity for the unwrapped beam was higher for all frequency levels than the wave velocity for the CFRP wrapped beam. However, as the number of cycles increased, the wave velocity at all frequencies for the unwrapped beam decreased more rapidly than the wave velocity for the CFRP wrapped beam until near the end of the fatigue life they became lower than those of the wrapped beam. The reductions in wave velocity for the unwrapped beam and the CFRP wrapped beam indicate a decrease in stiffness of the material along the lap splice and may be used as an indicator of the damage that has occurred in the lap splice region of the beam.

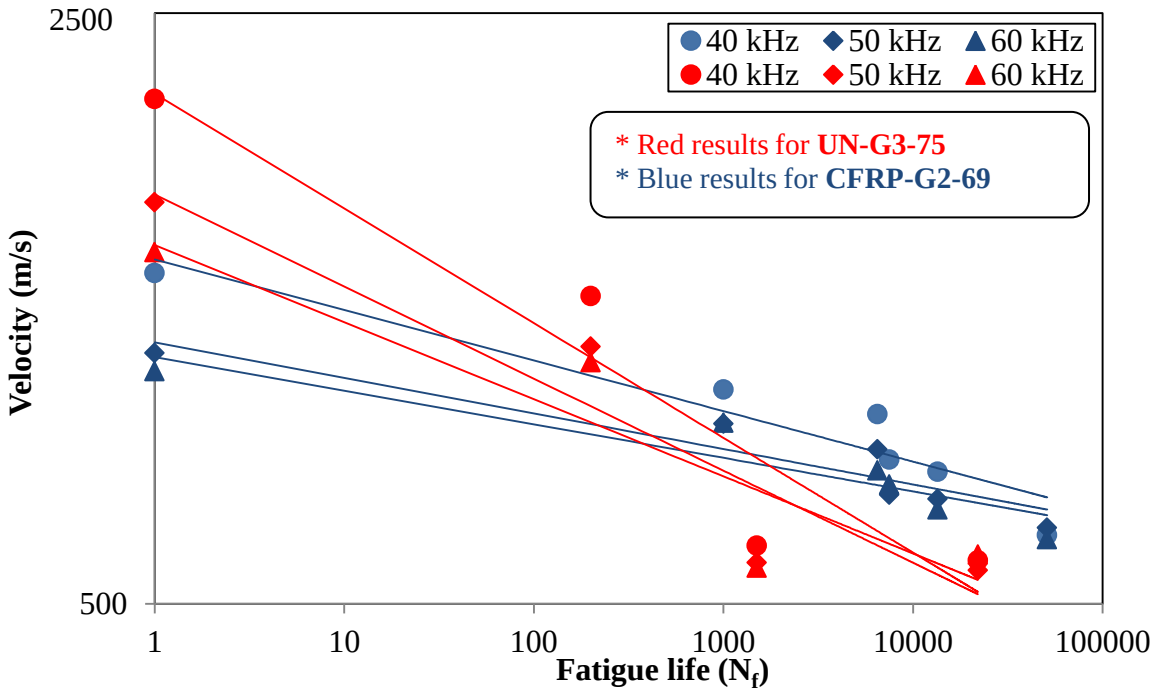

Figure 6.7 The change of the wave velocity versus fatigue life for different frequency levels for UN-G3-75 and CFRP-G2-69 beams

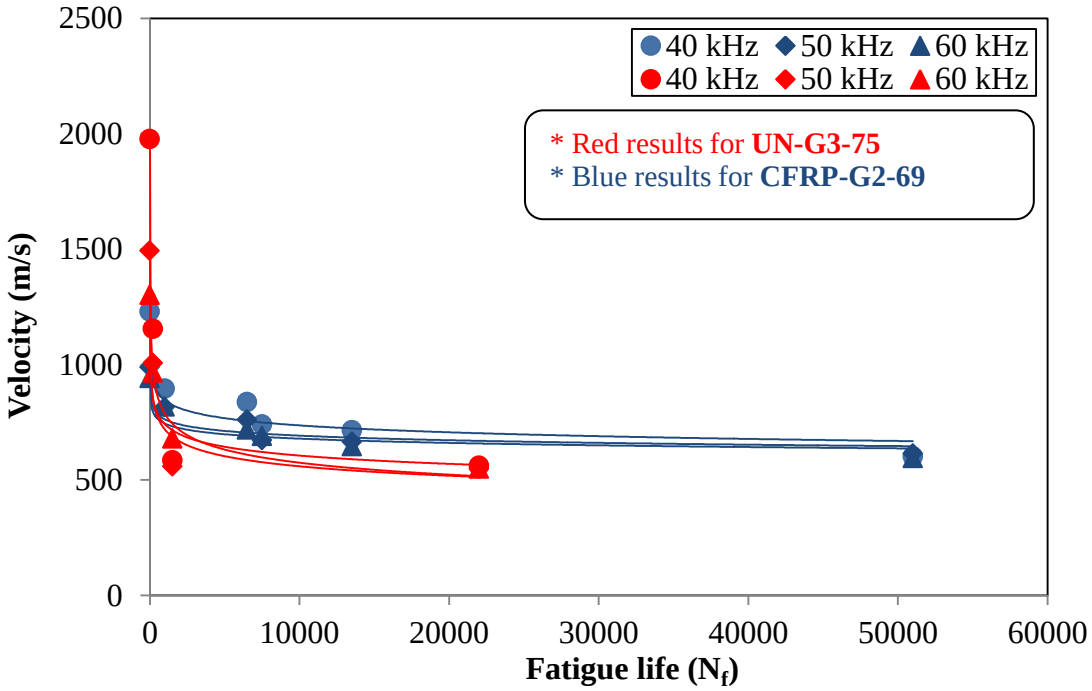

Figure 6.8 The change of the wave velocity versus fatigue life for different frequency level for UN-G3-75 and CFRP-G2-69 beams

6.3.2 Relationship between the Wave Velocity with the Deflection and Crack Length

Figure 6.9 and Figure 6.10 show plots of wave velocity versus deflection and crack length respectively. The large amount of deflection and crack growth during the first few cycles found earlier is shown here as a significant decrease in velocity. However, the decrease in wave velocity with these variables is more rapid thereafter. Since the wave velocity is proportional to the stiffness of the material that the wave passes through, we suggest that this second phase corresponds to the progressive breaking up of the concrete adjacent to the spliced bars noted at failure. The initial wave velocity is greater for the unwrapped specimen than for the wrapped specimen but its decrease of frequency with cycling is more rapid so that at the end of the fatigue life its velocity is lower than that of the wrapped specimen.

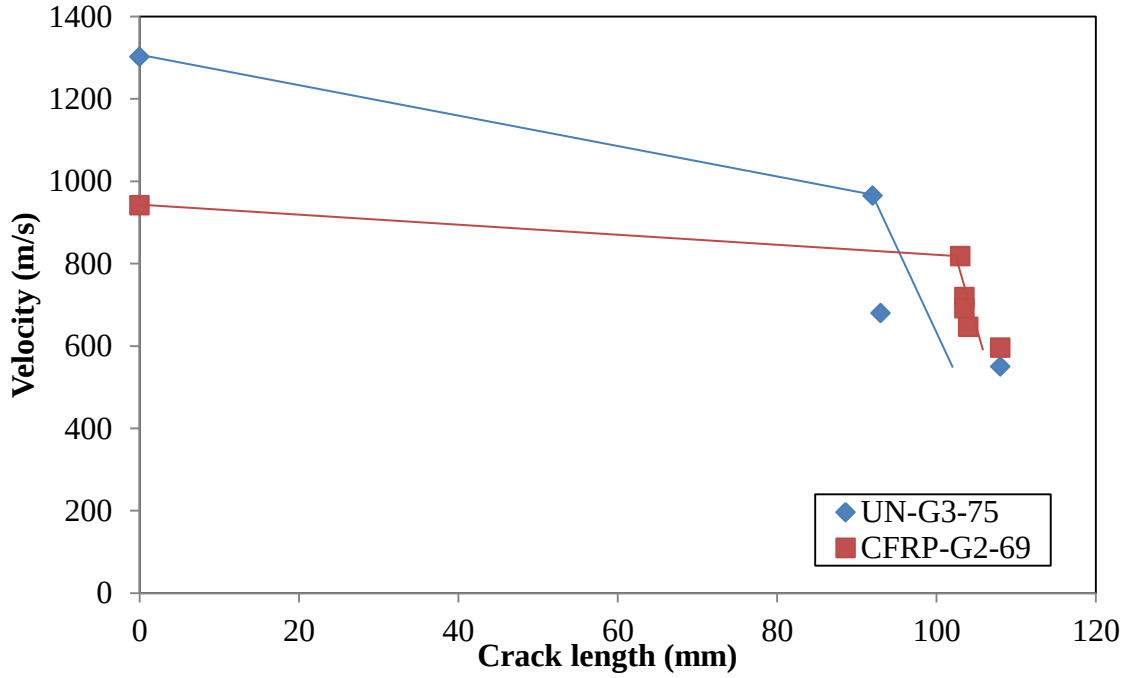

Figure 6.9 Changes in wave velocity with crack length

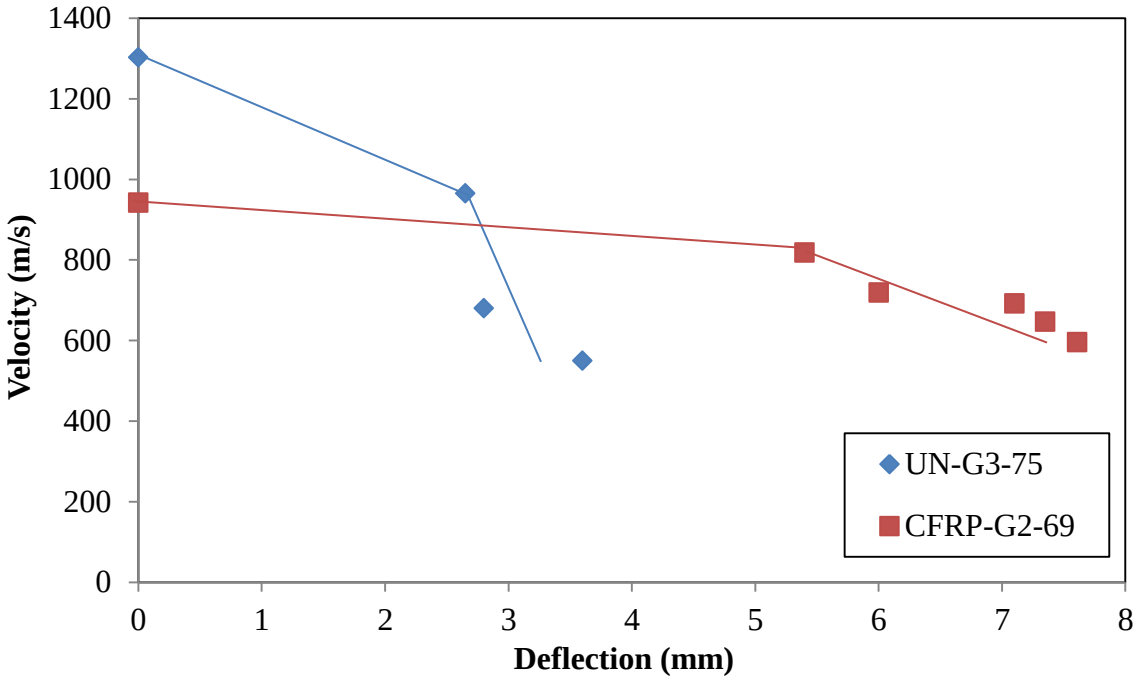

Figure 6.10 Changes in wave velocity with deflection

6.3.3 Discussion

The wave velocity decreases with cycling while the crack length and deflection increase. Taking any one of the number of cycles, the crack length or the deflection as measures of damage during fatigue we have a correlation with decreasing wave velocity as a test progresses. It is hoped that further work on this non-destructive monitoring may make it a useful tool for the inspection of lap splice deterioration with fatigue cycling.

Chapter 7 Conclusions, Contributions and Recommendations for Future Work

7.1 Introduction

This chapter presents the conclusions for this study and recommendations for future work. This study investigated the effect on lap splice bond fatigue behaviour of wrapping the lap splice region with FRP sheet for different concrete cover thicknesses. A total of 53 beams with three different wrapping conditions and three different concrete cover thicknesses were cast and tested under monotonic and fatigue loading. The following conclusions were drawn from the observations and an analysis of the results:

7.2 Conclusions

7.2.1 Monotonic Beam Tests

The conclusions drawn from the monotonic tests are listed below:

- The failure for almost all the beams with different wrapping conditions and different concrete cover thicknesses under monotonic loading was by a simple splitting bond failure. Only for two beams (CFRP-G1-ST and CFRP-G3-ST) out of the nine beams tested under monotonic loading, did the steel bar reach the yield stress level. Those beams also failed by a splitting bond failure.
- The GFRP wrapping increased the normalized bond strengths for the 20 mm, 30 mm and 50 mm concrete cover beams by 128%, 124% and 127% compared to those of the unwrapped beams, respectively.
- The CFRP wrapping increased the normalized bond strengths for the 20 mm, 30 mm and 50 mm concrete cover beams compared to those of the unwrapped beams by 171%, 160% and 144%, respectively.

- Increases in the thickness of the concrete cover resulted in increases in the ultimate load and deflection at failure for all wrapping conditions.
- The Orangun et al. (1977) and Hamad et al. (2004) equations gave good predictions of the average bond strength for all concrete cover thicknesses and wrapping conditions.
- The longitudinal splitting cracks of the unwrapped beams were wider than those of the FRP wrapped beams.
- For Group 1 (20 mm concrete cover), the FRP sheet along the lap splice delayed and confined the growth of the splitting cracks before failure and improved the bond strength compared to the unwrapped beams.

7.2.2 Fatigue Tests

The conclusions drawn from the fatigue tests are listed below:

- The failure for all the unwrapped beams under fatigue loading was by a splitting bond failure. The absence of the FRP sheet in the unwrapped beams allowed a separation of the bottom concrete cover from the beam and failure as the rebar lost support.
- The failure of all FRP wrapped beams was also by a splitting bond failure except for those beams that exceeded the fatigue life limits for a longitudinal bar proposed by Helgason and Hanson (1974). These beams failed by fatigue rupture of the longitudinal steel bars.
- The longitudinal splitting cracks for the FRP wrapped beams were finer in width and larger in number compared to those cracks for the unwrapped beams.
- It is worthy of mention that, the presence of the FRP sheets along lap splice resulted in smaller chunks of broken concrete than those observed for the unwrapped beam. Also, the concrete in front of the steel bar lugs was crushed and abraded for the FRP wrapped beams. Moreover, the presence of the FRP sheets delayed the separation of

the bottom concrete cover which provided the rebar with support to continue resisting load.

- The GFRP and CFRP sheets increased the fatigue strength (measured as the applied load range) of the wrapped beams for all concrete covers compared to that of the unwrapped beams.
- Beams strengthened with CFRP and GFRP sheets had significantly greater deflections at failure than unstrengthened beams for both monotonic and fatigue loading.
- For all the beams loaded in fatigue the deflection increased abruptly during the first cycle then slowed to a low rate of increase after the first 5 % of the fatigue life. This slow increase in deflection with cycles persisted to about 90 % of the fatigue life followed by an increasingly rapid increase until failure.
- For Group 1 (20 mm concrete cover) beams, the slip versus fatigue cycles behaviour was similar to the deflection versus cycles behaviour. The slip at failure of the FRP wrapped beams was greater than that of the unwrapped beams.
- The monotonic failure test results fell close to the intercept of the fatigue life curves at one cycle for all concrete covers and wrapping conditions of the beams. This suggests that a single mechanism is responsible for the monotonic and fatigue failures for all wrapping conditions and concrete cover thicknesses and that the percentage changes in fatigue strength and monotonic failure strength with wrapping condition and cover thickness are the same.
- There was a good correlation between the best fit fatigue life curves obtained by enforcing an average slope of the fatigue life curves for all the groups and the fatigue data.

7.2.2.1 Analysis

- A crack growth model based on a mechanism of crack growth similar to that reported

by Wahab et al., 2015 was developed to calculate the fatigue life of the bond specimens. The calculated number of cycles was in good agreement with the actual fatigue data for all wrapping conditions and concrete cover thicknesses. Also, the model was used to calculate the slip and the deflection due to changes in the stress of the steel and concrete due to cracking and compare their sum to the measured slip and deflection.

- It is worthy of mention that, only a small amount of the inelastic slip and deflection are due to the stress changes in the steel and concrete due to cracking. The remaining changes in slip and deflection with cycling which are due to deformation of the concrete in front of the steel rebar lugs are much larger.

7.2.2.2 Non-Destructive Test

- The NDT test results showed a reduction in the wave velocity as a fatigue test progressed. Data for the changes in wave velocity with cycles, crack length and deflection were presented. It is anticipated that these correlations can be used to relate NDT measured changes in wave velocity to bond deterioration in a lap splice.

7.3 Contributions

- The outcome of this research will enable engineers to use FRP sheet wrapping to strengthen and repair RC beams containing a lap splice under fatigue loading conditions.
- The outcome of this research will enable engineers to predict the fatigue life for RC beams containing a lap splice under fatigue loading conditions.

7.4 Recommendations for Future Work

The current study has contributed information on the performance of a lap splice under fatigue loading for three different concrete covers and three wrapping conditions. Additional work to increase our knowledge of lap splice bond behaviour in fatigue should include:

- the use of different bond lengths ranging from 100 to 500 mm,
- the use of different steel bar diameters (12 to 36 mm) to a cover wide range of bond strength where the bar diameter has a major role,
- the use of high strength concrete due to its effect on the bond strength of concrete beams and there are different criteria to model bond mechanism using high strength concrete,
- an investigation of the effect of corrosion and repair on the strength of a lap splice under fatigue loading due to the impact of the corrosion product on deteriorating the bond strength,
- the use of bidirectional FRP sheets for the wrapping reinforcement to prevent the split of the FRP sheet using the unidirectional sheet as seen in this study, and
- the use of the new cement based thin sheet composite rather than an epoxy based sheet to enhance the fire resistance, and lower the wrapping cost, in addition to its structural compatibility with concrete material.

References

American Concrete Institute (ACI). (1974). "Considerations for Design of Concrete Structures Subjected to Fatigue Loading." *ACI215-74*, Farmington Hills, MI.

American Concrete Institute (ACI). (1992). "State of the Art Report on Bond under Cyclic Loads." ACI408.2-92, Farmington Hills, MI.

American Concrete Institute (ACI). (1996). "State-of-the-Art Report on Fiber Reinforced Plastic Reinforcement for Concrete Structures, Manual of Concrete Practice." ACI440R-96, Farmington Hills, MI.

American Concrete Institute (ACI). (2003). "Bond and Development of Straight Reinforcing Bars in Tension." ACI408-03, Farmington Hills, MI.

American Concrete Institute (ACI). (2008). "Guide for the Design and Construction of Externally Bonded FRP Systems for Strengthening Concrete Structures." *ACI440-08*, Farmington Hills, MI.

American Concrete Institute (ACI). (2012). "Report on Bond of Steel Reinforcing Bars Under Cyclic Loads." *ACI408.2R-12*, Farmington Hills, MI.

American Concrete Institute (ACI). (2013). "Report on NDT methods for evaluation of concrete in structures." *ACI228.2R-13*, Farmington Hills, MI.

Aggelis, D. G., Shiotani, T., and Polyzos, D. (2009). "Characterization of surface crack depth and repair evaluation using Rayleigh waves." *Cement and Concrete Composites*, *31*(1), 77-83.

Alavi-Fard, M. and Marzouk, H. (2002). "Bond behavior of high strength concrete under reversed pull-out cyclic loading." *Canadian Journal of Civil Engineering*, 2002. 29(2): p. 191-200.

Al-Hammoud, Rania. (2007). “Bond Behaviour of Corroded and CFRP Repaired RC Beams Subjected to Monotonic and Repeated Loading.” PhD. Thesis, Department of Civil and Environmental Engineering, University of Waterloo.

Alyousef, R., Topper, T., and Al-Mayah, A. (2015). "Effect of FRP Wrapping on Fatigue Bond Behavior of Spliced Concrete Beams." *J. Compos. Constr.*, 10.1061/(ASCE)CC.1943-5614.0000588, 04015030.

Alyousef, R., Topper, T., and Al-Mayah, A. (2016). "Fatigue Bond Stress–Slip Behavior of Lap Splices in the Reinforcement of Unwrapped and FRP-Wrapped Concrete Beams." *J. Compos. Constr.*, 10.1061/(ASCE)CC.1943-5614.0000699 , 04016039.

Alyousef, R., Topper, T., and Al-Mayah, A. (2016). “Effect of the thickness of concrete cover on the fatigue bond strength of GFRP wrapped and non-wrapped reinforced concrete beams containing a lap splice." *J. Structures.*, 6(1), 1-8.

Alyousef, R., Topper, T., and Al-Mayah, A. (2016). “Effect of FRP Wrapping Stiffness and Concrete Cover on Lap Splice Failure Behavior." ACI Special Publication., (Accepted).

Alyousef, R., Topper, T., and Al-Mayah, A. (2016). “Crack Growth Modeling of Tension Lap Spliced Reinforced Concrete Beams Strengthened with Fibre Reinforced Polymer Wrapping Under Fatigue Loading." *Engineering Structures*., (Submitted).

Azizinamini, A., Pavel, R., Hatfield, E., and Ghosh, SK.. (1999). “Behavior of lap-spliced reinforcing bars embedded in high-strength concrete.” ACI Structural Journal, V. 96(5), 826-835, September 1999.

Badawi, M. A. (2007). “Monotonic and fatigue flexural behaviour of RC beams strengthened with prestressed NSM CFRP rods.” PhD. thesis, Department of Civil and Environmental Engineering, University of Waterloo., Waterloo, Ontario.

Bakis, C., Bank, L. C., Brown, V., Cosenza, E., Davalos, J. F., Lesko, J. J., and Triantafillou, T. C. (2002). "Fiber-reinforced polymer composites for construction-state-of-the-art review". Journal of composites for construction, 6(2), 73-87.

Balazs, G. (1991). "Fatigue of Bond." *ACI Materials Journal*., 88(6), 620-630.

Balazs, G. and Koch, R. (1992). "Influence of Load History on Bond Behaviour." *Proceedings: Bond in Concrete*- From Research to Practice, Riga, Latvia, October pp.7.1-7.10.

Bannantine J.A. (1990). "Fundamental of Metal Fatigue Analysis." *Prentice Hall*, NJ, USA, First Edition, 1990.

Bousias, S., Spathis, A., and Fardis, M. (2007). "Seismic retrofitting of columns with lap spliced smooth bars through FRP or concrete jackets." *J. Earthquake Eng.*, 11(5), 653–674

Bournas, D. and Triantafillou, T. (2011). "Bond Strength of Lap-Spliced Bars in Concrete Confined with Composite Jackets." *J. Compos. Constr.* 15, Special Issue in Honor of Professor Urs Meier, 156–167.

Breysse, D. (2012). "Non-destructive Assessment of Concrete Structures: Reliability and Limits of Single and Combined Techniques: State-of-the-art Report of the RILEM Technical Committee 207-INR." Springer Science and Business Media.

Canbay E, and Frosch R. (2005). "Bond Strength of Lap-Spliced Bars." *ACI Structural Journal*, 102(4), 605-614.

Carino, N.J. and H. Lew., 1982. "Re-examination of the relation between splitting tensile and compressive strength of normal weight concrete." *ACI Journal Proceedings*, 79(3), 214-219.

CSA, Design of concrete structures, CSA A23. 3–04. CSA, Rexdale, Ontario, 2004.

Darwin, D., Tholen, M. L., Idun, E. K., and Zuo, J. (1996). "Splice Strength of High Relative Rib Area Reinforcing Bars." *ACI Structural Journal*, 93(1), 95-107.

Eligehausen, R. (1979) "Bond in Tensile Lapped Splices of Ribbed Bars with Straight Anchorages," *Publication 301*, German Institute for Reinforced Concrete, Berlin, 118 pp.

Eligehausen, R., Popov, E., and Bertero, V. (1983). "Local bond stress-slip relationships of deformed bars under generalized excitations." *Rep. No. UCB/EERC-83/23*, Univ. of California, Berkeley.

El-Azab, M. A., Mohamed, H. M., and Farahat, A. (2014). "Effect of tension lap splice on the behavior of high strength self-compacted concrete beams." *Alexandria Engineering Journal*, *53*(2), 319-328.

FIB (International Federation for Structure Concrete). (2000). "Bond of Reinforcement in Concrete." *FIB 10*, Lausanne, Switzerland.

Fagundo, F., Gergely, P., and Whute, R. (1979). "The behavior of lapped spliced in reinforced concrete beam subject to repeated loads." *Report No.79-1*, Department of Structural Engineering, Cornell University, Ithaca, NY.

Ferguson, P. M., and Briceno, E. A., (1969) "Tensile Lap Splices-Part I: Retaining Wall Type, Varying Moment Zone," *Research Report* No. 113-2, Center for Highway Research, The University of Texas at Austin, Austin, Tex., July, 39 pp.

Garcia, R., Helal, Y., Pilakoutas, K., and Guadagnini, M. (2013). "Bond strength of short lap splices in RC beams confined with steel stirrups or external CFRP." *Mater. Struct.*, 48(1-2), 277–293.

Goto, Y. (1971). "Cracks Formed in Concrete around Deformed Tension Bars." *ACI Journal Proceedings*, 68(4), 244-251.

Goueygou, M., Abraham, O., and Lataste, J. F. (2008). “A comparative study of two non-destructive testing methods to assess near-surface mechanical damage in concrete structures.” *NDT & E International*, 41(6), 448-456.

Hamad, B.S., Rteil, A.A. and Soudki, K.A., (2004a). “Bond Strength of Tension Lap Splices in High Strength Concrete Beams Strengthened with Glass Fiber Reinforced Polymer Wraps,” *Journal of Composites for Construction*, 8(1),14-21.

Hamad, B.S.; Rteil, A.A.; Selwan, B. and Soudki, K.A. (2004b). “Behavior of Bond-Critical Regions Wrapped with Fiber-Reinforced Polymer Sheets in Normal and High-Strength Concrete,” *Journal of Composites for Construction*, 8(3), 248-257.

Hamad, B.S., Soudki, K.A., Rteil, A.A. and Harajli, M.H. (2004c). “Experimental and Analytical Evaluation of the Bond Strength of Reinforcement in Fiber Reinforced Polymer-Wrapped High Strength Concrete Beams,” *ACI Structural Journal*, 101(6), 747-754.

Hamad, B. and Rteil, A. (2006). “Comparison of Roles of FRP Sheets, Stirrups, and Steel Fibres in Confining Bond Critical Regions.” *J. Compos. Constr.*, 10(4), 330–336.

Harajli, M. H. (2006). “Effect of confinement using steel, FRC, or FRP on the bond stress-slip response of steel bars under cyclic loading.” *Materials and structures*, *39*(6), 621-634.

Harajli, M., H. (2009). “Bond strengthening of lap spliced reinforcement using external FRP jackets: An effective technique for seismic retrofit of rectangular or circular RC columns.” *Construction and Building Materials*, 23(3), 1265-1278.

Harajli, M., Hamad, B., and Karam, K. (2002). “Bond-slip Response of Reinforcing Bars Embedded in Plain and Fiber Concrete.” *J. Mater. Civ. Eng.*, 14(6), 503–511.

Harajli, M. H., Hamad, B. S., and Rteil, A. A. (2004). “Effect of confinement on bond strength between steel bars and concrete.” *ACI Structural Journal*, 101(5), 595-603.

Helgason, T., and Hanson, J. M. (1974). "Investigation of design factors affecting fatigue strength of reinforcing steel—Statistical analysis." *ACI SP-41*, 107–138.

Hevin, G., Abraham, O., Pedersen, H. A., and Campillo, M. (1998). "Characterization of surface cracks with Rayleigh waves: a numerical model." *NDT & E International*, 31(4), 289-297.

Hungspreug, S., Gergely, P., Ingraffia, AR., and White, RN. (1981). "Local bond between a reinforcing bar and concrete under high intensity cyclic load." *NASA STI/Recon Technical Report* N, 83, 11372.

ISIS Canada 2001. "Reinforcing Concrete Structures with Fibre Reinforced Polymers." Intelligent Sensing for Innovative Structures (ISIS) Manual, No. 2. Winnipeg, Manitoba, Canada.

ISIS Canada 2008. "Prestressing Concrete Structures with Fibre-Reinforced Polymers." Design Manual No. 5 Winnipeg, Manitoba, Canada.

Jones, R., Swamy, R.N., Bloxham J., and Bouderdalah A. (1988). "Composite Behaviour of Concrete Beams with Epoxy Bonded External Reinforcement," *International Journal of Cement Composite 2*, 2, 91-107.

Kajfasz S., Belki, b., and Wzmocnione K. (1970). "Concrete Beams with External Reinforcement bond by gluing," *Colloque RILEM*, synthetic, Resin in Building Construction, Paris, France, 142-151.

Kirlangiç, Ahmet. (2013). "Condition Assessment of Concrete Beams Using Ultrasonic Surface Waves." PhD. Thesis, Department of Civil and Environmental Engineering, University

Lerchental H. (1970). "Bonded Steel Metal Reinforcement of Concrete Slabs," *RILEM International Symposium*, Resin in Building Construction, Part 2, Paris, France, 165-173.

Lukose, K., Gergely, P., and White, R. N. (1982). "Behavior of reinforced concrete lapped splices for inelastic cyclic loading." *Journal Proceedings,* 79(5), 355-365.

MacKay, B., Schmidt, D., and Rezansoff, T. (1989). "Effectiveness of concrete confinement on lap splice performance in concrete beams under reversed inelastic loading." *Canadian Journal of Civil Engineering*, 16(1), 36-44.

Mallet, G. (1991). "Fatigue of Reinforced Concrete, State of the Art Review/2, Transport and Road Research Laboratory." *London: HMSO, ISBN 0*, *11*(550979), 8

Oh, B.H. and Kim, S.H. (2007). "Realistic Models for Local Bond Stress-Slip of Reinforced Concrete under Repeated Loading." J*ournal of Structural Engineering*, 133(2), 216-224.

Oehlers, D. (1992). "Reinforced Concrete Beams with Plates Glued to Their Soffits." *Journal of Structural Engineering*, 118(8), 2023-2038.

Orangun, C., J. Jirsa, and J. Breen. (1977). "A reevaluation of test data on development length and splices." *ACI Journal,* 74(3), 114-122.

Pacholka, K., Rezansoff, T., and Sparling, B. F. (1999). "Stirrup distribution across the beam width in tension lap splices." Canadian Journal of Civil Engineering, 26(1), 83-95.

Parvin, A., and Brighton, D. (2014). "FRP composites strengthening of concrete columns under various loading conditions". *Polymers*, 6(4), 1040-1056.

Perry, E. and Jundi, N., (1969). "Pullout Bond Stress Distribution under Static and Dynamic Repeated Loading," *ACI Journal,* 66(5), 377-380.

Plizzari, G., Lundgren, K., and Balazs, G. (2002). "Bond and Splitting in Fibre Reinforced Concrete under Repeated Loading." *Proceedings: Bond in Concrete-From Research to Standards,* Budapest, Hungary, 221-229.

Rabbat, B., and Corley, W. (1984). "Long-time fatigue properties of high yield reinforcing bars." *Matériaux et Construction,* 17-1.

Rehm, G., and Eligehausen, R. (1979). "Bond of Ribbed Bars under High Cycle Repeated Loads." *ACI Journal*, 76(2), 297-309.

Reynolds, GC., and Beeby, AW. (1982). "Bond strength of deformed bars." *Proceedings of the 2nd International Conference on Bond in Concrete*, Paisley, Scotland. Applied Science, London, UK, 434–445.

Rezansoff, T. (1978). "Performance of lapped splices in reinforced concrete loaded beyond yielding of the steel." *Canadian Journal of Civil Engineering*, 5(4), 489-496.

Rezansoff, T., Konkankar, US., and Fu, YC. (1992). "Confinement limits for tension lap slices under static loading." *Canadian Journal of Civil Engineering*, 19(3), 447-453.

Rezansoff, T., Zacaruk, J. A., and Topping, R. (1988). "Tensile lap splices in reinforced concrete beams under inelastic cyclic loading." *ACI Structural Journal*, 85(1), 46-52.

Rezansoff, T., Zacaruk, J.A., and Afseth, J.G. (1993). "High cycle (fatigue) resistance of reinforced concrete beams with lap splices." *Canadian Journal of Civil Engineering*, 20(4), 642-649.

Rteil, Ahmad. (2002). "Analytical and Experimental Evaluation of Bond Strength of Tension Lap Splice in High Strength Concrete Wrapped With Fiber Reinforced Polymer." MSc. Thesis, Department of Civil and Environmental Engineering, American University of Beirut.

Rteil, Ahmad. (2007). "Fatigue Bond Behaviour of Corroded Reinforcement and CFRP Confined Concrete." PhD. Thesis, Department of Civil and Environmental Engineering, University of Waterloo.

Rteil, A., Soudki, K., and Topper, T. (2007). "Preliminary experimental investigation of the fatigue bond behavior of CFRP confined RC beams." *Construction and Building Materials*, 21(4), 746-755.

Sakurada, T., Morohashi, N., and Tanaka, R. (1993). “Effect of transverse reinforcement on bond splitting strength of lap splices.” *Transactions of the Japan Concrete Institute*, *15*, 573-580.

Seliem, H., Hosny, A., Rizkalla, S., Zia, P., Briggs, M., Miller, S., Darwin, D., Browning, J., Glass, G., Hoyt, K., Donnelly, K., and Jirsa, J. (2009). “Bond characteristics of ASTM A1035 steel reinforcing bars.” *ACI Structural Journal*, 106(4), 530-539.

Shah, S. P., and Chung, L. (1986). “Effect of cyclic loading rate on response of model beam-column joints and anchorage bond.” In *Proceeding of the 3rd US National Conference on Earhquake Eng*.

Shihata, Ayman. (2011). “CFRP strengthening of RC beams with corroded lap spliced steel bars.” MSc. Thesis, Department of Civil and Environmental Engineering, University of Waterloo.

Soretz, S. (1974). “Contribution to the fatigue strength of reinforced concrete.” *ACI Special Publication*, 41, 35-58.

Soudki, K., and Sherwood, T. (2000). “Behaviour of Reinforced Concrete Beams Strengthened with Carbon Fibre Reinforced Polymer Laminates Subjected to Corrosion Damage.” *Canadian Journal of Civil Engineering*, 27(5), 1005-1010.

Soudki, K., and Sherwood, T. (2003). “Bond behavior of corroded steel reinforcement in concrete wrapped with carbon fiber reinforced polymer sheets.” *J. Mater. Civ. Eng*., 15(4), 358–370.

Sparling, B., and Rezansoff, T. (1986). “The effect of confinement on lap splices in reversed cyclic loading.” *Canadian Journal of Civil Engineering*, 13(6), 681-692.

Swamy, R., Jones, R., and Blxham, J. (1987). “Structural Behaviour of Reinforced Structured Strengthened by Epoxy-Bonded Steel Plates.” *Structural Engineer*, 65A, 1.

Tarabia, AM., Shoukry, MS., and Diab, MA. (2010). “Improving the behavior of reinforced concrete beams with lap splice reinforcement.” Taylor and Francis Group. UK.

Tastani, S. P., and Pantazopoulou, S. J. (2012). “Reinforcement and concrete bond: State determination along the development length.” *Journal of Structural Engineering*, *139*(9), 1567-1581.

Tepfers, R. (1973). “A theory of bond applied to overlapped tensile reinforcement splices for deformed bars.” *Chalmers University of Technology*, Sweden.

Tepfers, R. (1980). "Bond stress along lapped reinforcing bars." *Magazine of Concrete Research* 32, 112, 135-142.

Tepfers, R. (1988). “Overlap splices for ribbed bars for free use in a concrete structure.” *Nordic concrete research*, (7), 273-283.

Tilly, G.P., and Tan K.H. (1979) “Fatigue of Steel Reinforcement Bars in Concrete” A Review,” *Fatigue of Engineering Materials and Structures*, 2(3), 251-278.

Tocci, AD. (1981). “The behavior and strength of lapped splices in reinforced concrete beams subjected to cyclic loading.” PhD thesis, Cornell University.

Untrauer, R. E., and Henry, R. L., (1965). “Influence of Normal Pressure on Bond Strength,” *ACI Journal*, 62(5), 577-585.

Wahab, N., Topper, T., and Soudki, K. A. (2015). “Modelling experimental bond fatigue failures of concrete beams strengthened with NSM CFRP rods.” *Composites Part B: Engineering*, *70*, 113-121.

Wahab, N. (2011). “Bond behaviour of beams reinforced with near surface mounted carbon fibre reinforced polymer rods under fatigue loading.” PhD. thesis, Department of Civil and Environmental Engineering, University of Waterloo., Waterloo, Ontario.

Yang, Y., Cascante, G., and Polak, M. A. (2009). "Depth detection of surface-breaking cracks in concrete plates using fundamental Lamb modes." *NDT and E International*, *42*(6), 501-512.

Zacaruk, A. (1990). "Performance of large size reinforced concrete beams containing a lap splice subjected to fatigue loads." MSc. Thesis, Department of Civil Engineering, University of Saskatchewan, SK.

Appendix

Bond prediction equation with FRP sheet:

$$u = \left[0.10 + \frac{c}{4d_b} + \frac{4.2d_b}{l_d} + K_{tr\prime f}\right]\sqrt{f_c'}$$

$K_{tr\prime f}$ is contraption factor of FRP sheet to bond strength which added by (Hamad et al. 2004) to bond equation.

$$c = 25\ mm, \qquad d_b = 20mm, \qquad l_d = 300mm, \qquad f_c'(Assume) = 40\ MPa$$

Steps:	GFRP	CFRP
The nominal strength and strain of the FRP sheet: $f_{fu} = C_E f_{fu}$ (C_E is environmental reduction factor = 1.0 to get nominal tensile strength) $\varepsilon_{fu} = C_E\ \varepsilon_{fu}$	$f_{fu} = 1 * 537 = 537\ MPa$ $\varepsilon_{fu} = 1 * 0.022 = 0.022$	$f_{fu} = 1 * 1120 = 1120\ MPa$ $\varepsilon_{fu} = 1 * 0.011 = 0.011$
I_e is active bond strength length. For U wraps: $I_e = \frac{23{,}300}{(n\ t_f\ E_f)^{0.58}}$	$I_e = \frac{23{,}300}{(1 * 0.51 * 26{,}500)^{0.58}} = 94mm$	$I_e = \frac{23{,}300}{(1 * 1.3 * 100{,}000)^{0.58}} = 25\ mm$
k_1 and k_2 are coefficients to account for concrete strength and sheet layout respectively: $k_1 = \left(\frac{f'_c}{27}\right)^{2/3}$ $k_2 = \left(\frac{d_f - I_e}{d_f}\right)$	$k_1 = \left(\frac{33}{27}\right)^{2/3}$=1.14 $k_2 = \left(\frac{350 - 94}{350}\right) = 0.73$	$k_1 = \left(\frac{33}{27}\right)^{2/3}$=1.14 $k_2 = \left(\frac{350 - 25}{350}\right) = 0.93$

Calculate stress reduction factor:

$$R = \frac{k_1 k_2 I_e}{11{,}900\varepsilon_{fu}} \leq \frac{0.004}{\varepsilon_{fu}}$$

$$R = \frac{1.14 * 0.73 * 94}{11{,}900 * 0.022} = 0.29 \qquad R = \frac{1.14 * 0.93 * 25}{11{,}900 * 0.011} = 0.20$$

$$\frac{0.004}{\varepsilon_{fu}} = 0.18 \qquad \frac{0.004}{\varepsilon_{fu}} = 0.36$$

$$R = 0.29 \leq 0.18 \qquad R = 0.20 \leq 0.36$$

Use $R = 0.18$ Use $R = 0.20$

Calculate effective stress of fiber reinforced polymer sheet:

$$f_{fe} = R * f_{fu}$$

$f_{fe} = 0.18 * 537 = 97\ MPa$ $f_{fe} = 0.2 * 1120 = 224\ MPa$

Calculate area of fiber reinforced polymer reinforcement as follows:

$$A_{tr,f} = 2\ n\ t_f\ w_f$$

$A_{tr,f} = 2 * 1 * 0.51 * 600 = 612\ mm^2$ $A_{tr,f} = 2 * 1 * 1.3 * 600 = 1560\ mm^2$

Calculate $K_{tr,f}$

$$K_{tr,f} = \frac{A_{tr,f}\ f_{fe}}{C\ d_b n_b s_f} \leq 0.25$$

$$K_{tr,f} = \frac{612 * 97}{16.6 * 20 * 2 * 600} = 0.148 \qquad K_{tr,f} = \frac{1560 * 224}{16.6 * 20 * 2 * 600} = 0.89$$

$K_{tr,f} = 0.148$ According to Hamad et al. (2004) $K_{tr,f}$ is limited to0.25